PROJECTING WILDFIRE EMISSIONS AND THEIR AIR QUALITY IMPACTS IN THE SOUTHEASTERN U.S. FROM 2010 TO MID-CENTURY

Uma Shankar

A dissertation submitted to the faculty at the University of North Carolina at Chapel Hill in partial fulfillment of the requirements for the degree of Doctor of Philosophy in the Department of Environmental Sciences and Engineering in the Gillings School of Global Public Health.

Chapel Hill
2019

Approved by:

William Vizuete

Francis S. Binkowski

David Leith

Jeffrey P. Prestemon

Jason West

ABSTRACT

Uma Shankar: Projecting Wildfire Emissions and Their Air Quality Impacts in the Southeastern U. S. from 2010 to Mid-century
(Under the direction of William Vizuete)

Wildfires can severely impair the health of ecosystems, life forms and regional economies. In the rapidly changing U. S. Southeast, both climate and socioeconomic factors (e.g., population and income) drive wildfires, and need to be represented in wildfire inventories to assess the air quality (AQ) impacts and health risks of wildfires long-term. This motivated the development of a wildfire emissions projection methodology leveraging published models of annual areas burned (AAB) based on county-level socioeconomic and climate projections for 2011-2060. It is applied to project two sets of AAB with different climate downscaling approaches, to estimate wildfire emissions for 2010 and four mid-century years. These are compared with emissions estimated using 18-year historical mean AAB without changes in climate and socioeconomics. Competing climate and socioeconomic factors result in 7% - 32% lower projected AAB than historical values, and 13% - 62% lower fine particulate matter ($PM_{2.5}$) emissions than estimated from historical AAB in the selected years, with climate driving their temporal variability.

Evaluation of the emissions projection methods in air quality (AQ) simulations against those using the National Emissions Inventory (NEI), and network observations for 2010 show little difference among the methods in ozone (0.08% - 0.93%) and $PM_{2.5}$ (1% - 8%). Larger, comparable biases relative to observations in all three methods for secondary species, especially in winter, are attributable to non-wildfire emissions or secondary chemical production. The

projection methods predict primary wildfire PM better than the NEI, providing confidence that they can assess current wildfire AQ impacts, while enabling longer-term AQ assessments unachievable with static inventories.

AQ simulations using the projected wildfire emissions, and projected emission reductions in SO_x and NO_x from energy and transportation (by ~80% at mid-century) show peak periods and locations of wildfire impacts on ozone and PM shifting from autumn in Midwestern locations in 2010, to warmer and drier summers east and south by mid-century, following the AAB spatiotemporal patterns. Although considerably lower than 2010 levels, summertime $PM_{2.5}$ increases by 4%-5% in 2040-2060 in this emission scenario, driven by increases in OC and unspeciated other PM.

In loving memory of my parents, Madhuram and K. V. Shankar, and my brother-in-law V. S. Mahesh, my examples in courage and joyful dedication to work.
To my grandnieces Maya, 7, and Eva, 1, and children everywhere, the reason for it.

ACKNOWLEDGMENTS

My deepest thanks go to my beloved family, including my family of friends, for their unwavering support and encouragement. I am most grateful to my friend Dr. Suzanne Elizabeth "Zz" Szabo (1951 – 2012), but for whose material support in the last two years, this work could not have been completed.

I owe thanks to many mentors: Dr. Frank Binkowski, for launching and nurturing my career; my advisor Dr. Will Vizuete, for his endless patience, critical review and advice on this work; my other committee members Dr. Jason West and Dr. David Leith, for their guidance on these analyses, and Dr. Jeff Prestemon, for inviting me into his research, and funding this work; Dr. Doug Fox, my first mentor and co-PI in wildfire research; Dr. Don McKenzie, fire science guru, for his guidance on the fire modeling approach, his excellent writing skills and good humor; and Dr. Adel Hanna, and colleagues and co-authors at the University of North Carolina–Institute for the Environment for many years of collaboration and support. I am indebted to my former colleague Jeanne Eichinger, whose extraordinary skills in technical editing have improved me as a writer. Special thanks to my former colleague Dr. Mohammed "MO" Omary, for his critical contributions to the emissions processing in this work. MO, this is for you!

My sincere thanks go to my friend and colleague Dr. Stefano Galmarini for his constant encouragement, camaraderie, and timely help in submitting part of this work to Atmospheric Chemistry and Physics for publication. This research was wholly supported by Joint Venture Agreement # 11-JV-11330143-080 between the U. S. Forest Service and UNC–Chapel Hill.

TABLE OF CONTENTS

LIST OF TABLES

LIST OF FIGURES

LIST OF ABBREVIATIONS

AAB	Annual areas burned
AMET	Atmospheric Model Evaluation Tool
AQ	Air quality
AQS	Air Quality System
AR3	Third Assessment Report (of the IPCC)
AR5	Fifth Assessment Report
cb05tucl	Carbon Bond 05 gas-phase mechanism with toluene and chlorine chemistry updates
CAP	Criteria air pollutant
CSN	Chemical Speciation Network
CFFDRS	Canadian Forest Fire Danger Rating System
CGCM3	Canadian General Circulation Model version 3
CGCM31	Canadian General Circulation Model version 3.1
CMAQ	Community Multiscale Air Quality model
CONUS	Conterminous U. S.
EC	Elemental carbon
EI	Emissions inventory
EPA	(U. S.) Environmental Protection Agency
FCCS	Fuel Characteristic Classification System
FEPS	Fire Emissions Processing System
FSB	Fire Scenario Builder
FWI	Fire Weather Index
GCAM	Global Change Assessment Model
GCM	General circulation model

GHG	Greenhouse gas
HadCM3	Hadley Centre Climate Model version 3
ICS 209	Incident Status Summary report by the National Interagency Fire Center
IMPROVE	Interagency Monitoring of PRotected Visual Environments
IPCC	Intergovernmental Panel on Climate Change
IVOCs	Intermediate volatile organic compounds
KBDI	Keetch-Byram Drought Index
LBC	Lateral boundary condition
LCC	Lambert Conformal Conic map projection
LSF	Land surface feedback
MB	Mean Bias
MCIP	Meteorology-Chemistry Interface Processor
MDA8	maximum daily value of the 8-h running average of ozone
MFB	Mean Fractional Bias
MFE	Mean Fractional Error
MODIS	Moderate Resolution Imaging Spectroradiometer
NARCCAP	North American Regional Climate Change Assessment Program
NEI	U. S. National Emissions Inventory
NMB	Normalized Mean Bias
NME	Normalized Mean Error
NMVOC	Non-methane volatile organic compound
NP	National Park
NWR	National Wildlife Refuge
OC	Organic carbon
PET	Potential evapotranspiration

PM	Particulate Matter
$PM_{2.5}$	PM below 2.5 μm in aerodynamic diameter
POA	Primary organic aerosol
RCP	Representative Concentration Pathway
RCP4.5	RCP that stabilizes anthropogenic components of radiative forcing to 4.5 W m^{-2} by 2100
RCM	Regional climate model
RPA	Resources Planning Act
RS	Remote sensing
SEARCH	Southeast Aerosol Research and Characterization
SMOKE	Sparse Matrix Operator Kernel Emissions processing system
SOA	Secondary organic aerosol
SRS	Southern Research Station, U. S. Forest Service
SVOCs	Semi-volatile organic compounds
VBS	Volatility basis set
VOC	Volatile organic compound
WRF	Weather Research and Forecasting model
WRFG	WRF with an improved scheme for convective parameters
WSM6	WRF Single- Moment 6-Class microphysics scheme w/ graupel
WUI	Wildland-urban interface
USDA	U. S. Department of Agriculture
USFS	U. S. Forest Service

CHAPTER 1: INTRODUCTION

Assessing the Impacts of Wildfire on Future Air Quality: Rationale

The adverse impacts of wildfires on the health of ecosystems, life forms and regional economies cannot be overstated. The loss of forested areas in catastrophic wildfires could increase their climate impacts through a reduction in the forest carbon sink depending on whether or not fire activity outpaces their ability to regenerate (Liu et al., 2011; King et al., 2012). Black carbon emitted in wildfires adds to the positive radiative forcing on climate, which was estimated to be as high as 1.1 W m^{-2} in a comprehensive review of the radiative impacts of black carbon (Bond et al., 2013). Climate change in turn has an impact on wildfires, due to an increase in conditions such as widespread drought coupled with warmer and drier weather patterns (Littell et al., 2010, 2016). These can increase the risk of fire recurring in the next wildfire season, particularly in the case of rainfall during the growing season that promotes new forest growth (Littell et al., 2010, 2016). Even when there is no further growth of vegetation to supply fuel for another fire, there is an increased risk of mudslides in sloping terrain denuded by fire, as happened in 2017 in the week following the Thomas Fire, one of the largest in California history; mudslides following wildfires resulted in 66 deaths in that year (Balch et al., 2018).

These adverse impacts are not limited to terrestrial ecosystems. The atmospheric emissions of particulate black and brown carbon in fire plumes have adverse consequences for air quality, which can be felt thousands of miles away, as evidenced by the fire season of 2017 (Balch et al., 2018) among many others. The health impacts from the toxicity of wildfire emissions are not

only on first responders (Wegesser et al., 2009), but on vulnerable populations exposed to the pollutant plumes in downwind areas (Fann et al., 2018; Rappold et al., 2011). These populations often lack the means for adequate protection measures and healthcare, adding to the wildfire health risks (Gaither et al., 2011). The extent of the wildland-urban interface (WUI) is increasing (USGCRP, 2018) alongside increasing wildfire, exacerbating the health risks of smoke exposure.

In this context, the economic costs associated with wildfires go far beyond those of fire suppression and recovery of values at risk. In a study of the health impacts of wildfires over the Northwestern and Southeastern U.S., Fann et al. (2018) estimated the economic impacts of wildfires in the form of additional premature deaths and hospital admissions between 2008 and 2012 in the range of $11B - $20B (2010$) per year, and far in excess of the cost of fire suppression. Using data from the 2008 Evans Road Fire in eastern North Carolina, Rappold et al. (2014) estimated the economic benefits of avoided short-term healthcare costs through interventions such as public health forecasts of smoke events to be a fraction ($1M) of the avoided long-term costs of additional mortality ($42M).

Given the evolving landscape of wildfires brought on at least in part by climate change, climate adaptation and resilience pivots on the availability of methods to project future impacts reliably over a longer time horizon than is typical for forecasting weather-related incidents. While climate change has been implicated as a driver of wildfires, society and economic factors are also important drivers (Syphard et al., 2017; Viedma et al., 2018). In their study of 37 counties across the U.S. by Syphard et al. (2017) found human presence and climate to have a complementary relationship in explaining fire activity in certain geographic areas, and in some areas, completely offset the climate drivers of wildfire. Balch et al. (2018) also cite human presence as a major switch for fire ignitions, responsible for starting 89% of the fires during the

2017 wildfire season. Human-ignited fires are closely related to socioeconomic drivers such as population and income (Prestemon et al., 2013, 2016), especially in the Southeastern U.S., where humans both cause and suppress a majority of wildfires (Mercer and Prestemon, 2005; Prestemon et al., 2013; Balch et al., 2017). As climate change is interconnected with changes in some of these socioeconomic drivers of wildfire, e.g., population and land use, integrated assessment methods that allow a simultaneous examination of their impacts on wildfires and downstream effects on ecosystems become even more important. Faced with fire activity patterns that are responding to evolving climate drivers as well as regional demographics, forest resource and air quality managers in the Southeast have a critical need to use such methods to develop effective plans for protecting the health and welfare of the public and the environment. The research described here is aimed at addressing this need.

Research Goal, Hypotheses, and Objectives

Background

Under the requirements of the Forest and Rangeland Renewable Resources Planning Act (RPA) of 1974, the U.S. Forest Service (USFS) and other federal agencies, along with researchers from several universities, generate a national RPA Assessment report every ten years. The report includes the current conditions of the US forest and rangeland, the drivers of changes in these resources, and the projections of these resources for the next 50 years (2011 - 2060). As part of its RPA Assessment the USDA Forest Service Southern Research Station (SRS) developed projections of annual area(s) burned (AAB) over the Southeast from 2011-2060 (Prestemon et al., 2016). The development of these AAB projections was the starting point for the wildfire emissions projections to mid-century done in this research (Shankar et al., 2018).

SRS had previously developed statistical models (Prestemon and Butry, 2005; Mercer and Prestemon, 2005) to estimate AAB by broad cause (lightning- and human-ignited) to mid-century. These models were updated using inputs of monthly-averaged climate variables for temperature, precipitation, and fuel aridity from nine different climate realizations remapped to a column-row grid over the Southeastern U.S. at 12-km x 12-km resolution, with the goal of eventually using the AAB projections in air quality applications (Prestemon et al., 2016). In addition to the climate model inputs, the AAB projection models used socioeconomic inputs of income and population growth rates, and population density, projected over the Southeast from the 2010 county-level data to 2060 and beyond, under the same greenhouse gas (GHG) emission scenarios as were used in the climate realizations. These same GHG emission scenario assumptions were also used to project county-level changes in the forest, cropland, pasture, and urban land use inputs to the AAB projections (Wear, 2013).

Human-caused ignitions are responsible for five times more wildfire AAB in the Southeast than lightning ignitions (Prestemon et al., 2016). Accordingly, annual fire activity was especially concentrated in the Western part of the Southeast, in Oklahoma, Arkansas and Missouri, along the Gulf coast, in Florida, up the Southeast Coast, and in the Appalachian region, where there are both an abundance of fuels, and human populations living near them. Lightning-ignited wildfires are projected to increase by 34%, with little or no response to socioeconomic changes in the Southeast, but human-ignited fires are projected to decrease by 6%, and are highly correlated with socioeconomic factors. The net effect is a 4% increase in AAB from their 2016-20 values to mid-century (2056-60) in the Southeast, with their temporal variability attributable to that of the climate system (Prestemon et al., 2016).

In addition to being used in long-term regional resource planning and land management, AAB projections such as these provide a critical input for estimating wildfire emissions that can be used to drive air quality simulations for long-term wildfire health risk assessments. However, current AAB projection methods lack the ability to allocate AAB to wildfire emissions even on monthly timescales. The need to bridge this gap to estimate wildfire emissions for assessing their future air quality impacts and health burden provides the impetus for this research.

Research Goal

The main goal of this research is to support effective land and air quality management practices in the coming decades in the Southeastern U.S. by developing reliable methods that include projected changes in the climate, socioeconomic and land use drivers of wildfires to estimate their emissions and assess their air quality impacts from the present to mid-century. The choice of the Southeast is not only motivated by changes evident in the climate system, but also by the rapid growth of this region, the expansion of the WUI, and the attendant increased access of populations to fuels as well as their increased risk of exposure to wildfire smoke.

Research Hypotheses

The following research hypotheses are tested in Chapters 2-4 of this dissertation.

Hypothesis 1: Expected changes in the climate and socioeconomic drivers of wildfires in the Southeast will cause wildfire emissions estimated with time-varying wildfire activity projection approaches to deviate significantly by mid-century from those estimated with (static) historical wildfire activity.

Hypothesis 2: AQ predictions with the dynamic wildfire emissions will be within published criteria for acceptable AQ model performance compared to retrospective observations, and will be comparable to those using a standard (empirical) inventory.

Hypothesis 3: Inclusion of climate and socioeconomic factors in the dynamic wildfire emissions estimation methods will result in considerably different ozone and $PM_{2.5}$ spatial distributions and seasonal-average concentrations by mid-century from their 2010 levels.

Objectives

The research hypotheses are tested by modeling wildfire emissions and air quality under scenarios for the Southeast that include projected changes in climate and socioeconomic factors from the present to mid-century, and by comparing those results with estimates of wildfire activity, emissions and air quality using static inventories based on historical or current data, and with observations for applicable periods. These studies address the following objectives:

1. Examine how wildfire emissions over the Southeast evolve relative to their historical levels under potential changes in climate and socioeconomic factors.
2. Evaluate how air quality predictions using the wildfire emissions projection methodology compare with those using benchmark (static) methods, and with observations when applied to a retrospective period.
3. Investigate the impacts of the projected wildfire emissions on air quality trends by mid-century relative to the retrospective period.

These objectives are addressed using an adaptation of the integrated modeling framework (Figure 1.1) of McKenzie et al. (2014). Wildfire emissions estimation methods have been developed leveraging the AAB projections of Prestemon et al. (2016) that take into account, for the first time, the simultaneous impacts of climate and socioeconomic factors on fire activity in the Southeast from 2011 to 2060. In the first study (Chapter 2), wildfire emissions are estimated at a spatial resolution suitable for annual air quality simulations for a contemporary year (2010), and four future years selected from 2040 – 2060 (Shankar et al., 2018). These emissions are

compared with emissions estimated using a static inventory based on 18-year historical mean AAB (1992-2010) that do not consider future changes in climate and socioeconomics. The second study (Chapter 3) evaluates the wildfire emissions projection methods by using their emissions estimates in AQ simulations of the criteria pollutants (ozone and particulate matter less than 2.5 μm in diameter, denoted $PM_{2.5}$) for 2010. The simulation results are compared to those using the (empirical) U. S. National Emissions Inventory (NEI) for 2010 wildfires, and to available network observations for 2010 (Shankar et al., 2019). The third study in this assessment (Chapter 4) examines the response of atmospheric concentrations of $PM_{2.5}$ and ozone to the projected emissions from wildfire and other anthropogenic sources by mid-century.

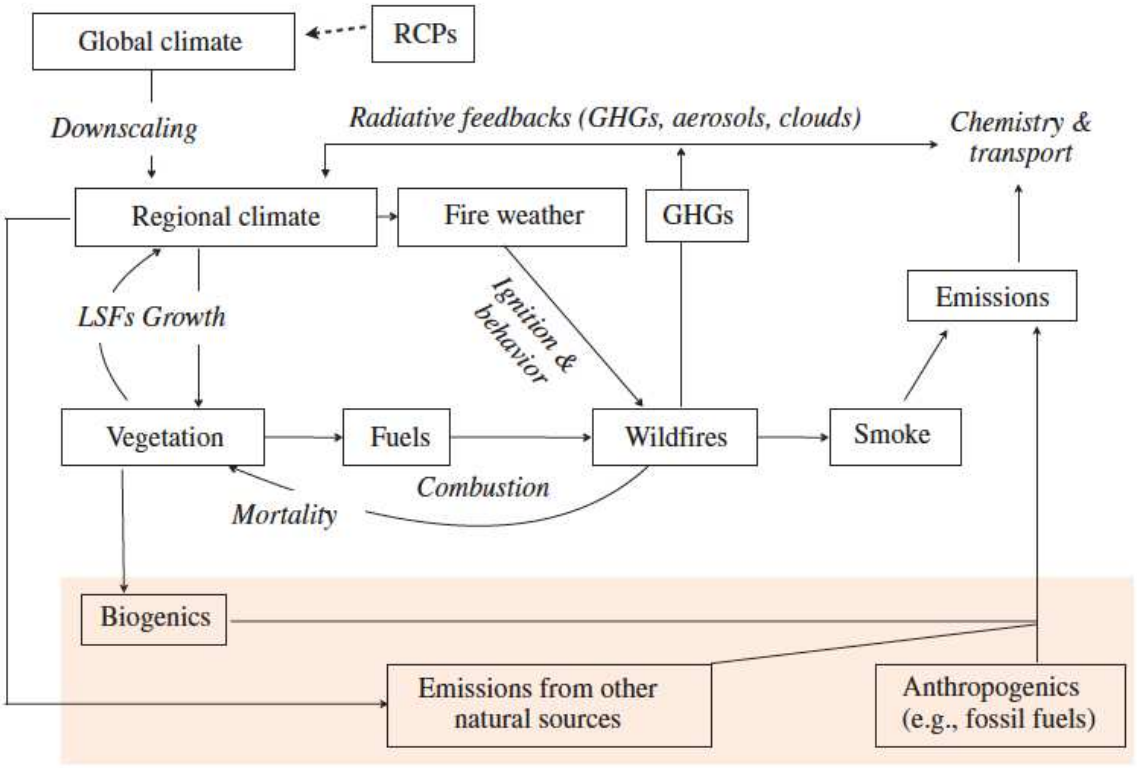

Figure 1.1. From McKenzie et al. (2014) (Fig. 3). Master flowchart for a modeling system to predict the smoke consequences of changing fire regimes in a warming climate. RCPs: Representative Concentration Pathways; GHGs: Greenhouse gases; LSFs: Land-surface feedbacks.

CHAPTER 2: PROJECTING WILDFIRE EMISSIONS OVER THE SOUTHEASTERN UNITED STATES TO MID-CENTURY[1]

Introduction

Wildfires have serious consequences for human health due to the dramatic increase in the concentrations of pollutants of known toxicity emitted in wildfire smoke. There have been several studies (Wegesser et al., 2009; Rappold et al., 2011; Fann et al., 2013) on the adverse health impacts of wildfire-emitted particulate matter (PM) and ozone. Wegesser et al., (2009) found the inherent toxicity of PM from wildfires to be greater than equal doses of PM in ambient air. These researchers have also attributed the toxicity of PM collected from Alaska wildfire sites in their study, in part, to reactive metals as a major source of carbon-centered free radicals, following the findings of Leonard et al., (2000, 2007). Toxic polychlorinated dibenzodioxins and dibenzofurans, and aromatic compounds are also emitted from forest and grassland fires (Gullett et al., 2008). In addition to their adverse health impacts, wildfires can cause extensive damage to human communities and structures and threaten the integrity of some ecosystems that are sensitive to disturbance. For example, in 2016, nearly $2 billion of federal funds were spent suppressing wildfires that totaled more than 2.2 million ha (5.5 million ac) on lands managed by

[1] This chapter previously appeared as an article in the International Journal of Wildland Fire. The original citation is as follows: Shankar, U. Prestemon, J. P., McKenzie, D., Talgo, K., Xiu, A., Omary, M., Baek, B. H., Yang, D., and Vizuete, W.: Projecting wildfire emissions over the south-eastern United States to mid-century, Int. J. Wildland Fire, 27, 313-328, https://doi.org/10.1071/WF17116, 2018.

the USDA Forest Service and the Department of the Interior (National Interagency Fire Center, 2017a). Of these, the overall South-wide costs in 2016 of wildfire suppression of more than 494,000 ha (1.22 million ac) burned were reported at $121 million (National Fire and Aviation Management, 2017). Wildfires in Smoky Mountain National Park, TN, alone caused up to $2 billion in damages by some estimates (National Park Service, 2017) in late November that year. These are not the only costs of wildfires, however. A large part of the economic impact of wildfires is due to the human health impacts of smoke exposure. Fann et al. (2018) estimate the present combined healthcare costs of mortality and morbidity due to exposure to wildfire-attributable PM below 2.5 μm in aerodynamic diameter (termed $PM_{2.5}$) to be $63 billion (2010$) for short-term exposures, and $495 billion for long-term exposures nationwide. Rappold et al. (2011, 2012, 2014) came to similar conclusions in their study of the health costs of a 45-day peat bog fire in 2008 at the Pocosin Lakes National Wildlife Refuge in rural North Carolina, which was ignited by lightning following a long drought. Rappold et al. (2014) put the costs of emergency department visits during the fire due to excess asthma and congestive heart failure at over $1M, but their estimated costs of general health outcomes, predominantly premature mortality, were $48.4 M, far in excess of the medical costs to treat short-term health outcomes.

Climate change has been increasingly implicated in the rise in the frequency and magnitude of large wildfires in the Western US due to the increasing frequency and severity of droughts (Dennison et al., 2014; Stavros et al., 2014; Abatzoglou and Williams, 2016). This increasing trend in total area burned has been observed even while the absolute numbers of wildfires has demonstrated a declining trend since the 1960s (National Interagency Fire Center, 2017b). Climate change is also expected to lead to longer fire seasons in the south-eastern US by mid-century, as shown in the regional climate model analyses of Liu et al., (2013). However,

wildfires in this region are more strongly connected to human factors (Prestemon et al., 2002; Mercer and Prestemon, 2005; Syphard et al., 2017). Humans both ignite more fires in this region (Balch et al., 2017) and actively participate in their suppression (Prestemon et al., 2013). Half of the major wildfires in late 2016 in and around Gatlinburg, TN, were attributed to human causes, punctuating the role of humans on wildfire occurrence in this region. Human factors also play a role in wildfire impacts via the demographics and income levels of the exposed populations (Gaither et al., 2011; Rappold et al., 2011, 2014). Increased urbanization and expansion of the Wildland-Urban Interface (WUI) is only expected to increase in the South in the coming decades, increasing the vulnerability of populations to wildfire smoke exposure. In their study of 37 regions across the continental US, Syphard et al., (2017) find wide geographical variability in both the fire-climate relationship, and the role of human presence in fire regimes; their study suggests a geographically complementary role for the two. Thus, region-specific methods of constructing wildfire emissions inventories that account for changes in both climate and societal factors are a critical need for better estimating how wildfire emissions and their air-quality impacts will change in the Southeast and managing wildfires and their associated health risks long-term.

Current wildfire-emissions inventories (EIs), like those used to provide high-resolution inputs (at 12-km x 12-km grid spacing or finer) required for air-quality simulations, are typically constructed from the most current data of fire activity and fuel loads selected for their completeness, reliability, and accessibility. Empirical data of fire counts for these inventories are provided at the county level in Situation Reports archived and maintained by the USDA Forest Service. They are often augmented by data from satellite remote sensing (RS) of fire pixels detected by the Moderate Resolution Imaging Spectroradiometer (MODIS) instrument, served

through the NOAA Hazard Mapping System (Ruminski et al., 2006) and reconciled with ground-based fire reports in the SMARTFIRE emissions processing system (Larkin et al., 2009). The EPA's National Emissions Inventory (NEI), for example, includes a fire-emissions inventory that is updated yearly for its base-year air-quality assessments and forecasting applications using fire activity from the USDA Forest Service Situation Reports, MODIS fire counts from HMS, and fire perimeters from the Monitoring Trends in Burn Severity project (Eidenshink et al., 2007), all of which are processed in SMARTFIRE (Pouliot et al., 2012; Larkin et al., 2014). On-the-ground data that are reported by state and local agencies can also be included once every three years, during the NEI release.

Wildfire-emissions inventories used in global and regional air-quality modeling characterize the atmospheric loadings due to wildfire emissions of pollutants and their precursors under *current* conditions. Using these inventories in future-year wildfire impact assessments will be wrong from the start (McKenzie et al., 2014) because they do not account for changes in climate, land use, population density, or income levels (which may affect emissions exposures—e.g., Rappold et al., 2012). All of these factors are regional drivers in initiating and sustaining wildfires (Mercer and Prestemon, 2005) as well as in suppressing them (e.g., Butry et al., 2001). Yet, wildfire inventories used in future-year air quality simulations are based very often on historical wildfire records, without accounting for how changes in climate and other factors could affect future wildfire activity. Future air-quality estimates need to address changes in weather patterns in future years to estimate daily area burned, and methods do exist to do so. For example, McKenzie et al. (2006) projected future daily wildfire activity in the Pacific Northwest region of the United States using a stochastic fire ignition model that estimates daily area burned. These estimates are based on fire weather indices calculated from a mesoscale meteorological

model simulation for the future modeling period. The results of McKenzie et al. (2006) showed that this stochastic method estimated area burned in a historical fire season (2003) over the Pacific Northwest to within 8% of actual burned areas. These estimations as such do not include the influences that future changes in population and income could have on wildfire activity. Such changes have been shown (Prestemon et al., 2002, 2016) to be important for the human factors dominating wildfire areas burned in the Southeast. Furthermore, these estimates were applied for a visibility assessment using the CALPUFF dispersion model, and were not designed for use in regional-scale grid-based air quality simulation models.

The statistical models developed by Prestemon et al. (2016) take into account the combined impacts of climate and socioeconomic factors on wildfire occurrence to estimate AAB at the county level. These multi-stage regression models of historical AABs over the Southeast were used to make multi-decadal projections of future AAB for the region, with fine-scale projections of future climate, socioeconomic factors and land use change as inputs. The statistical models were validated in each stage of their construction against out-of-sample historical observations to eliminate bias. These models of AAB thus provide a framework for the construction of wildfire EIs that allow air quality and exposure assessments to be based on an evolving landscape of natural and human factors influencing fire occurrence, and to project future air quality in the coming decades more realistically in response to potential changes in climate and society.

In this work, we leverage the AAB projection models of Prestemon et al. (2016) that incorporate regional changes in climate, population, income, and land use to project daily wildfire emissions in the Southeast, and present the results herein for selected years in 2010-2060. We hypothesize and show that wildfire-emissions inventories for the Southeast, if based on historical AABs, will yield significantly different emission levels for criteria pollutants from

inventories that do account for these changes. Consequently, we suggest that historical AABs cannot be used to represent the impacts of projected changes in climate and society in the region over the next four decades adequately. Given the uncertainties in the climate change estimates, and the importance of human influences on south-eastern US wildfires, both present and future (Prestemon et al., 2016), realistic emissions inventories for the Southeast require an integrated method that accounts for expected changes in both climate and society. Model projections of changes in fire activity and fuel loads due to climate change, coupled with projections of human-caused wildfire, could lead to more effective land and wildfire management in a manner that reduces the adverse air-quality impacts of wildfires in future years (McKenzie et al., 2014; Prestemon et al., 2016). The research presented here proposes and tests such a methodology in the south-eastern US. This work is not intended to be an exhaustive study of climate and socioeconomic drivers of wildfires in the Southeast, but rather the description of a feasible, scientifically sound, and regionally relevant methodology of constructing wildfire emissions projections that include the impacts of those drivers, and how they might change in the future.

The emissions projection methodology developed in this work addresses the stochastic process of wildfires. Although prescribed burning accounts for more ignitions in the Southeast than wildfires, these are, by definition, planned fires that therefore need very different projection methodologies, e.g., incorporating demographic and socioeconomic factors explicitly rather than implicitly through the AABs, as is done here, as well as incorporating different criteria for selecting the burn days. We address these and related issues in the "Conclusions" section.

Methods

This section describes a dynamic approach to constructing inventories of daily future wildfire emissions by leveraging a readily available statistical model that estimates AAB accounting for

changes in climate and society over the five decades from 2010-2060. It describes our application of the statistical AAB estimation model of Prestemon et al., (2016) and of the Fire Scenario Builder (FSB) model (McKenzie et al., 2006), which uses these AABs as constraints to estimate daily areas burned based on wildfire ignition probabilities. The daily burned areas are then used in the BlueSky fire emissions model (Larkin et al., 2009) to estimate daily wildfire emissions that are needed as inputs for future air-quality simulations. Figure 2.1 shows a schematic of these various models and data flows in constructing a wildfire emissions inventory.

Annual area burned estimation

To evaluate the effects of including changes in regional climate and socioeconomics on wildfire activity in the Southeast, our current- and future-year AAB estimates using two different climate downscaling methods are compared against a base case of AABs over the region with no projections of climate or societal influences. A summary of the three AAB estimation methods is provided in Table 2.1. These are (1) a base case of historical mean AABs at the county-level calculated with data from 1992 to 2010; (2) a case with AABs that were estimated with the published statistical model of Prestemon et al. (2016) using statistically downscaled meteorological inputs, and (3) a case with AABs estimated with the statistical model of Prestemon et al. (2016) using dynamically downscaled meteorological inputs. The base case, hereafter called "historical", consists of historical mean AABs from the wildfire burned areas compiled from Situation Reports at the county level for 1992-2011 (Short 2014; 2015), because in this first-time application of the FSB to the south-eastern US, we aimed for as similar an implementation to its north-western applications (McKenzie et al., 2006) as feasible. The historical data also provided the AABs used in a static case, i.e., one that does not include changes in climate and socioeconomic factors, to contrast with the other two AAB estimation

methods. As empirically accounted for in Prestemon et al. (2016), some counties and years of the 1992-2010 historical had potentially invalid observations of wildfire areas burned in the Short (2014) database (K.C. Short, private communication). Gap-filling of these invalid observations of historical data was done by replacing potentially invalid observations in the Short (2014) database with in-sample predictions of AAB generated with the statistical models of Prestemon et al. (2016). Gap-filling accounted for 35.1% of the observations in the region, 1992-2010. The county-level historical mean AABs were remapped using a GIS tool on a column-row grid at 12-km x 12-km grid spacing over the south-eastern US modeling domain (D02) shown in Figure 2.2 for the wildfire inventory development; their sum over this domain is estimated at 450 499 ha (Figure 2.3). The historical case is equivalent to a projection of future wildfires in the Southeast that ignores changes in climate and socioeconomic factors, and the 19-year historical mean of AAB (1992-2010) is used as its representative constant value, as shown in the time slices in Figure 2.3. For reference, the actual-year AAB for 2010 is also shown in the figure.

To compare against the historical case, two AAB projections were made that do account for changes in climate and socioeconomic factors. Both of them projected the statistical models of Prestemon et al. (2016) onto both 2010 and to future climatology. The first case, hereafter called "statistical d-s", used monthly average values of daily maximum temperature, minimum temperature and potential evapotranspiration (PET – Linacre, 1977), and monthly total precipitation as meteorological inputs to the statistical models of Prestemon et al. (2016). In that work, these inputs were taken from historical and projected climate data that were statistically downscaled at 5′ x 5′ resolution (Joyce et al., 2014) using the downscaling relationship of Daly et al. (2002) from each of nine general circulation model (GCM) realizations. The downscaled climate model inputs were remapped using a Lambert Conformal Conic (LCC) map projection

over the south-eastern US, to domain D02 (Figure 2.2) at 12-km x 12-km grid spacing, and aggregated to the required monthly values.

Other key inputs for the statistical model are income and population growth. Projections of these variables were based on three of the greenhouse gas (GHG) emission scenarios (Nakicenovic and Steward, 2000) formulated by the Intergovernmental Panel on Climate Change (IPCC) in support of its Third Assessment Report (AR3), which were used in the nine climate realizations (3 GCMs x 3 GHG emission scenarios) reported in Prestemon et al. (2016). The emissions scenarios A1B, representing high economic growth and low population growth, A2, representing moderate economic growth and high population growth, and B2, representing moderate economic growth and low population growth, provided the basis for the income and population growth rates used by Prestemon et al. (2016) for the Southeast from the 2010 county-level data to 2060. Historical data needed for projecting population growth at the county level were obtained from the US Census Bureau (2012). Historical annual personal income data by county came from the US Bureau of Economic Analysis (2013a) and were converted to real values (in constant 2005 dollars) using the US gross domestic product deflator (US Bureau of Economic Analysis 2013b). Projections of population and income at 5-year increments for each scenario were obtained from the USDA Forest Service (2014), and linearly interpolated for the intervening years. Finally, inputs to the statistical model of changes in land use expected under the future climate scenarios, including those due to changes in the use of forest, cropland, pasture, and urban lands, were estimated at the county level by Wear (2013).

Prestemon et al. (2016) provide justification for using the AR3 scenarios rather than the more currently used Representative Concentration Pathways (RCPs) developed under the IPCC's Fifth Assessment Report (AR5): unlike the RCPs, the AR3 emission scenarios are directly and

mechanistically linked to projections of economic and population growth. These internally consistent socioeconomic projections were also the basis for the county-level projections used by Prestemon et al. (2016) for income and population growth and by Wear (2013) for land uses, which provided the input variables known to be connected to wildfires in the Southeast. Updating those projections to be consistent with the RCPs would have required a complete revamp of these region-specific projection data, and was beyond the scope of their work.

The second AAB projection used dynamical, rather than statistical, downscaling of climate model results to provide the meteorological inputs to the AAB estimator, and is hereafter called "dynamical d-s". Meteorological fields for this projection were simulated by a mesoscale meteorological model, the Advanced Research Weather Research and Forecasting (WRF) model version 3.4.1 (Skamarock et al., 2008), forced by dynamically downscaled climate model inputs at its lateral boundaries. The dynamical d-s projection was motivated by the need to examine the effects of using consistent meteorological inputs throughout the inventory development, beginning with the annual area burned projections, and continuing on to the daily wildfire emissions estimates, as they would also be used later in the hourly air quality impact assessments. Dynamical, rather than statistical, downscaling has been the practice over the past few decades for generating meteorological inputs for air quality models, because it provides a complete and consistent framework of hourly, 3-D meteorological fields needed to process emissions from all the meteorologically-driven sectors (e.g., vegetation, dust, sea spray, fires) and drive the air quality simulations, at the spatiotemporal scales appropriate for tropospheric chemistry and transport of trace pollutants. It is, therefore, important to understand its performance and its limitations to improve the reliability of its projections of wildfire activity and emissions. For comparison with statistical d-s AAB projections, the relevant hourly

meteorological fields (minimum and maximum daily temperature, PET and precipitation) from WRF were aggregated to the temporal resolution (monthly) of the predictor variables in the statistical model. Due to its high computational cost, the dynamical downscaling for this comparative study could be done only in selected years over the south-eastern US (domain D02 in Figure 2.2), whereas the statistical downscaling could be done for every year from 2010-2060.

The GCM realization used for the dynamical downscaling and comparison with the statistical d-s results was selected from the publicly available outputs in the North American Regional Climate Change Assessment Program (NARCCAP – Mearns et al., 2009) archive. Provided in this archive were GCM outputs that had been dynamically downscaled with WRF at 50-km x 50-km horizontal resolution over the conterminous US (CONUS) domain D01 in Figure 2.2. We examined the NARCCAP archive for parent GCM/GHG scenario combinations that matched those used for the statistical downscaling from Joyce et al. (2014), finding only one, the Canadian General Circulation Model version 3 (CGCM3) using the A2 GHG emission scenario, which best fit this criterion. The WRF model results in NARCCAP downscaled from this GCM realization were then used to provide the lateral boundary conditions (LBCs) for a nested WRF simulation at 12-km x 12-km horizontal grid spacing over the Southeast domain. To the extent possible, the same physics options were chosen in WRF 3.4.1 for domain D02 as were used in NARCCAP for domain D01; these options are listed in Table 2.2. There were differences in the shortwave and longwave radiation schemes and the microphysics parameterizations, due to updates to the WRF model options since the time of the NARCCAP simulations. However, our Southeastern WRF simulations were performed using the nest-down feature in WRF, i.e., using archived boundary inputs extracted from the D01 simulation, rather than as part of a two-way

nested multi-domain simulation with D01. The nest-down feature eliminates the possibility of undesired feedbacks from inconsistent schemes between the two domains.

Wildfire emissions for the three cases were estimated for a historical year, 2010, for eventual use in air quality simulations that will be evaluated against ambient observations. Since no downscaled data were available for the 2020-2040 period in NARCCAP, the future fire emissions were projected every five years beginning with an arbitrarily selected future year close to the beginning of the 2040-2060 period– in our case, 2043 – providing inventories for 2043, 2048, 2053 and 2058 (thus the data gap 2010-2043). The random year selection seems reasonable in light of the interannual variability seen in the AAB projections of Prestemon et al. (2016), which nevertheless showed a small but significant increase in projected median AAB over the region, 2056-2060, relative to 2016-2020.

To ensure a robust comparison between the statistical and dynamical d-s methodologies, the AAB projections for statistical d-s were then redone in this work using only the downscaled inputs from the CGCM31/A2 climate model realization. The AABs presented here for the statistical d-s therefore differ somewhat from those published in Prestemon et al. (2016), who reported projected median and uncertainty bands of AABs calculated using all nine climate realizations, even though the underlying statistical models remain the same.

Fire Scenario Builder

The Fire Scenario Builder model (McKenzie et al., 2006) is a stochastic model that estimates daily areas burned at the spatial scales associated with regional climate and air-quality models. The FSB was designed specifically to provide coarse-scale fire areas (as opposed to individual fire perimeters) as inputs to current and future projections of daily fire emissions and smoke dispersion. A detailed schematic of the FSB model is provided in supplemental Figure 2.S1. Two

key assumptions of the FSB are (a) that a fire event in a grid cell will only occur once in a fire season (assuming that fuels cannot return to the landscape within the season), and (b) that a fire season is entirely contained within the calendar year. Using mean AAB associated with some baseline climatology, which is usually historical but not necessarily, the FSB samples a fire-start day randomly from the fire season based on an assigned probability distribution of fire likelihood. This is typically uniform unless informed by particular fire-start data. Here, we use our three estimates of mean AAB – historical, statistical d-s, and dynamical d-s – as baselines for the historical case and the two projections. Although changes in socioeconomic variables are not explicitly input to the FSB, it implicitly includes the response of wildfires to changes in socioeconomic factors via the AAB projections. For each model grid cell, the FSB constructs a cumulative distribution of area burned with the AAB for that grid cell as the mean, using a mixed model that is a negative exponential up to the 95th percentile and a truncated Pareto distribution beyond that value. The beginning and end dates of the fire season appropriate for the Bailey ecoregion province (Bailey, 1995) allocated to each model grid cell are read from a national database maintained by the USDA Forest Service. Fires are further constrained to burn only if precipitation is less than 5 mm/day. If it is above that, another fire-start day is sampled.

A fire-weather metric from the historical climatology that can be simulated for the future is chosen as an indicator of potential fire size. The fire-weather metric used in this study is the fire weather index (FWI – Van Wagner and Pickett, 1985) from the Canadian Forest Fire Danger Rating System (CFFDRS), and the calculation of this metric is accomplished through its Canadian Forest Fire Weather Index system shown schematically in supplemental Figure 2.S2. FWI is a comprehensive metric that incorporates several measures of heat and dryness, and is used in fire-danger projections in forests within and outside Canada (Liu et al., 2010; Stavros et

al., 2014). It is computed from the dynamically downscaled daily meteorology for all selected years. We note that the use of this metric necessitated the use of dynamically downscaled meteorological data in all daily fire emissions estimates, even in the case where the AABs were estimated with statistically downscaled meteorological inputs, because the temporal aggregation (monthly) at which the statistical d-s inputs were available was too coarse to calculate daily FWI. Area burned on the randomly selected fire-start day for each case is calculated as the quantile from the cumulative distribution of AAB that corresponds to the quantile of the FWI from the climatology for that case matching that day's FWI. Fires as treated by the FSB can burn up to 4047 ha (10 000 acres) per day; larger fires are modeled as multiday fires.

At first glance, the use of our 12-km x 12-km spatial resolution may seem too coarse for the FSB, but our selection of this resolution can be understood as follows. The FSB is really simulating annual fire activity as a surrogate for real fire simulation. Actual fires do not burn contiguously for 144 km^2 except in extreme events, but the coarse scale (relative to that of typical fires) of the FSB application for air quality modeling requires a stochastic representation of AAB, the relevant fire metric. Therefore, the area burned in a single year ("fire") is simulated by the FSB, constrained probabilistically by the historical mean (or a future-year annual mean). Lumping all possible "fires" in a year into a single "event" would cause drastic information loss at the scale of fire-spread models, but at our coarser scale it is the only tractable way to represent AAB, and actually limits the error propagation that would ensue from attempts to partition burned area into individual "fires" (somewhere within a 12-km x 12-km grid cell).

BlueSky fire emissions model

Using the results from the FSB, daily fire emissions were estimated using the BlueSky smoke emissions modeling framework (Larkin et al., 2009) for each of the cases discussed (historical,

statistical d-s, and dynamical d-s). The BlueSky model accomplishes this by using the gridded daily burned areas in conjunction with fuel load data available in the Fuel Characteristic Classification System (FCCS) database (McKenzie et al., 2007) to estimate daily fire emission rates. BlueSky is a highly modular framework that links state-of-the-science models of meteorology, fuels consumption, and emissions, and provides flexibility in the data sources for fire activity and fuel load inputs. Fuels consumption in BlueSky is based on the CONSUME model version 3.0 (Ottmar et al., 2006), the default modeling option, which is an empirical model developed by the USDA Forest Service based on 106 different pre- and post-burn plots covering several vegetation types and fire conditions. Emissions are estimated as daily rates by a fire emissions module for CO, CO_2, CH_4 and $PM_{2.5}$. In our application, BlueSky is used at the latitude-longitude location of each fire strictly for estimating total emission magnitudes of the various emitted species. The fire emissions estimated in BlueSky for the "fire" modeled by the FSB are processed in the SMOKE emissions processing system similarly to other point sources, which are vertically distributed in the air-quality model simulation in a later step (not presented here), using the plume-rise algorithm within that model.

Results

This section presents the comparisons of the historical mean AABs from a retrospective period against those estimated using the climate downscaling approaches described previously, examining both time slices of AABs aggregated over the south-eastern modeling domain, and their spatial distributions in each modeled year. Similar analyses are then presented of the wildfire emissions of $PM_{2.5}$ estimated using each set of these AABs.

Comparisons of AAB estimation methods

The purpose of these analyses is to examine the sensitivity of the statistical model estimates of AABs to the downscaling method used to provide their meteorological inputs, since the AABs are used as constraints on the daily burned area estimates needed to calculate wildfire emissions. AABs from the historical mean over a 19-year period, 1992-2010 (inclusive), provide a benchmark to compare against the modeled estimates of AABs using the downscaled climate inputs. These historical mean AABs summed over the domain D02 add up to 450 499 ha, shown as a constant value in Figure 2.3 for all years modeled. The spatial pattern of the historical mean AABs is shown in Figure 2.4. Prestemon et al. (2016) found that human-caused ignitions, whether accidental or intentional, dominate over lightning-caused ignitions in the peak locations shown in Figure 2.4. These occur in the Western part of the domain, in Oklahoma, Arkansas and Missouri, along the Gulf coast, in Florida, up the Southeast Coast, and in the Appalachian region. These are regions where there are both an abundance of fuels and ample human populations with access to those fuels.

The domain-total AAB estimate in 2048 is much lower than in the other modeled years for the case of statistically downscaled meteorology (Figure 2.3). This low estimate can be explained through the interannual variability of the AAB from 2010-2060 shown in supplemental Figure 2.S3. As previously noted, the years for our study were selected at an arbitrary interval of five years beginning at a randomly chosen 2043. In a random year such as 2048, there can be as much as ±50 000 ha difference from the domain-total mean AAB value. The statistical d-s AAB estimates summed over the D02 domain are distributed around, and fall within ±7% of the historical mean AABs, but there are larger negative deviations from the historical mean in 2048 (-20%), and 2058 (-13%). Given the excellent agreement seen in Figure 2.3 for this case with the

actual AAB value for 2010, the deviation of its AABs projections from the historical mean is a clear consequence of the influences of climate and socioeconomic factors, each with its own variability.

The spatial differences in AAB for the statistical d-s case from the historical case (Figure 2.5, left panels) show that in 2010, the positive and negative differences are smaller than those in other years, and largely offset each other. In 2043, there are large negative differences (i.e., historical AABs are much greater than the statistical d-s estimates) in the ecoregion provinces to the north in northern Missouri, offset by a large positive difference in ecoprovinces in Florida and along the Gulf coast. In 2048, the positive differences in these coastal ecoprovinces are not large enough to offset the negative differences in the interior of the domain, and the domain-wide difference is a net negative, consistent with the time-slice plot in Figure 2.3. In 2053, the small net positive difference is due to the positive AAB differences in these coastal ecoregion provinces and much of Texas, outweighing the negative differences in the interior of the domain. Finally, in 2058, the spatial pattern once again shows negative differences dominating over larger areas of the domain, and to a greater extent than in 2010, with little or no contribution from Texas. The net result overall is a negative difference, i.e., lower AAB values in the statistical d-s case than in the historical.

AAB estimates for the dynamical d-s case are significantly lower than in the other two cases in each of the five modeled years (Figure 2.3). The temporal variability in AAB is also quite different between the two downscaling methods, with the closest agreement in 2048 (a difference of 10 814 ha), and the greatest differences in 2053 and 2010 (182 591 ha and 148 249 ha, respectively). Spatial differences in AAB for the dynamical d-s case relative to the historical case (Figure 2.5, right panels) show less temporal variability than for the statistical d-s case (Figure

2.5, left panels). The greatest negative differences are seen to occur along the Gulf coast and Eastern seaboard, while the portion of the domain west and northwest of Missouri is the main contributor to positive differences. These positive differences offset the negative differences across the domain significantly in 2048, consistent with the smallest domain-wide difference in all the years shown in Figure 2.3 between the historical and dynamical d-s AAB estimates. Similar spatial offsets of positive and negative differences occur to a lesser degree in 2043 and 2053, although the net result domain-wide in each of these years is still a negative difference (i.e., the historical AABs are greater than dynamical d-s estimates). Unlike the case of the statistical d-s, the Appalachian region in the right panels has a persistent large negative difference, as do parts of the Gulf coast; these are also areas where the historical mean AABs had the largest values (see Figure 2.4). As both the downscaling methods used the same parent climate model realization, these differences in the spatial patterns in Figure 2.5 are a result of the differences in the downscaling methods themselves.

The right panels of Figure 2.5 indicate that dynamical downscaling leads to much less wildfire activity in the Southeast, relative to the 19-year historical mean, while statistical downscaling preserves more of the large-scale circulation patterns in the region in the future decade and shows smaller differences from the historical fire activity. Liu et al. (2013) also found such spatial differences in their analyses of future wildfire activity in the dynamically downscaled results with the HRM3 regional climate model (RCM) compared to the HadCM3 climate model used in their previous analysis (Liu et al., 2010). Their study over North American regions used the Keetch-Byram Drought Index (KBDI – Keetch and Byram, 1968) as the indicator of fire potential and compared the results of the KBDI calculation from RCM results for the different GCM/RCM downscaling combinations in NARCCAP. While the climate system

showed a warming overall in the 2041-2070 period over North America relative to the 1971-2000 period, there were pronounced differences in the locations of peak precipitation and temperature between the HRM3 and the HadGCM. It is worth noting that their 2013 results are at a coarser resolution (50-km x 50-km) for the various regions, and used a different GCM/RCM combination to calculate future climate change from the one used in our study (CGCM3/WRFG) over the Southeast. The HRM3 model that they used for their Southeast assessments had the smallest KBDI increase of all the RCMs in NARCCAP in the future decades in the Central Plains and Deep South, the region of our study. By comparison, the WRFG, used to provide boundary inputs for our Southeast WRF simulation, showed more mixed results, with a moderate KBDI increase from warming and drying in the Deep South, but a KBDI decrease in the Central Plains due to increased precipitation in the future. However, our WRF model results for the Southeast are from a nest-down simulation at a 12-km x 12-km spatial resolution from the dynamically downscaled WRFG model results in NARCCAP. Any biases, particularly in precipitation, relative to the GCM will be propagated in the boundary inputs extracted from those results and input to our Southeast WRF simulations. Another major difference in our method from the Liu et al., (2013) study is that their study did not consider county-level socioeconomic factors, and used a different indicator of wildfire, the KBDI, from our fire weather metric (FWI) and would be expected to produce different results. We explain this further under "Discussion".

$PM_{2.5}$ predictions from wildfires

The AABs estimated from the three cases described previously were used to develop wildfire emission inventories suitable for air quality model simulations needed in impact assessments of ambient $PM_{2.5}$. Figure 2.6 shows the variability of $PM_{2.5}$ emissions from wildfires among the selected years. For this figure, the emission rate of total $PM_{2.5}$ calculated for each point fire by

the BlueSky fire emission model was mapped to the south-eastern US domain (D02) modeling grid using the Sparse Matrix Operator Kernel Emissions (SMOKE) processor (Houyoux et al., 2000, Baek and Seppanen, 2018), and the gridded daily emissions were vertically integrated and summed over the year in each grid column for each year modeled. Consistent with the AAB estimates from the three cases shown in Figure 2.3, the $PM_{2.5}$ emissions estimates are highest for the historical case, followed by the cases using AABs estimated with statistically and dynamically downscaled meteorology. The historical and statistical d-s total $PM_{2.5}$ emission trends follow each other closely in 2010 and 2043, while the dynamical d-s trends are 50% and 20% lower in these years, and even lower in the later years, except for the maximum in 2048 leading to good agreement with a correspondingly low value mentioned previously in the statistical d-s case. The dynamical d-s estimates of $PM_{2.5}$ emissions are also the closest of all three cases to the NEI 2010 emission levels from point wildfires, which are shown here for reference. There is slightly less variability in the time slices of wildfire $PM_{2.5}$ emissions using the historical mean AABs than in the case using statistically downscaled meteorology. As the AAB estimates used to constrain the daily burned areas are constant for the historical case, this emissions variability can be attributed to the mesoscale model calculation of the daily FWI. The tendency of the WRF meteorology is to lower the daily wildfire activity, and therefore the emissions, and this is once again evident in these emissions estimates for the historical case, albeit to a far lesser degree than in the dynamical d-s case.

Figure 2.7 compares the spatial distributions of $PM_{2.5}$ emissions using the historical AABs (left panels) against those estimated using dynamical d-s (right panels). For simplicity, the statistical d-s results are not included here, but the comparison of the domain-wide historical vs. statistical d-s estimates of wildfire $PM_{2.5}$ emissions is available as supplemental Figure 2.S4. The

$PM_{2.5}$ emissions for the historical (and statistical) case show greater spatial variability within a given year than for the dynamical d-s case and higher values in the interior Southeast due to the underlying higher wildfire activity in this case. Significant differences in the spatial distributions of emissions can be seen between the two cases in any year along the Southeast coastal areas, the Appalachian region, eastern Texas and Oklahoma, and Arkansas and Missouri. Of these, the states to the west (the southern part of 'Central Plains' in Liu et al., 2013, 2014) were part of the region where the NARCCAP model combination of CGCM3/WRFG tended to predict more seasonal precipitation in the future years (2041-2070), in both summer and winter, compared to the historical period (1970-2000). The remaining regions, which roughly map to the 'Deep South' of Liu et al., (2013, 2014), saw a decrease in precipitation in the summer in the future years, but this decrease was among the lowest for all the model combinations in the NARCCAP suite. These spatial differences in wildfire $PM_{2.5}$ emissions distributions between the statistical and the dynamical d-s cases therefore suggest that precipitation increases have an overriding influence on emissions compared to the temperature increases seen in future years.

The spatial distributions of $PM_{2.5}$ emissions in Figure 2.7 in each of the future years are generally consistent with the trends of annual total AABs shown in Figure 2.3. The much lower AABs in 2048 for the dynamical d-s case translate into smaller, albeit more numerous, wildfires with lower annual total $PM_{2.5}$ emissions in Figure 2.7. The biggest spatial differences in 2048 relative to the historical case are seen to occur in Appalachia, North and Central Florida, in eastern Texas and Oklahoma, and around the Arkansas-Missouri state boundary.

Figure 2.8 shows the total seasonal $PM_{2.5}$ emission estimates for spring, summer and fall in each selected year using the historical mean AABs, and those estimated with dynamically downscaled meteorology. Differences in each season between the historical and dynamical d-s

cases show the impact of the AAB constraints imposed on the $PM_{2.5}$ emission rates. Furthermore, the impact of the dynamically downscaled meteorology is seen in the seasonal variability of these emissions. Both the historical AABs and those from the dynamical d-s yield the lowest emissions of $PM_{2.5}$ in the spring and the highest in the summer, while the NEI estimates for 2010 had the lowest emissions in the summer and higher $PM_{2.5}$ emissions in both spring and fall. These seasonal plots indicate that the common feature among the historical and dynamical d-s cases, which is the WRF meteorology used to calculate daily FWI, dictates the seasonal variability in wildfire activity in any given year, as well as the variability among the modeled years in each season. In all years, there is also a consistently more pronounced summer high in $PM_{2.5}$ emissions in the historical than in the dynamical d-s case due to its (constant) higher AAB values. The variability of $PM_{2.5}$ emissions among the modeled years also somewhat reflects the AAB difference patterns shown in Figure 2.5.

Discussion

Prestemon et al., (2016) showed that the statistical d-s estimates of AAB reflected the counteracting influences of the climate and socioeconomic variables driving wildfire activity in the Southeast. According to those analyses, the 2056-2060 average annual wildfire areas burned in the Southeast due to human causes would decrease by 6% over the 2016-2020 average in response to changes in socioeconomic influences, but a comparison of the averages over the same periods would show a 34% increase due to lightning-ignited fires, which were minimally influenced by socioeconomic factors. As a majority of areas burned in the Southern US are from human causes, the conclusion in that work was that the projected average AAB for 2056-2060 would be higher by about 4% relative to that for 2016-2020 from all causes, with its temporal variability attributable mainly to that of the climate system (see supplemental Figure 2.S3). This

variability can also be seen in this work, in the frequency distributions of Figure 2.9 of domain-wide totals around the annual mean of the gridded AABs in each year for each of the estimation methods. Due to the wide range of the data, values of AAB below 10 ha are not shown so that the trends around the median values can be seen more clearly. The historical mean AABs used to represent 2010 have a higher median value than either of the other two estimation methods, consistent with the time slices shown in Figure 2.3. The statistical d-s AAB distributions have higher maxima than the dynamical d-s distributions in every year, even though their median values are slightly lower than for the dynamical d-s in 2048 and 2058. The higher statistical d-s AABs are also consistent with the domain-total AAB time slices for these two cases (Figure 2.3). The effects of competing climate and socioeconomic factors in the AABs for the statistical d-s are also clear in Figure 2.3: any biases due to the dynamically downscaled meteorological inputs are not applicable in these AABs. Those biases would therefore also have a smaller impact on the $PM_{2.5}$ emissions in this case (Figure 2.6) than in the dynamical d-s case.

The WRF model used in the dynamical downscaling yields very different spatial patterns of AAB from the statistical d-s AAB estimates. The differences between the AABs estimated from statistical and dynamical d-s are a consequence of differences between the downscaling methods themselves, as they are both using the same climate model (CGCM3.1), as well as GHG, population, and income growth assumptions, corresponding to IPCC AR3 scenario A2.

The role of the GCM/GHG scenario in the differences seen in the AAB estimates with climate downscaling can be better understood through an examination of their mean changes in temperature and precipitation. Figure 2.10 shows the expected changes in precipitation and temperature from 2000 to 2060 from the GCM/emission scenario combinations for the conterminous US, and for the Southeast. In this figure, the CGCM3.1 scenario A2 shows an

increase in precipitation from 2000 to 2060 in both the US and the Southeast, of ~ 4% and ~ 6% respectively, over the ensemble mean for scenario A2. Although this GCM simulation shows a higher-than-mean increase in temperature US-wide, it also shows a slightly smaller-than-mean increase in temperature in the Southeast from 2000 to 2060, compared to the "SE A1B&A2" value. These changes are small for the five-decade period. The change in precipitation is in the correct direction toward explaining the changes seen in the dynamical d-s estimates relative to the historical case, as well as the statistical case, but would likely not be the sole cause of the dramatically lower AAB values for the dynamical d-s case compared to the other two cases.

A more likely explanation of these lower AAB values is two-fold. One possible reason is the difference between the mesoscale and synoptic-scale predictions, as shown in the regional analyses of wildfire regimes by Liu et al., (2013, 2014). In their work, the dynamical downscaling of climate showed increases in summertime precipitation in the future decades (2041-2070) for the Southeast region (moderate), and South Central region (small) compared to the historical period (1971 -2000). This was different from the predictions of the GCM used in their previous studies (Liu et al. 2010). The second likely explanation is the known high bias in precipitation in WRF (Alapaty et al., 2012; Spero et al., 2014), which would also tend to lower the AAB estimates. Dynamical d-s is also used in the D01 domain to produce the lateral boundary conditions for the Southeast domain, and thus inherits biases in the NARCCAP downscaling with WRF; thus, the influence of the high bias in precipitation in WRF could become magnified, producing consistently lower AABs. This may also account for the differences in our results from those of Liu et al., (2013) for the Southeast, which showed increases in the fire potential indicator (KBDI) by at least one level, and an increase in the length of the fire season in nearly all months. Of note, the Liu et al., (2013) analyses used a single level

of dynamical downscaling from the GCM, i.e., only for domain D01, a coarser resolution (50-km x 50-km), a different fire potential index, the KBDI, from that of our work (FWI), and did not include county-level socioeconomic changes.

The historical case, which uses historical mean AABs to constrain daily area burned, estimates higher total $PM_{2.5}$ emissions than the dynamical d-s case for every year and season except in the fall of 2043. These higher values could be partly because of the much higher AABs in some years in the 19-year fire history (e.g., in 2000 and 2006) than in the future projections, as indicated by the lower actual-year AAB for 2010 compared to the 19-year historical mean shown in Figure 2.3. Equally important, the historical mean AABs do not include the socioeconomic changes projected in the dynamical d-s case, which were shown to offset the influences of climate warming on the AAB projections in the Southeast (Prestemon et al., 2016). The projected variability in climate and socioeconomic factors from the CGCM3 scenario A2 climate simulation influences the dynamical d-s AAB projections but has no role in the historical AABs. The effects of a wet bias in WRF on the AABs would also be compounded in the $PM_{2.5}$ emissions by those on the daily FWI inputs to the FSB, leading to lower annual totals and peak values in spatial distributions of $PM_{2.5}$ emissions in the dynamical d-s than in the historical case.

The fall wildfire emission levels are lower than summer levels in all years and cases modeled. The possible WRF v3.4.1 overprediction of precipitation and underprediction of temperature appear to have the greatest impact in the fall season fire activity, translating into lower wildfire $PM_{2.5}$ emissions. Overall, we would expect $PM_{2.5}$ trends to follow those of the AABs, although the relationship is clearly nonlinear, due to the stochastic nature of the daily disaggregation of the AABs in the FSB as well as the spatiotemporal variability in the

downscaled predictions of fire weather. It is clear that the latter will, at a minimum, introduce variability that cannot be inferred from the historical data.

Conclusions and Future Work

Wildfire area burned, and the resulting emissions of $PM_{2.5}$ in the Southeast for the period 2010-2060 are seen to be a result of two competing drivers, climate and socioeconomics, each with its own spatiotemporal variability. This may not always lead to uniform increases in wildfire activity and emissions in future climate regimes. The historical mean AABs are higher than those estimated from statistically downscaled meteorology in most of the years modeled, and higher in all years than those estimated with dynamically downscaled meteorology. Historically based estimates of wildfire emissions in the Southeast are consistently higher (by 13% - 62%) for $PM_{2.5}$ than those estimated by either of the projection methodologies. The large differences in the temporal variability and spatial patterns of $PM_{2.5}$ emissions in future years compared to their historical values are attributable in part to the temporal variability of the future climate and socioeconomics underlying the annual area burned projections, and to the dynamically downscaled meteorology used to estimate future daily fire activity. The wildfire emissions estimated from a historical mean of areas burned, even for the most recent 19-year period, do not appear to be representative of how the climate and socioeconomic variables driving wildfire activity and emissions could change in future decades. Our results therefore suggest that the use of historical AABs is not sufficient to construct wildfire emission inventories for simulating future-year air quality by mid-century, be they for climate change impact assessments, or for projecting population health risks from wildfire smoke.

This work also shows significant variability among the modeled years in the AABs and the corresponding wildfire $PM_{2.5}$ emissions as a result of the natural variability of the climate system.

Better inferences of temporal trends can be obtained in the dynamical downscaling by ensemble simulations that bracket the extremes in climate and societal change over the 2010-2060 period using representative high- and low-fire frequency years from among a number of GCM/GHG emission scenarios.

Another finding of this work is that the high bias in precipitation in the WRF model could be the reason for significantly lower wildfire emissions estimates from dynamical downscaling than from statistical downscaling of climate in the AAB estimation model inputs. The impact of the dynamical downscaling of climate on wildfire emissions is important, because this is the most consistent method in current use to calculate meteorological inputs for estimating daily wildfire activity and wildfire emissions, and for driving the air-quality simulations. Thus, we need to understand and correct biases in the dynamical downscaling, particularly as regards precipitation in the Southeast, because of its strong influence on fire weather, and soil and fuel conditions. Less biased downscaling would provide more reliable support of natural resource management and wildfire health risk assessments.

Future contributions from ongoing work will examine the current (2010) and future-year air quality impacts based on these emissions estimates. Furthermore, fuel loads are expected to respond both to climate and to evolving fire suppression activities in the Southeast. Excessive fuel buildup, for example, has been cited as the cause of the large wildfires in the past two fire seasons in the south-eastern and western US. Fuel load changes were not explicitly included in the modeled wildfire emission estimates, although the land use changes included in the AAB projections do indirectly account for them in the aggregate. Decisions on where and what to burn in managed fires may benefit from tools that incorporate fuel load changes in these dynamic estimates of wildfire emissions.

Acknowledgments

The authors[2] thank Dr. Natasha Stavros for her guidance on the use of the Fire Scenario Builder, Dr. Linda Joyce for her guidance on the use of the statistically downscaled climate data, and Dr. Jared Bowden and Dr. Shannon Koplitz for their insightful editorial comments on the manuscript. Dr. Michelle Snyder's assistance with the R package used in the plots is also gratefully acknowledged. We also thank the North American Regional Climate Change Assessment Program (NARCCAP) for providing the data used in this paper. NARCCAP is funded by the US National Science Foundation, the US Department of Energy, the US National Oceanic and Atmospheric Administration, and the US Environmental Protection Agency Office of Research and Development. This research was supported entirely through funding provided by USDA Forest Service to the University of North Carolina at Chapel Hill under joint venture agreement 11-JV-11330143-080.

Conflicts of Interest

The authors declare that they have no conflicts of interest.

---

[2] Author Contributions: US, DM, and JPP designed the research. US directed and quality-assured the development of custom software used in remapping the statistically and dynamically downscaled climate data to the Southeastern column-row modeling grid. AX and KT prepared all meteorological data used in the AAB estimates, and daily FWI calculations. For all emissions estimation methods described, KT and US estimated the daily area burned for input to the BlueSky smoke emissions model. BHB and MO prepared the wildfire emissions and processed them in CMAQ-model ready form, and US quality-assured these wildfire emissions data. US prepared all drafts of the manuscript and US, DM, JPP, and WV edited the manuscript.

Table 2.1. Annual area burned data used in the wildfire inventories for the south-eastern US

Note: "Statistical model" refers to the statistical AAB projection model of Prestemon et al. (2016). The modeling domains D01 and D02 are shown in Figure 2.2. CGCM3, CGCM31, Canadian General Circulation Model, ver. 3, ver. 3.1; WRF, Weather Research and Forecasting model

Case Name	Annual Area Burned	Climate Scenario	Time Dependence	Spatial Resolution of Meteorology
Historical	County-level historical mean of 1992-2010 Situation Report data remapped to domain D02	None	Static	N/A
Statistical d-s	Estimated from statistical model with statistically downscaled climate, county-level projections of socioeceonomics for domain D02	CGCM3, scenario A2	Varies yearly	5′ x 5′ (lat-long) from climate model, remapped to domain D02 at 12-km x 12-km
Dynamical d-s	Estimated from statistical model with dynamically downscaled climate, county-level projections of socioeceonomics for domain D02	CGCM3, scenario A2, dynamically downscaled with WRFG over domain D01	Varies yearly	Dynamically downscaled over domain D02 at 12-km x 12-km from domain D01 WRFG output at 50-km x 50-km

Table 2.2. WRF model physics options for the D01 and D02 modeling domains

Domain	Long-wave radiation	Short-wave radiation	Micro-physics	Cumulus Scheme	Boundary layer scheme	Land Surface Model
D01 (CONUS)	CAM3[3]	CAM3	Prognostic cloud liquid and ice, rain, snow[4]	Grell 3D ensemble[5]	Yonsei University explicit entrain-ment scheme[6]	Noah[7]
D02 (Southeast)	RRTMG[8]	RRTMG	WRF Single-Moment 6-Class (WSM6) microphysics w/ graupel[9]	Grell 3D ensemble	Yonsei University explicit entrain-ment scheme	Noah

[3] Collins et al., 2004

[4] Hong et al., 2004

[5] Grell, 1993; Grell and Devenyi, 2002

[6] Hong et al., 2006

[7] Niu et al., 2011; Yang et al., 2011

[8] Iacono et al., 2008

[9] Hong and Lim, 2006

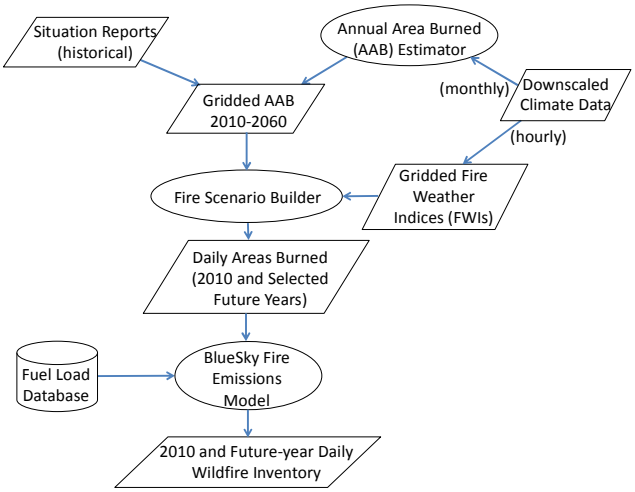

Figure 2.1. Flow diagram of various models and data needed for estimating benchmark (2010) and future wildfire emissions. AAB, annual area burned; FWIs, fire weather indices.

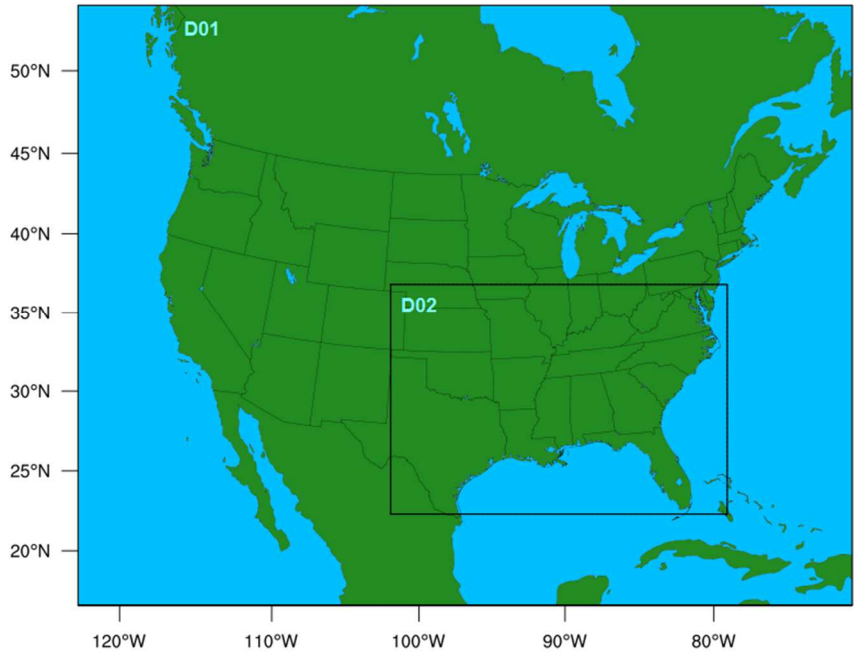

Figure 2.2. Modeling domains: D01 at 50-km x 50-km grid spacing; D02 at 12-km x 12-km grid spacing.

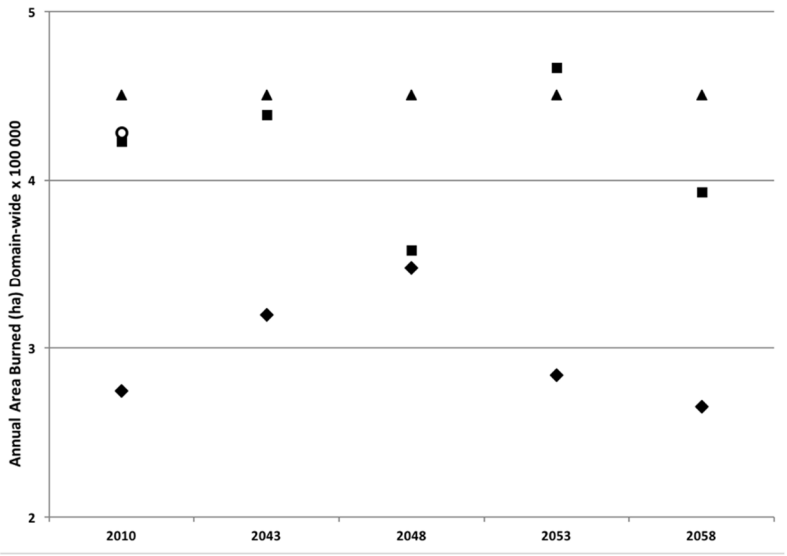

Figure 2.3. Time slices of total annual area burned (AAB) domain-wide (10^5 ha) in domain D02 of Figure 2.2: historical (triangles) – historical mean value for 1992-2010 replicated in all years; statistical d-s (squares) – estimated using statistically downscaled meteorology from the Canadian General Circulation Model, ver. 3.1 (CGCM3.1) and A2 scenario realization; dynamical d-s (diamonds) – estimated with dynamically downscaled meteorology from the Canadian General Circulation Model, ver. 3 (CGCM3) and A2 scenario realization; open circle – historical 2010-only data.

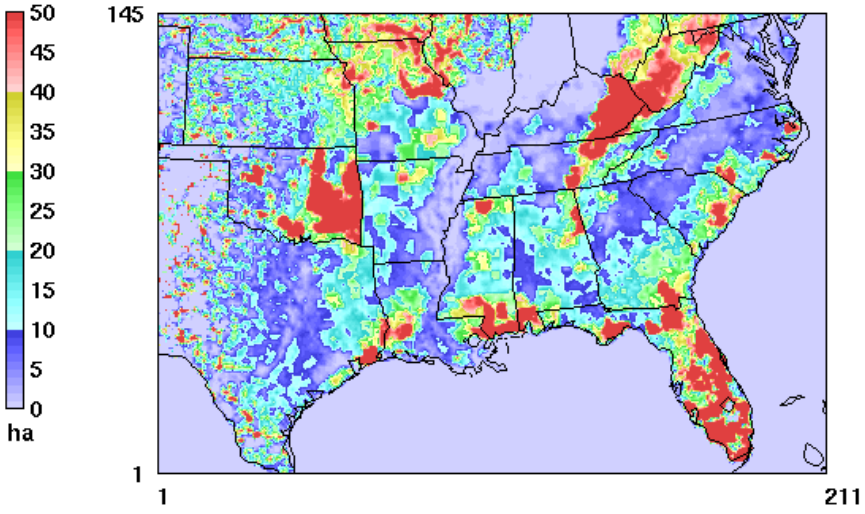

Figure 2.4. Spatial distribution of historical mean AAB (ha) for 1992-2010.

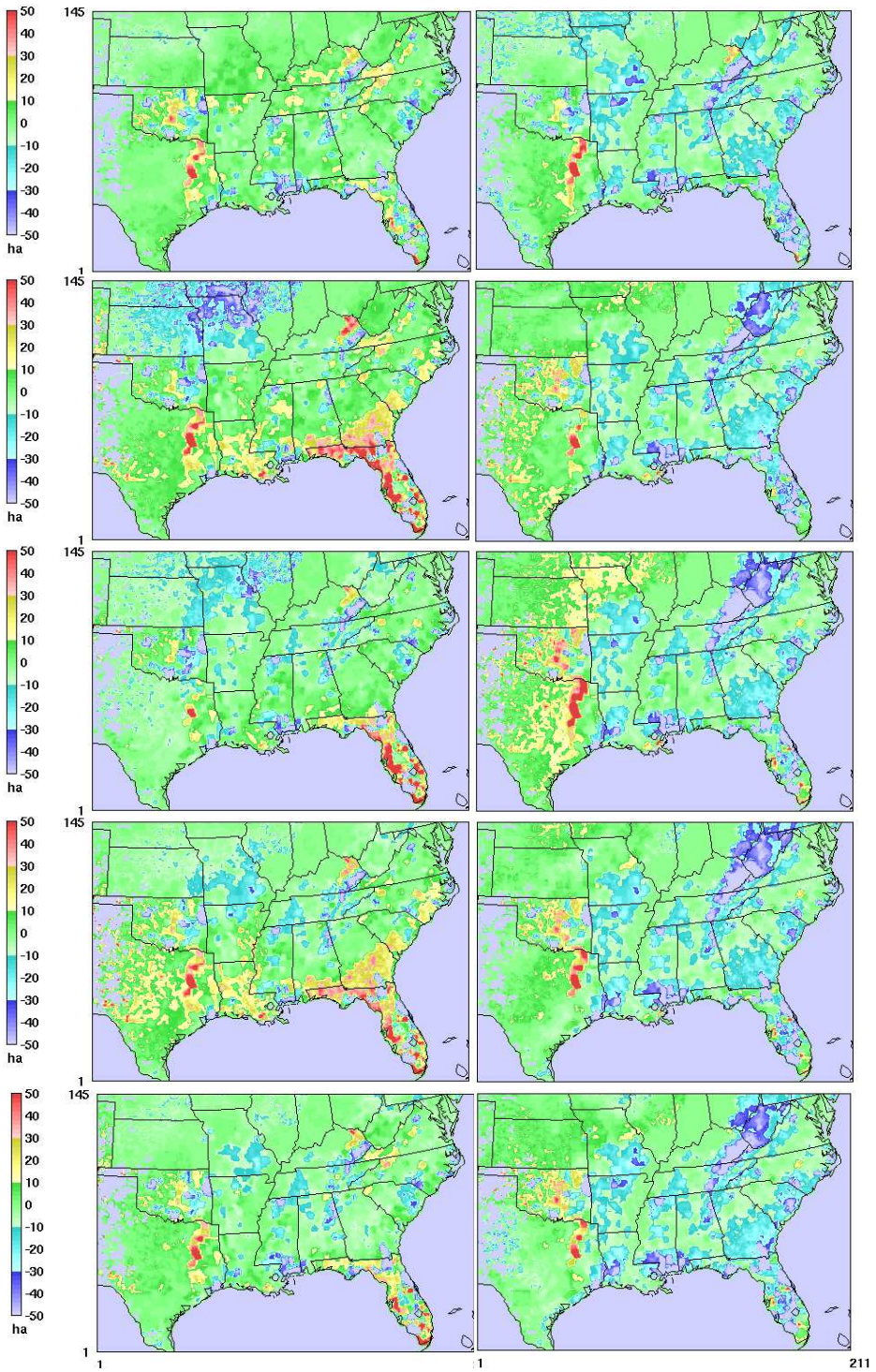

Figure 2.5. Annual area burned (AAB) differences (ha) in future years above the historical mean of Figure 2.4 for (L) statistical d-s (i.e., statistical d-s - historical) and (R) dynamical d-s (i.e., dynamical d-s - historical): Row 1, 2010; Row 2, 2043; Row 3, 2048; Row 4, 2053; Row 5, 2058.

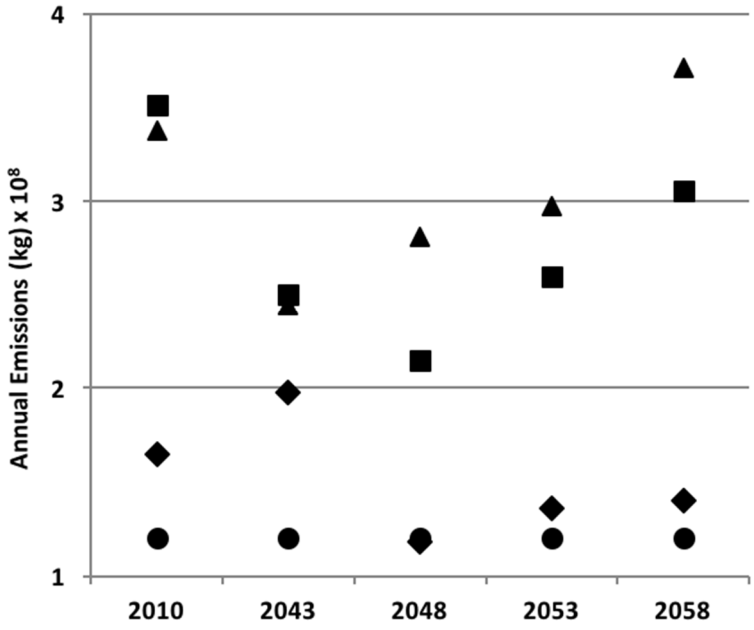

Figure 2.6. Time slices of annual domain-wide total wildfire $PM_{2.5}$ emissions (10^8 kg) for domain D02 of Figure 2.2 using historical (triangles), statistical d-s (squares) and dynamical d-s (diamonds) estimates of annual area burned (AAB). Shown for reference is the annual domain-wide total $PM_{2.5}$ emissions level from point wildfires only in the 2010 NEI (circles), replicated in all other years.

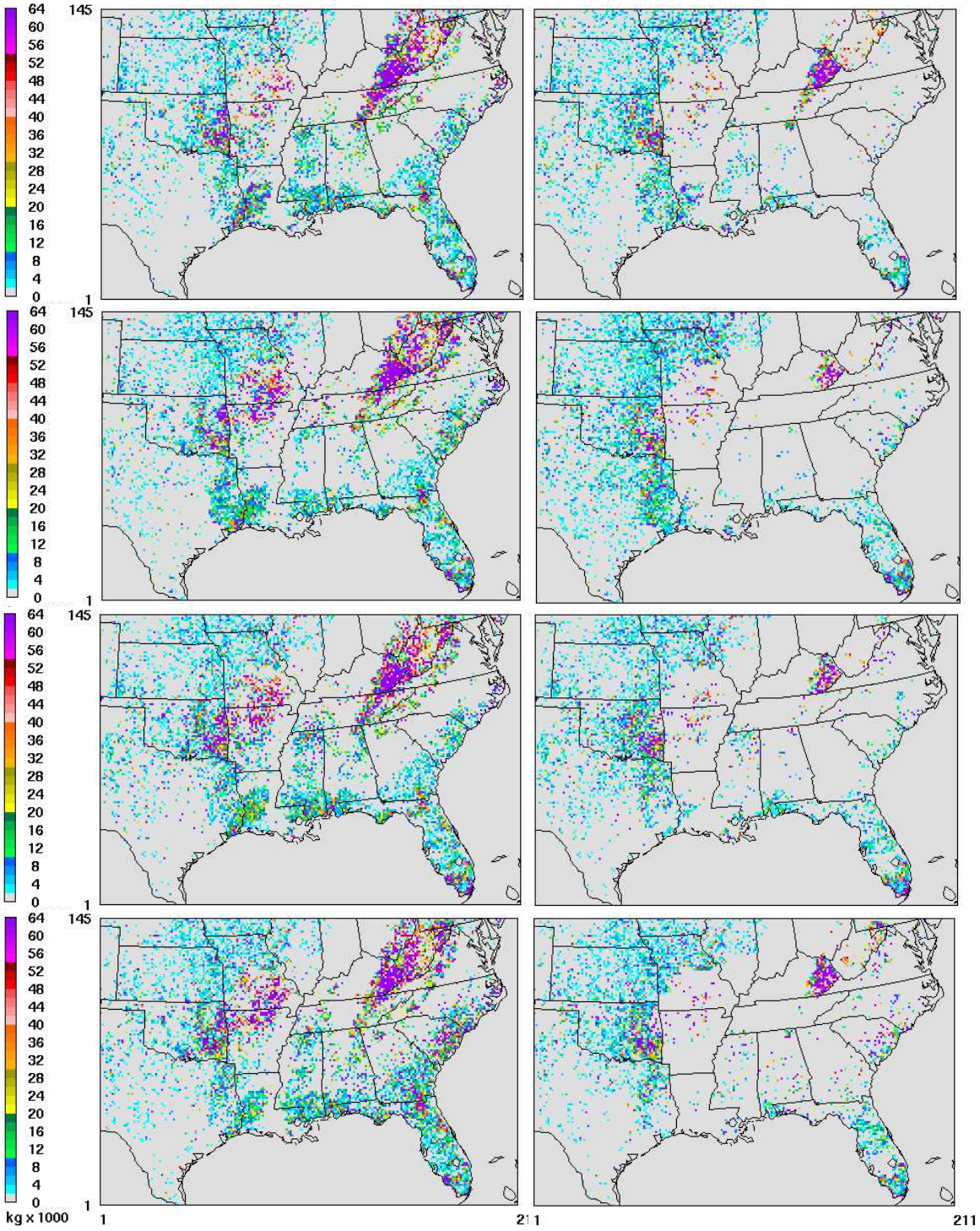

Figure 2.7. Spatial distribution of annual column total wildfire $PM_{2.5}$ emissions (10^3 kg) based on two AAB estimation methods: historical means (left panels) and dynamical d-s (right panels), for the future years: 1st row, 2043; 2nd row, 2048; 3rd row, 2053; 4th row, 2058.

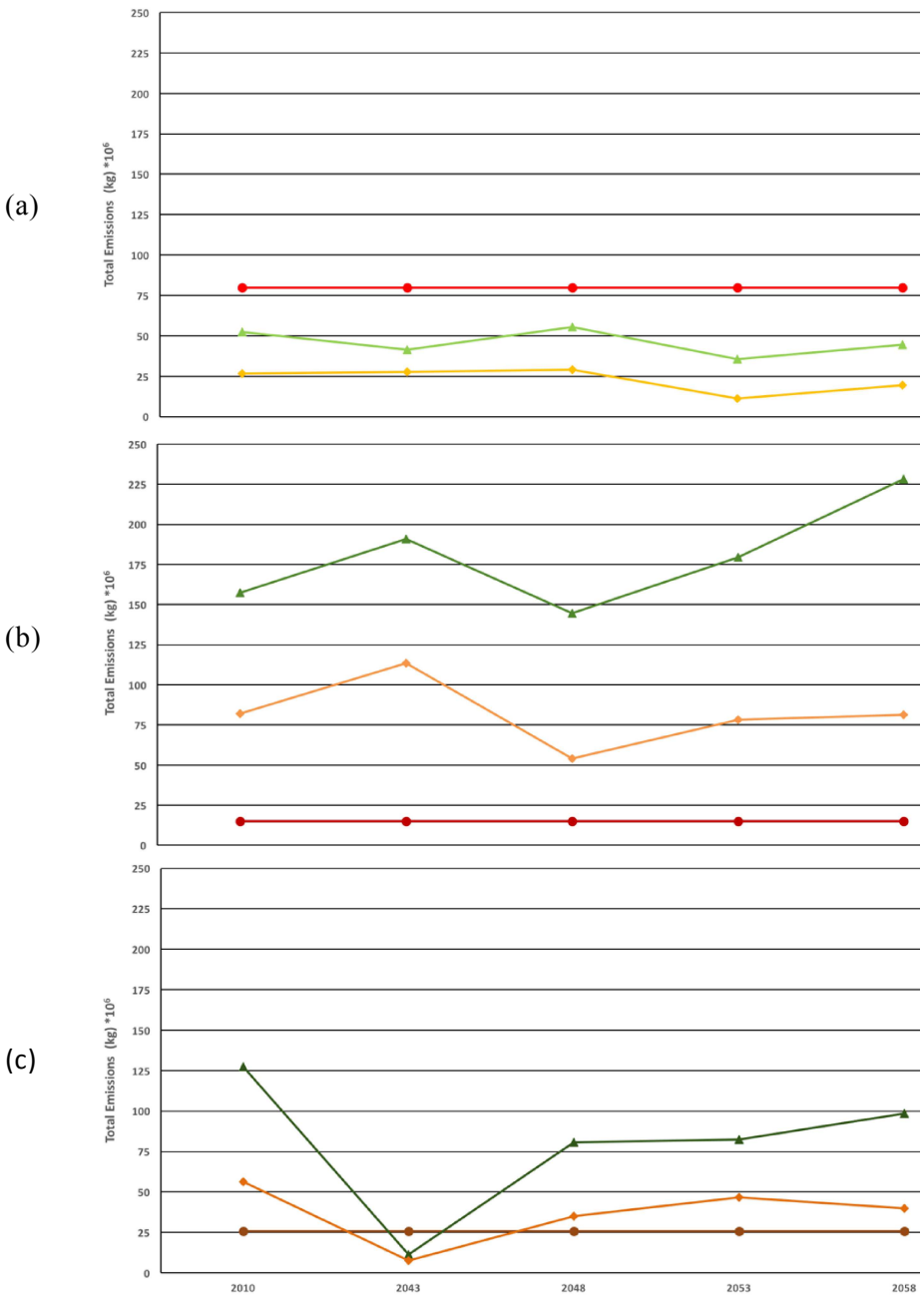

Figure 2.8. Variability of seasonal domain-wide total wildfire $PM_{2.5}$ emissions (10^6 kg) for domain D02 of Figure 2.2 for (a) spring, (b) summer, and (c) fall, in the modeled years, shown for two sets of annual areas burned (AAB), historical (triangles), and dynamical d-s (diamonds). Shown for reference are the seasonal domain-wide total wildfire $PM_{2.5}$ emissions in the 2010 NEI (circles), which are replicated in future years.

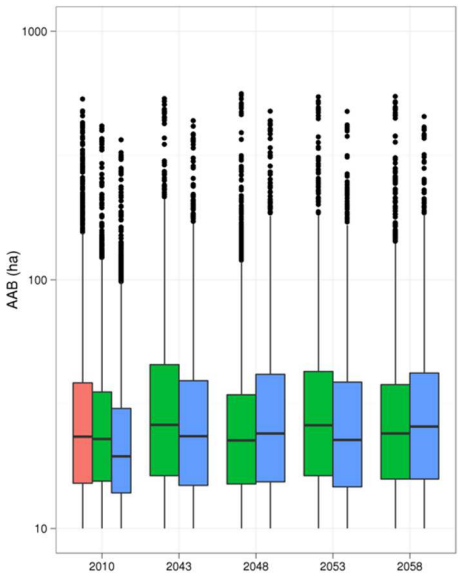

Figure 2.9. Spread of domain-wide AAB values around the annual mean for the AAB estimation methods in each of the modeled years: red: historical; green: statistical d-s; and blue: dynamical d-s. Note that the 2010 value for the historical mean represents a multiyear average (1992-2010).

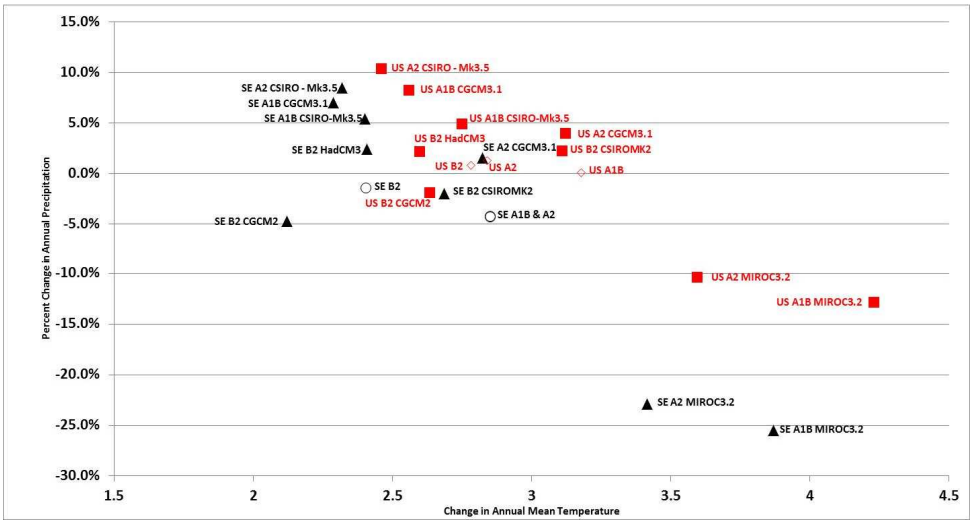

Figure 2.10. Precipitation and temperature differences between 2000 and 2060 decadal averages for the conterminous US and the Southeast from nine downscaled climate models (L. Joyce, private communication; updated from Joyce et al. 2014). US data are represented by red squares and open diamonds, and the Southeast data, by black triangles and open circles.

Supplemental Material for Chapter 2

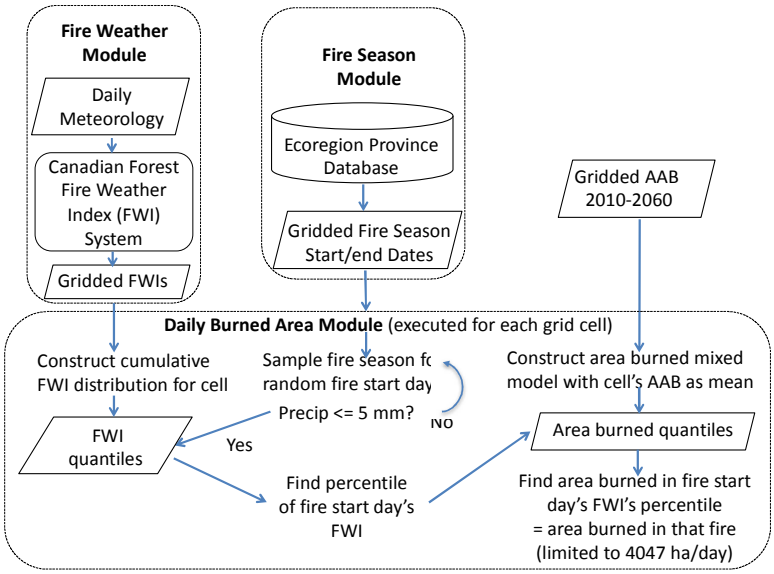

Figure 2.S1. Schematic of the Fire Scenario Builder; FWI, Fire weather index; AAB, annual area burned.

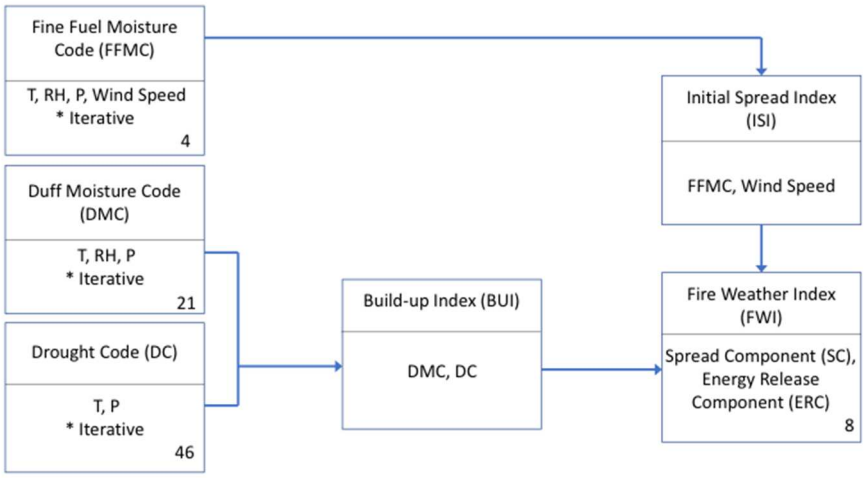

Figure 2.S2. Schematic of the Canadian Forest Fire Danger Rating System's Fire Weather Index System. Reproduced from Stavros et al. (2014). Numbers at the lower right corner of the modules denote the number of days that any given calculated index has an effect on subsequent calculated indices. (Note: T, temperature; P, pressure; RH, relative humidity)

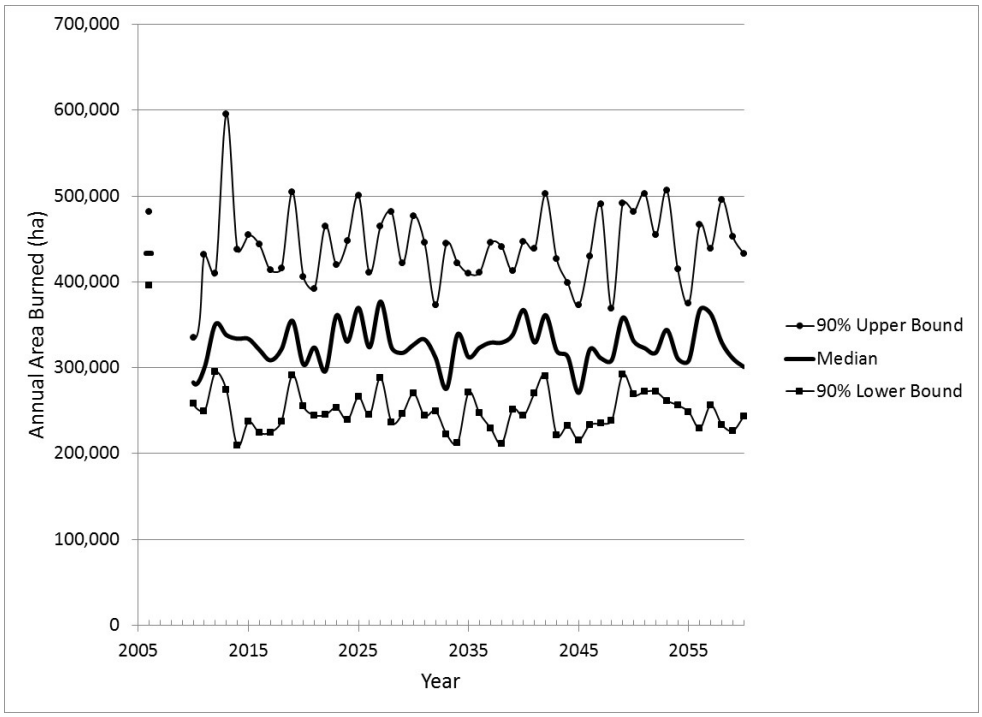

Figure 2.S3. From Prestemon et al., 2016 (Figure 4). Projections of all wildfires combined for the south-eastern US in aggregate (i.e., sum of all areas burned for all counties in the region) for 2006, and 2010 – 2060, including upper and lower 90% bounds of 2250 Monte Carlo iterations of models under nine climate model realizations. Note: No projections were made for 2005, 2007, 2008, or 2009.

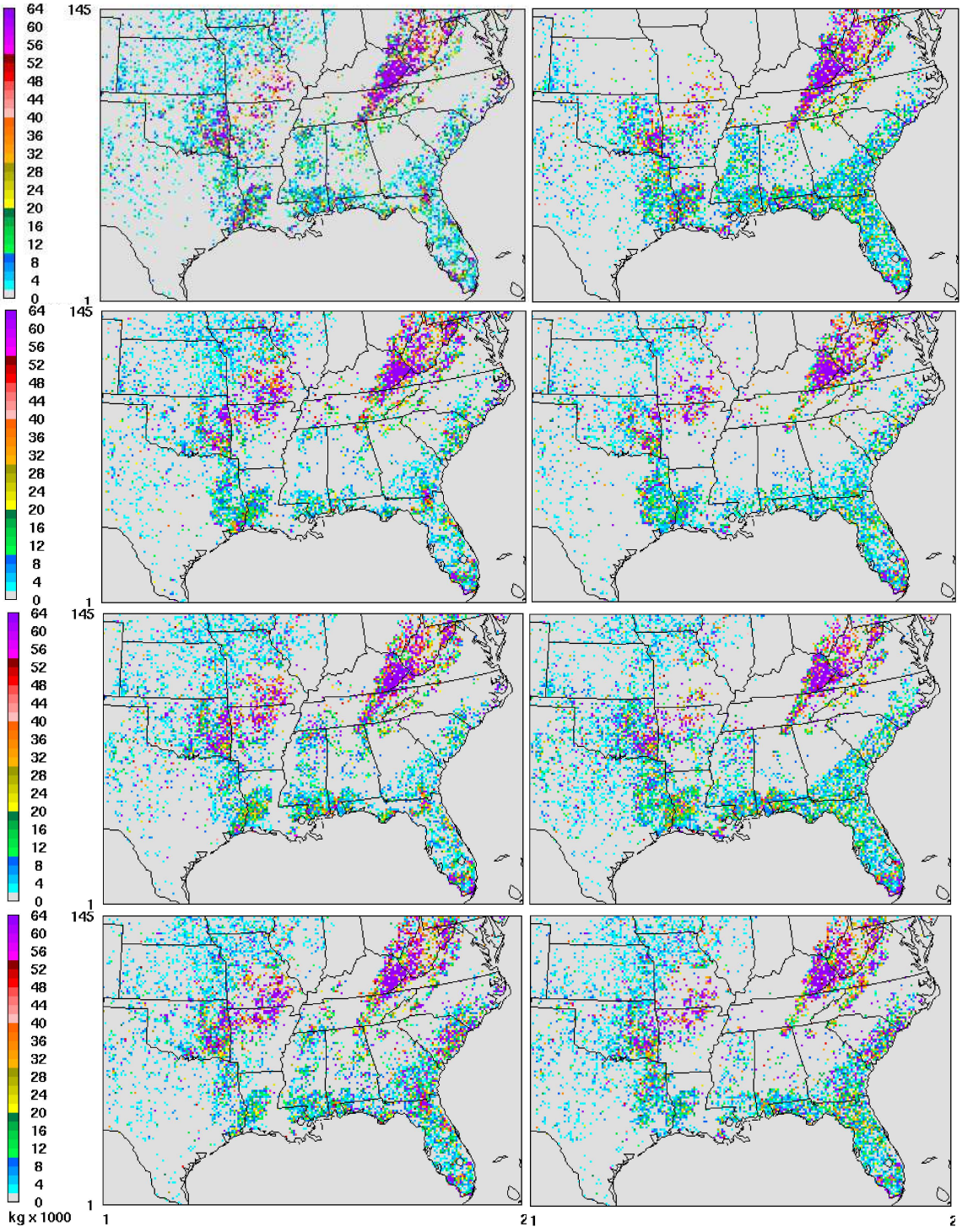

Figure 2.S4. Spatial distribution of annual column total wildfire $PM_{2.5}$ emissions (103 kg) based on two annual area burned (AAB) estimation methods: historical means (left panels), and statistical d-s, (right panels) for the future years: 1st row, 2043; 2nd row, 2048; 3rd row, 2053; 4th row, 2058.

CHAPTER 3: EVALUATING WILDFIRE EMISSIONS PROJECTION METHODS IN COMPARISONS OF SIMULATED AND OBSERVED AIR QUALITY[10]

Introduction

Wildfires can have catastrophic impacts on air quality and health in the United States and around the world. At this writing, the death toll from the Camp Fire that destroyed the town of Paradise, California in November 2018 is still mounting. Earlier, in the summer of 2018, catastrophic wildfires in Sweden required international aid for their mitigation, while Mendocino county in Northern California saw the largest wildfire in that state's history. In October 2017, multiple wildfires in Northern California burned 850 km^2 of a fragile ecoregion, causing at least 44 fatalities and nearly 200 hospitalizations. Only two months later, the Thomas Fire in Ventura County in Southern California burned more than 300 km^2 in its first week alone, with a total area burned exceeding 1,100 km^2. These events underscore the human, economic, and environmental toll of large wildfires. In addition to damaging human and wildlife communities, structures, and ecosystems sensitive to disturbance, wildfires can also have adverse health consequences for vulnerable populations through exposure to the emitted pollutants, notably particulate matter

[10] This chapter previously appeared in an article in Atmospheric Chemistry and Physics Discussions. The original citation is as follows: Shankar, U., McKenzie, D., Prestemon, J., Baek, B., Omary, M., Yang, D., Xiu, A., Talgo, K., and Vizuete, W.: Evaluating emissions projection methods in comparisons of simulated and observed air quality, Atm. Chem. Phys. Discuss., https://doi.org/10.5194/acp-2018-1296, in review, 2019.

(PM) below 2.5 μm in diameter, denoted $PM_{2.5}$, and ozone. In a study of the health impacts of wildfires over the Northwestern and Southeastern U.S., Fann et al. (2018) estimated the economic impacts of wildfires in the form of additional premature deaths and hospital admissions between 2008 and 2012 to be $11B - $20B (2010$) per year. In the Southeastern U.S., the economically disadvantaged populations in rural areas are most vulnerable to these health impacts, due to limited resources for preventive healthcare and wildfire mitigation (Gaither et al., 2011; Rappold et al., 2011, 2012, 2014). In their study of the Pocosin Lakes peat bog fire in eastern North Carolina in 2008, Rappold et al. (2014) estimated the long-term healthcare costs of the fire at ~ $48 M, far in excess of their estimates for short-term exposure (~ $1 M).

Climate change leading to prolonged droughts that affect soil and fuel conditions has been implicated as a driver in many Western wildfires (Dennison et al., 2014; Stavros et al., 2014; Abatzoglou and Williams, 2016). Statistical analysis of nearly a century of wildfires in 19 ecoprovinces in the western U.S. (Littell et al., 2009; 2018) found that climate variables (precipitation, temperature and drought severity) were able to explain up to 94% of the variability in annual areas burned (AAB). In a climate-limited ecosystem (no limitation due to fuel availability), the current fire season's climate was the biggest driver of wildfires in a given year (Littell et al., 2009, 2018). In analyses of regional climate model predictions over the continental U.S. from 2000 - 2070, Liu et al (2013) also projected increases in the length of the wildfire season by mid-century, and found increasing temperatures to be the main driver of increasing fire potential, outweighing the mitigating effects of increases in precipitation in some regions.

Wildfire occurrences vary widely geographically in response not only to these climate drivers, but also to human factors (Prestemon et al., 2002, Mercer and Prestemon, 2005; Syphard et al., 2017). Humans both ignite and suppress the majority of wildfires, especially in the Southeastern U. S. (Prestemon et al., 2013; Balch et al., 2017). Analyses by Syphard et al. (2017) of over 37 regions across the continental U.S. suggest that human populations and climate may play complementary roles in determining the spatial patterns of wildfire in the Southeastern U.S., currently considered among the fastest-growing regions in the country (U.S. Census Bureau, 2018). Fire regimes in the Southeast may be responding to both a changing climate and population shifts. Thus, there is a critical need in Southeastern land and air quality management to consider both these drivers to plan effectively for protecting the public and the environment. This has motivated the recent development of methodologies that include these drivers in projections of wildfire activity (Prestemon et al., 2016) from the present to 2060, and their use in assessing not only current, but also future air quality (Shankar et al., 2018).

Prestemon et al. (2016) estimated annual areas burned (AAB) over 13 states in the U.S. Southeast using county-level projections of the major wildfire drivers in the Southeast (climate, population and income, and land use). These projected drivers of their statistical models of AAB were based on the Intergovernmental Panel on Climate Change emissions scenarios (Nakicenovic and Steward, 2000). Their median projection of aggregate wildfire activity in the Southeast over hundreds of iterations in a Monte Carlo framework shows an increase, albeit by a small amount (4%), from 2011 to 2060 due to the combined influences of these climate and socioeconomic factors (Prestemon et al., 2016). Shankar et al. (2018) leveraged the AAB projections of Prestemon et al. (2016) to estimate wildfire emissions over a Southeastern modeling grid at 12-km x 12-km spatial resolution suitable for air quality impact assessments.

They applied the methodology in that first study to project daily wildfire emissions, which include the influence of both climate and socioeconomic changes in selected years from 2011 to 2060. The study also compared their wildfire emissions projections to those using 19-year historical mean AAB. Because the future AAB of Prestemon et al. (2016) that were used in their wildfire emissions projection method were lower (7% - 38%) than the historical mean AAB in the years selected, future wildfire emissions were also lower (by 13% - 62%) than those based on the historical AAB. The offsetting influences of socioeconomic variables, which decreased AAB, and climate variables, which increased AAB, played an important role in these lower projected AAB and emissions in the selected years.

Various methods are available to derive the climate inputs for the AAB estimation models that provide the basis of these regional-scale wildfire emissions projections. Prestemon et al. (2016) used *statistically* downscaled outputs of nine general circulation model (GCM) realizations to provide the needed meteorological inputs at a fine spatial resolution (12-km x 12-km) for their statistical model estimates of AAB at the county-level. These meteorological inputs, however, do not include all the variables needed for an air quality simulation; nor are the available variables at the temporal resolution (hourly) needed for such simulations (Shankar et al., 2018). Thus, the use of AAB estimated with statistically downscaled climate inputs in air quality studies requires additional mesoscale meteorological modeling. An alternative approach is to use a mesoscale meteorological model to downscale these climate variables *dynamically* from one or more GCMs to start with. This provides the spatial resolution needed to project the AAB, along with a higher temporal resolution of all the prognostic meteorological variables, allowing for a consistent set of inputs from AAB estimates to air quality simulations. An evaluation of both methods, through air quality simulations and a comparison of the modeled air

quality against observations, would provide insights into how well (or poorly) these projection methods represent real-world conditions, their effects on the modeled fire emissions, and their air quality impacts. Retrospective model performance evaluations have a long history of use in atmospheric modeling (see, e.g., Fox, 1981; Appel et al., 2007, 2008; Wong et al., 2012; Katragkou et al., 2015). They are critical for evaluating models used for predictive applications, and for establishing the baseline against which future modeled trends can be compared. Issues to be considered in evaluating the performance of a model or modeling system have been reviewed by several authors (see, e.g., Chang and Hanna, 2004; Dennis et al., 2010; McKenzie et al., 2014, and references therein).

In this study, we examine the model performance of retrospective air quality (AQ) simulations using wildfire emissions (Shankar et al., 2018) that are a function of changes in climate and socioeconomic factors, with both the statistical and the dynamical climate downscaling methods for the underlying AAB estimates. We compare the AQ model results using these two emissions estimates to those with a standard wildfire inventory compiled from observed daily fire activity without considering changes in climate and socioeconomic factors. The performance of all three wildfire emissions methods is also evaluated by comparing these model results to ground-based air quality observations for 2010. This year was chosen for the retrospective evaluation because it provided the latest historical year of AAB that was used by Prestemon et al. (2016) to calibrate their statistical AAB projection models. Thus, the choice of this year both ensured the robustness of the underlying AAB data used in the wildfire emissions estimates, and allowed the use of reliable and relatively recent emissions inventories for the non-wildfire sectors in the AQ simulations.

Our evaluations compare selected outputs from the AQ models for ozone and speciated $PM_{2.5,}$ to observations from long-term monitoring networks, seasonally and spatially across the Southeast. If results based on either our emissions modeling or the standard inventory, or both, show systematic departures or bias with respect to the observations, it will provide critical feedback for improvements in national emissions inventories and modeling techniques designed for future AQ projections. For example, if the wet bias in our dynamical downscaling (Shankar et al., 2018) were to persist into predictions of ozone and $PM_{2.5}$, it would signal the need for re-evaluation of the mesoscale meteorological model's usefulness for projecting air-quality changes from wildfire. Similarly, if model output based on the standard inventory departs significantly from observations, it might suggest specific changes in some of the many assumptions that go into national wildfire emissions inventories (see, e.g., Pouliot et al., 2008). Based on our initial analyses of our wildfire emissions projection methods (Shankar et al., 2018), we hypothesize that they will yield results within published criteria for acceptable AQ model performance with respect to observations, and that their predictions will closely match those using the benchmark inventory for the historical period.

Methods

Predictions of ozone and $PM_{2.5}$ were generated for 2010 using version 5.0.2 of the Community Multiscale Air Quality model (CMAQ – Byun and Schere, 2006) using emissions estimates from each of the two wildfire projection methods of Shankar et al. (2018) in combination with emissions from other sectors. We compared the AQ model results for these two cases with those using the National Emissions Inventory (NEI) compiled and distributed by the U.S. Environmental Protection Agency (EPA), and also against AQ network observations.

Emissions Inventories

We used two projected wildfire emission inventories from Shankar et al. (2018), and one from 2010 compiled by the EPA, hereafter "NEI benchmark". The projected inventories were developed using AAB estimated by the statistical models of Prestemon et al. (2016) with input meteorological variables either from (a) statistically interpolated output of a GCM (hereafter "statistical d-s") or (b) dynamically downscaled from a GCM using a mesoscale meteorological model (hereafter "dynamical d-s"). Regardless of the climate downscaling method used to project AAB, the distinguishing feature of our emissions projection methods compared to the NEI (and other empirical inventories) is that they can estimate future-year wildfire emissions based on expected county-level changes in climate and socioeconomics built into the underlying AAB estimates.

The statistical d-s case was based on output from a realization of the Canadian General Circulation Model version 3.1 (CGCM31 – Gachon et al., 2008) using the A2 greenhouse gas (GHG) emissions scenario (Nakicenovic and Steward, 2000) characterized by moderate economic growth and high population growth. Selected outputs from this climate model realization were statistically downscaled following Daly et al. (2002) over the Southeastern U. S. (domain D02 in Figure 3.1) at 5′ x 5′ resolution to provide the meteorological inputs required for the AAB projections (Joyce et al., 2014). These included maximum and minimum daily temperature, monthly cumulative precipitation and potential evapotranspiration. These data were then remapped to a 12-km x 12-km grid over the D02 domain and aggregated or averaged to the required monthly values.

The dynamical d-s case provided meteorological inputs for the AAB estimates from the Weather Research and Forecasting model (WRF -- Skamarock et al., 2008) over domain D02.

This involved the use of WRFG (WRF with an improved scheme for convective parameters -- Grell and Devenyi, 2002) model outputs archived in the North American Climate Change Assessment Program (NARCCAP – Mearns et al., 2009) database for the D01 domain (Figure 3.1) at 50-km x 50-km spatial resolution from the dynamic downscaling of a CGCM version 3.0 (Flato, 2005; Jeong et al., 2012) realization with the same A2 scenario for GHG emissions as in the previous case. These D01 WRFG outputs were used at the boundaries of domain D02 for a WRF version 3.4.1 simulation using its nest-down feature at 12-km x 12-km resolution to calculate the meteorological inputs needed for the AAB estimates. The model differences between WRFG and WRF version 3.4.1 and their implications for the dynamical d-s wildfire emissions inventory are discussed in Shankar et al. (2018).

Each set of estimated AAB was used to calculate daily wildfire emissions (Shankar et al., 2018) with the BlueSky/CONSUME fire consumptions and emissions model (Larkin et al., 2009). A critical step in this process is the disaggregation of the AAB estimates into daily fire activity with a daily metric of ignition probability, the fire weather index (FWI -- Stavros et al., 2014), using the Fire Scenario Builder (McKenzie et al., 2006). Due to the finer (daily) temporal resolution of the meteorological data needed to calculate the FWI than is available from statistical downscaling, the same WRF model outputs were used to disaggregate the AAB to daily area burned for both statistical d-s and dynamical d-s (Shankar et al., 2018).

As a baseline inventory, the 2010 NEI for wildfire emissions draws on a variety of data sources, including fire counts, i.e., fire pixels at 1-km^2 resolution, from the Moderate Resolution Imaging Spectroradiometer (MODIS) on board the Aqua and Terra satellites, available in the National Oceanic and Atmospheric Administration's Hazard Mapping System. These are matched in the SMARTFIRE system (SMARTFIRE -- Pouliot et al., 2012, and references

therein) to ground-based wildfire activity data reported in Incident Status Summary (denoted ICS 209) reports by the National Interagency Fire Center. The daily areas burned estimated by SMARTFIRE are input to the Fire Emissions Processing System (FEPS) in BlueSky (Larkin et al., 2009) to estimate daily point wildfire emissions for the NEI (Pouliot et al., 2008). Being an empirical inventory, the NEI does not include changes in climate and socioeconomic variables, and is intended for use in AQ simulations close to the time period of the inventory data.

Each of the three wildfire inventories was processed in the Sparse Matrix Operator Kernel Emissions (SMOKE) processing system (Houyoux et al., 2000; Baek and Seppanen, 2018) to provide the necessary spatiotemporal wildfire emission magnitudes for the respective AQ simulation, which were then vertically allocated inline by the AQ model. The diurnal profiles and fire emissions speciation for PM used in the NEI benchmark inventory were also applied in processing the other two inventories, to avoid any artifacts from them in the inventory comparisons. Emissions for all other source sectors were provided by the EPA's 2005 NEI for all three cases. Table 3.1 summarizes these details.

Air Quality Simulations

The CMAQ v5.0.2 model simulations for the 2010 evaluation study were performed over the Southeastern U. S. domain shown in Figure 3.1 (D02) at a 12-km x 12-km horizontal grid spacing. Representative hourly chemical boundary inputs at the lateral boundaries of the domain were extracted from an annual simulation for the conterminous U. S. (CONUS) at 36-km x 36-km grid spacing (Vennam et al., 2014) for all three simulations. All simulations also used the same aerosol and gas-phase chemical mechanisms. The Carbon Bond 05 gas-phase mechanism (cb05tucl) used in our simulations includes updates to toluene chemistry, homogeneous hydrolysis rate constants for N_2O_5, and updates to the chlorine chemistry (Sarwar et al., 2011;

Whitten et al., 2010). The aerosol mechanism, AERO6, includes a primary organic aerosol aging scheme (Simon and Bhave, 2012), and an improved representation of fugitive dust; primary speciated emissions needed to model dust are based on Reff et al. (2009).

Observational Networks

Observations for ozone and speciated $PM_{2.5}$ for 2010 were extracted from three long-term monitoring networks: the Air Quality System (AQS -- https://www.epa.gov/aqs), a national network of over 1000 sites maintained by the EPA; the Interagency Monitoring of Protected Visual Environments (IMPROVE – Sisler et al., 1993), a network of mostly rural sites concentrated in the western half of the U. S.; the EPA's Chemical Speciation Network (CSN -- https://www3.epa.gov/ttnamti1/speciepg.html) of mostly urban sites. AQS consolidates and distributes data on samples taken at hourly and daily intervals. The IMPROVE and CSN observations are for two 24-hour periods per week, with many collocated sites so that they provide observations of rural vs. urban air sheds in close proximity. We also compared simulations results to available observations of hourly ozone and daily-averaged speciated PM from the Southeast Aerosol Research and Characterization (SEARCH – Blanchard et al., 2013, and references therein) network for the continuous monitoring of particulate matter (PM) over a limited set of 8 sites in the Southeast.

Model Evaluation Tools and Data

The Atmospheric Model Evaluation Tool (AMET -- Appel et al., 2011) was used to compare the modeled cases against each other, and against the network observations, using Mean Fractional Error (MFE), Mean Fractional Bias (MFB), Normalized Mean Error (NME) and Normalized Mean Bias (NMB) as the key indicators of model performance. In model-to-observation comparisons all four metrics are meaningful, but in intermodel comparisons AMET

also calculates "bias" of one model with respect to another, which is useful for testing our hypothesis regarding the performance of our projection methods with respect to the NEI benchmark. The AMET version used here (version 1.2.2) contains several updates to the tool since the initial distribution, along with corrections to the observational data originally distributed with the software. In our intermodel comparisons, we filtered the model results to display only monitored grid cells that had wildfires, defined as those with non-zero AAB estimated for the statistical d-s case described in Shankar et al. (2018). This case was deemed to have the most number of grid cells with fires among the three inventories, and to have AAB most similar to the gap-filled AAB data (Prestemon et al., 2016) created for the historical period 1992-2010. Most model grid cells in this dataset had some fires, and therefore our analyses apply to most of the domain.

Results

Ozone

Model evaluation against observations

In this section, we compare the performance of the two downscaling methods to observations for ozone. We also provide results using the NEI benchmark wildfire inventory for reference. We evaluate the ozone model performance against AQS observations over all of 2010. Boylan and Russell (2006) provide the performance guidelines in current use in AQ model evaluation for MFB and MFE with respect to observations for ozone and PM that are considered good, acceptable or needing further investigation. We apply their ozone performance measures also for monthly-averaged NMB and NME, shown in Table 3.S1 in the Supplement along with mean modeled and observed ozone. We compare the Southeast-wide MFB and MFE for modeled monthly-averaged 1-h ozone relative to AQS measurements in the soccer goal plots of Figure

3.2, with the performance goals and criteria of Boylan and Russell (2006) shown as dotted lines. The ozone performance statistics show very small differences in the CMAQ results from the three sets of wildfire emissions. Table 3.S1 shows that in all three modeled cases, ozone is overestimated in all months of the fire season (March – November), and the ozone model performance falls outside the performance goals of NME ≤ +35% and NMB ≤ ±15% in all except March and April. MFB and MFE in Figure 3.2 are in the acceptable range of performance for ozone (≤ 50% and ≤ ±30%, respectively) from March to July, but fall just outside of it from August to November. The overprediction is greatest in the summer, especially August, being 8.4 ppb for the statistical d-s, while the best agreement with observations within the fire season is for April in all three cases (Table 3.S1). However, differences among the three cases are negligible. Of the three cases, the statistical d-s case has the largest MFB, albeit by a very small margin, in October. There is virtually no disagreement between the dynamical d-s and NEI benchmark cases throughout the fire season except in September. It is important to note that there are no wildfires in January, February and December in any of the inventories, and thus the emissions for these months are the same across all three modeled cases, corresponding to the NEI 2005 (default) inventory.

Based on the statistics in Table 3.S1 and Figure 3.2 there are no discernible differences in their monthly average performance over all sites and hours in any month, with a small exception in October for the statistical d-s. This is confirmed by the lack of distinction among the cases in the seasonal spatial distributions of MFB (Figure 3.S1 in the Supplement), with the exception of one AQS site on the Kentucky-Illinois border in autumn (Figure 3.S1, bottom row). The MFB has some of its largest values in the eastern half of the domain in spring, and is lowest in autumn domain-wide. Comparing hourly ozone across networks in Figure 3.S1, the SEARCH network

sites (four rural, four urban) in the deep South show lower biases than the AQS sites across the three cases and seasons. The lack of distinction across the modeled cases for either network is consistent with the results for the absolute difference in hourly ozone between the two downscaling methods in the 24-hour domain-wide trend (Figure 3.S2 in the Supplement), that is, at most hours of a given day over the whole domain, 75% of the values modeled by these two methods differ by ~0.1 ppb or less.

To better understand the relative contributions of the magnitude and location of the wildfire emissions to the October 1-h ozone performance differences among our three methods, we filtered the three sets of modeled data over the range of values showing the largest differences, at all grid cells that contained monitors and also had some fire during the fire season. We then examined the hourly O_3 for October at a few of these selected locations (Figure 3.S3 in the Supplement). The top four panels of Figure 3.S3 show the time series of ozone mixing ratios and bias with respect to observations for all three modeled cases at two AQS sites, 2105900005 and 210910012, close to the Kentucky (KY) –Ohio (OH) border, respectively labeled KY-OH (1) and KY-OH (2). The bottom four panels display the time series for the same metrics at AQS sites 291831002 and 295100085 farther west, on the Missouri (MO) –Illinois (IL) border (labeled MO-IL (1) and MO-IL (2), respectively). These four sites had some of the largest differences in the statistical d-s case relative to the other two cases in the low-to-middle range of values (0-70 ppb) during the fire season (see Table 3.2). With the exception of short periods of large positive differences in the statistical d-s case from the other two cases on specific days in October, they are all closely aligned; some smaller differences are also seen between the dynamical d-s and the NEI benchmark. At the KY-OH sites, all model simulations underpredict the ozone peaks during October 9-11 with the NEI having the greatest underprediction, while all models have an equally

high bias during October 24-26. The statistical d-s case shows a large overprediction on October 30. The similarity of the temporal trends at these two proximal sites suggests similar sources of the biases. The two sites at the MO-IL border show less negative bias in the models relative to AQS observations, but once again the statistical d-s has large positive biases with respect to the other cases and to AQS for short periods mid-month and at the end of the month; its negative biases with respect to observations also tend not to be as large as in the other two cases, e.g., on October 11 at KY-OH (1) site. This would be expected, as this case had the largest AAB values of the three inventories (Shankar et al., 2018).

Results of our time series analyses at these and other AQS sites are tabulated in Table 3.2, highlighting periods and locations of large differences either between the two downscaled cases, or between one or the other case and AQS observations. Most of these occurred in October 2010, but there were also a few outlier locations/times in early September. Ozone is underpredicted at half the locations and times in the statistical d-s case, and at 76% of them in the dynamical d-s. The model biases with respect to AQS vary between -49 ppb and +47 ppb for statistical d-s, and between -62 ppb and +13 ppb for dynamical d-s. The largest intermodel differences occur in grid cells on days with little or no fire activity within, or near the cells; most of the grid cells indicated as no-fire locations in Table 3.2 had fewer than 5 ha burned annually. Thus, the biases are not proportional to daily fire activity within the grid cell, but in general, when there is a large difference in ozone between the two modeled cases, there is a comparable difference between them in daily area burned in an adjacent cell upwind, which is larger for the statistical d-s due to its larger AAB as noted previously. There are also some dates, e.g., October 30, on which the model biases with respect to observations are comparably large at multiple monitor locations,

suggesting the impact of the same upwind fire event(s) at these locations. We explore this further in the next section.

Intermodel comparisons

(a) Hourly ozone

The modeling bias with respect to AQS observations is shown in the previous analyses to be very comparable among the three wildfire emission estimation methods; this may mask intermodel differences and prevent understanding of important sources of modeling uncertainties. Therefore, we compare the differences in modeled 1-h O_3 mixing ratios between each pair of the three CMAQ simulations at AQS sites for the whole fire season (March 1 – November 30) and for the months with the maximum differences (Figure 3.3). For the whole wildfire season, the statistical d-s ozone values are the highest, and the NEI values are the lowest. The maximum difference with respect to the NEI exceeds 45 ppb for both downscaling methods (Figure 3.3, rows 1 and 2). Of these, statistical d-s has the largest maximum difference compared to the other cases (> 67 ppb), and systematically positive domain-wide mean differences (denoted MB in the figure) compared to dynamical d-s and NEI, of 0.12 ppb and 0.23 ppb respectively over the fire season (Figure 3.3, top and bottom left panels). Comparable maximum differences of > 67 ppb between the statistical d-s and either of the other cases occur on October 29 (Figure 3.3, top and bottom right panels) due to an outlier value in the statistical d-s predictions at AQS station 291893001, and nearly identical low ozone values there in the dynamical d-s and the NEI cases for that hour. The maximum difference between the dynamical d-s and the NEI of 45.7 ppb occurs on July 6 at a different station (540390010), and even with a positive mean difference with respect to the NEI of 0.1 ppb over the fire season (0.17 ppb in July), most of the dynamical d-s values are within 50% of the NEI (Figure 3.3, middle row).

To better distinguish between outlier values and more systematic biases in ozone, we compared the three cases in each season (Figure 3.4). Seasonally, the springtime differences are the smallest between each pair of cases compared, as would be expected due to low fire activity. Summer ozone differences between each pair of cases (Figure 3.4, middle panels) have a smaller range and lower values (0.12 ppb – 0.28 ppb) than in autumn (0.11 ppb – 0.32 ppb; Figure 3.4, right panels). Comparing across modeled cases, the systematic positive mean ozone differences in either downscaling method compared to the NEI persist in each season (Figure 3.4, left and middle panels). The largest seasonal mean difference from NEI is in autumn in the case of statistical d-s (0.32 ppb), and in summer in the case of dynamical d-s (0.15 ppb); the latter difference is likely due to a few outlier locations, as autumn actually shows a greater range of differences from NEI for this case. Over all seasons, there is better agreement between the dynamical d-s and NEI than between the statistical d-s and NEI. The previously noted positive mean difference in the statistical d-s results relative to the dynamical d-s increases progressively from 0.05 ppb to 0.21 ppb from spring to autumn (Figure 3.4, bottom row).

(b) Daily maximum 8-h average ozone

Although hourly ozone performance is a good indicator of the robustness of the gas-phase chemical mechanism in the model, in regulatory compliance modeling in the U.S., the maximum value of the 8-h running average of ozone mixing ratio over a given day (denoted MDA8) is the metric of relevance. Its calculation is a requirement for state-level demonstrations of attainment of the annual ozone standard (U.S. EPA, 2007). Our comparisons of MDA8 between each pair of CMAQ simulations (Figure 3.S4 and Figure 3.S5 in the Supplement) show similar characteristics to those for 1-h ozone. Overall, most of the MDA8 values show better agreement between the cases than the 1-h values (within ± 50% of each other), as might be expected from the longer

averaging periods for this metric. However, as for 1-h ozone, the mostly positive differences remain for either downscaling case with respect to NEI, and for the statistical d-s with respect to the dynamical d-s case. There is also more variability in the timing and location of these maximum intermodel differences (Figure 3.S4, right panels). They occur on July 6 for the statistical d-s case vs. NEI (33.4 ppb), on September 3 for the dynamical d-s vs. NEI (30.2 ppb), and on October 16 for the statistical d-s vs. dynamical d-s (28.3 ppb). Seasonally (Figure 3.S5), both downscaling cases have large differences from the NEI at the upper end of the range in autumn, an indication of their higher wildfire emissions estimates than in the NEI in this season.

(c) Ozone modeling uncertainties

Table 3.2 and Figure 3.S3 illustrate the large differences among the downscaled inventories in relatively fire-free locations, possibly due to a greater impact in these environments from the transport of precursors and ozone from fires upwind. This is supported by the spatial distribution of the maximum absolute difference in O_3 and its precursor emissions between statistical d-s and dynamical d-s in each modeled grid cell over the entire fire season (Figure 3.5). In this comparison "fire season" is defined as April 23 – November 30, 2010, because that was the period of occurrence of these maximum differences. The spatial pattern for O_3 (Figure 3.5, right panel) shows that the geographic areas of greatest difference in O_3 are in the Appalachian region centered in West Virginia, and also in "plumes" into the Southwestern corner of Missouri and out of its eastern border. The spatial pattern of these differences appears to be aligned with an underlying circulation, suggestive of transport from upwind source regions. This possibility is borne out by the spatial patterns of the maximum absolute difference in the column totals of VOC and NO_x point emissions between the two respective wildfire inventories (Figure 3.5, left and middle panels, respectively) over the same period. Column emission totals, rather than

emissions in model layer 1 are used in this comparison, because they constitute the wildfire emissions from each inventory, including what is allocated to aloft layers and transported downwind in the AQ simulation, and which would be missed if the comparison had been limited to emissions in layer 1. The largest differences are seen in VOC emissions due to their much greater magnitude than those of NO_x, but both precursors have similar spatial patterns of maximum absolute difference between the inventories. Peak differences occur in both species emissions from the Southwestern corner of Missouri and across its lower third, as well as at the KY-OH border in Appalachia, south and east of the ozone difference peak in West Virginia seen in the right panel of Figure 3.5.

Discussion

Overall, our analyses of ozone model performance over the fire season show very little difference among the three modeled cases with respect to each other, but a consistent and near-identical overprediction of ozone across all three, with the largest MFE (55%) occurring in the winter. The sharp differences seen in our results at individual locations and times in the intermodel comparisons (Figure 3.3, Figure 3.4, Figure 3.S4 and Figure 3.S5) between the two downscaled cases do not translate into major differences in the overall 1-h and MDA8 ozone model performance, with the possible exception of statistical d-s in October. In all cases the largest MFEs occur in winter, outside the fire season (Figure 3.2). As the three inventories used in the simulations differ only in the wildfire emissions, the occurrence of the maximum MFE in winter indicates that those emissions are not the major contributor to the ozone biases for any of the cases. This is consistent with the findings of Wilkins et al. (2018), whose brute-force zero-out

analyses of wildfire emissions impacts on air quality showed only a 1% increase in ozone due to wildfire from 2008 – 2012 over the CONUS.

Despite the very slight differences in error statistics among the three modeled cases for hourly ozone during the fire season, our intermodel comparisons do show sporadic large differences between the statistical d-s and the other two cases, and somewhat smaller ones between the dynamical d-s and the NEI. Differences in model formulations used in the two meteorological downscaling methods, which can lead to spatiotemporal differences in their predictions of peaks and troughs in wildfire emissions, are discussed in Shankar et al. (2018). The biases between the two downscaling methods are due to fundamentally different formulations of the underlying models used to provide the climate inputs for the AAB estimation. Statistical downscaling is a closer representation of the large-scale circulations modeled by the GCM used in the climate downscaling, while the dynamical d-s captures more of the prevailing local meteorological features, which may be quite different in a given period from the large-scale circulation. Furthermore, the WRF 3.4.1 model used in the AAB estimates for the dynamical d-s inventory has a known high precipitation bias (Alapaty et al., 2012; Spero et al., 2014). The prediction of too much precipitation in the AAB estimation model inputs could be another reason for the lower wildfire emissions overall in the dynamical d-s case (Shankar et al., 2018); this would account for its lower ozone precursor emissions and mixing ratios compared to the statistical d-s case. Temporally, some of the largest differences in 1-h ozone between the two downscaling cases occur on the same day, e.g., October 30, at multiple locations. Spatially, they occur in relatively clean, i.e., low- or no-fire grid cells. These results suggest that the greatest impact of their different wildfire emissions magnitudes is on ozone mixing ratios in low- or no-

fire grid cells due to the transport of those emissions (and ozone) from upwind locations with significant fire activity.

The seasonal intermodel comparisons of Figure 3.4 (top and middle row) show that the two downscaling methods differ not only in the magnitude, but also the timing of the maximum difference with respect to the NEI. The NEI predicts less ozone than the other cases in all the warmer months (summer and autumn). These warmer months are dominated by fires in a denser canopy. MODIS fire counts, which are used to estimate area burned in the NEI, are known to be underestimated in the earliest versions of that inventory for wildfires, in part due to the difficulty of under-canopy fire detection by the MODIS instrument (Pouliot et al., 2008, Soja et al., 2009). In addition to any ozone overestimates that are present in the downscaling cases in these months (e.g., statistical d-s in October), application of the MODIS estimates during canopy-heavy months could also contribute to these lower values in the NEI relative to the downscaling cases. The seasonal (positive) differences in ozone among the models are largest between either downscaling case and the NEI in autumn, at the upper end of the range, and can be attributed to the effect of less convective precipitation in autumn than in summer in the Southeast, which would increase the daily fire activity estimates in the downscaling cases.

$PM_{2.5}$

Model evaluation against observations

In this section, we compare the performance of the two downscaling methods, and the NEI wildfire inventory to $PM_{2.5}$ observations. We evaluate $PM_{2.5}$ model performance over all of the 2010 fire season (March 1 – November 30), as well as its seasonal variability, using observations from the IMPROVE, CSN, and the SEARCH networks for $PM_{2.5}$ and its constituents.

(a) Monthly variability

Table 3.S2 in the Supplement summarizes the performance statistics (NME and NMB) for $PM_{2.5}$ compared to observations from the IMPROVE network. There is more variability in these metrics seasonally and among the three simulation cases, than in the results for ozone (Table 3.S1). Figure 3.6 shows the range of MFE and MFB for total $PM_{2.5}$, and for two key co-emitted PM constituents from wildfires, elemental carbon (EC) and organic carbon (OC). The overall performance for $PM_{2.5}$ (Figure 3.6, top row) is in the acceptable range for MFE and MFB ($\leq$ 75% and $\leq \pm$ 60%, respectively). Unlike ozone, which is overpredicted in the summer months, total $PM_{2.5}$ has the greatest underprediction in these months in all three cases, with the statistical d-s having the least negative bias with respect to observations, followed by the dynamical d-s (except in July). The best performance statistics are in April and May, while the greatest overpredictions during the fire season are in November and March. However, these last two months appear to be in a continuum of overpredictions from late autumn when they are largest, to early spring when they are smallest, across all cases. The NEI has the best performance of the three cases for total $PM_{2.5}$ in the spring and autumn months, and the most underprediction in the summer months, though by small margins.

To investigate the possible source(s) of the $PM_{2.5}$ biases, we examined these error metrics for all the major PM constituents. The results for EC and OC are shown in Figure 3.6 (middle and bottom rows, respectively), and for the inorganic constituents (SO_4, NH_4, and NO_3) in Figure 3.S6 in the Supplement. EC performance for all three cases meets the PM performance goal (MFE $\leq$ 50% and MFB $\leq \pm$ 30%) in April, June, August and September, and meets performance criteria (MFE $\leq$ 75% and MFB $\leq \pm$ 60%) in the remainder of the year. MFB for EC is nearly zero for the two downscaled cases, and slightly negative for the NEI in June and August, but is positive in July for all three cases. These results indicate that the pronounced

negative bias in $PM_{2.5}$ in the summer months over all cases is not attributable to EC. All three cases overpredict EC in autumn, albeit within the good-to-acceptable range of performance. As there are no fires in the winter months, the performance for EC during that period is identical in all cases, and the large positive winter bias in EC is clearly due to combustion sources other than wildfires.

There is a severe underprediction in OC for all three cases except in winter (Figure 3.6, bottom row), with MFB from April – September being outside the range of acceptable performance. The negative biases are smallest for the statistical d-s, followed by the dynamical d-s, and largest for the NEI, particularly in summer and autumn, consistent with the progressive decrease in their respective wildfire $PM_{2.5}$ emission magnitudes (Shankar et al., 2018) in these seasons. The negative biases in $PM_{2.5}$ in the summer months, which are common to all three cases, are attributable in part to the OC underpredictions, although species with larger mass fractions of total PM could also be responsible. This is further examined in Figure 3.7. OC performance is best in the winter months when there are no differences in the input emissions among the three cases; the performance also improves throughout the fire season from the warmest to the coolest months in all cases. We discuss some possible explanations for this under "Discussion".

(b) Variability across network observations

The IMPROVE network is located mainly in the Federal Class I Areas with monitoring provided by the National Park Service (NPS), and administered by a consortium of several resource management agencies such as the National Fish and Wildlife Service, the USDA Forest Service, the Bureau of Land Management. As such, IMPROVE monitors are placed in rural areas, which allow reliable measurements of ambient concentrations in the vicinity of fires. To

evaluate the performance of our wildfire inventories in simulating air quality downwind and farther away from fires, we compared the model results at IMPROVE sites with those across the CSN and SEARCH networks for the species common to all. There are some limitations in these observations: the geographical coverage in SEARCH is limited to eight stations located in Mississippi, Alabama, Florida, and Georgia, and CSN had no EC measurements available beyond March in 2010. Nevertheless, these cross-network comparisons can provide additional insights into the geographical variability of model performance for PM, e.g., urban vs. rural, or the Atlantic seaboard vs. the high-fire areas in the interior of the domain.

Total $PM_{2.5}$ comparisons among IMPROVE and CSN (Figure 3.S7 in the Supplement) show that the model performance at the CSN sites is better than at IMPROVE sites, with lower bias and error, especially in the summer and autumn, for all the three cases. In these warmer months, the least negative bias at the CSN sites is for statistical d-s in August, and the least positive bias is for the NEI in September, but the differences among the cases are very small. Figure 3.S8 in the Supplement compares the spatial distribution of MFB among the three modeled cases across available networks for total $PM_{2.5}$ (IMPROVE and CSN) in each season. As with the ozone spatial comparisons of MFB (Figure 3.S1), the differences among the cases in Figure 3.S8 are too slight to be resolved in the color map. However, the bias differences across networks for $PM_{2.5}$ in Figure 3.S7 indicate better performance in some of the constituent species in the warmer months at the urban sites than at the rural sites.

To investigate this further we compared monthly-averaged model bias and error against IMPROVE, CSN, and SEARCH daily measurements (Figure 3.S9 in the Supplement) for OC and NO_3. These are the two PM constituents with poor model performance at the IMPROVE sites (Figure 3.6 and Figure 3.S6). As differences in model performance among the modeled

cases were small in those comparisons, the Figure 3.S9 comparisons are shown for a single case, statistical d-s, which had large negative biases for OC and NO_3, but also predicts higher $PM_{2.5}$ than the other cases. The errors and biases for OC are comparably high at the IMPROVE and SEARCH networks, and considerably less at the (urban) CSN monitors than at IMPROVE (rural) sites. However, the monthly variability of the bias is seen at the SEARCH and CSN monitors as well, and goes from negative to positive progressively from the warm to cool months, as at the IMPROVE sites.

NO_3 performance falls outside the acceptable range at all network sites, in almost all months, with CSN being the exception in winter. The results for NO_3 are somewhat better at the IMPROVE and CSN sites than at SEARCH sites, which have considerably more underprediction from May – September. The seasonal variability of the bias at all three networks is similar to that of OC, at least in these months. As with OC, the greatest negative bias in NO_3 is at the SEARCH sites in summer, with MFE in excess of 150%. One contribution to this large value is from the low concentrations of NO_3 in the Southeast, and the small numbers involved in the error estimates. The NO_3 bias is discussed further in a subsequent section (see "Discussion").

(c) PM composition

There is a wide range of bias and error among PM and its constituents in Figure 3.6, Figure 3.S6 and Figure 3.S9, and in Tables 3.S2-3.S5 in the Supplement, although total $PM_{2.5}$ meets the criteria for acceptable PM performance throughout the year and across all cases. To further examine the contributions of individual PM species to total $PM_{2.5}$ performance we compared the seasonally averaged $PM_{2.5}$ composition (Figure 3.7) over the fire season between IMPROVE observations and the model simulations. Overall, modeled PM composition is overpredicted in sulfate and nitrate, underpredicted in OC, and has mixed results for the other

constituents. Total $PM_{2.5}$ mass is overpredicted in the spring and autumn, and underpredicted in the summer in all cases; the summer underprediction is driven by the underprediction of most species other than sulfate, particularly the severe underprediction of the lumped species labelled "Other", which includes fugitive dust. There is a decrease in predicted total $PM_{2.5}$ mass across the three cases, statistical d-s, dynamical d-s and the NEI, and in the same direction as the decrease in their wildfire emissions. This translates into a monotonic decrease in the springtime average $PM_{2.5}$ concentration of ~ 1% from statistical d-s to dynamical d-s to NEI. In the summer and autumn, there is a 5% decrease from statistical d-s to dynamical d-s, and a ~ 2% – 3% decrease from the dynamical d-s to the NEI. The differences of modeled PM from the observations are much larger, from a low of -20% in the summer for the NEI to a high of 50% for the statistical d-s in the autumn, as noted in here and previously.

The contribution of sulfate to total PM concentration over the Southeastern U.S. is substantial (26% – 32%) in the IMPROVE observations throughout the year, and is overpredicted in every season across the three cases, although Figure 3.S6 (top row) shows it to be within the acceptable range in all months except October. The sulfate overprediction also persists in two months of the winter (January and February), when all three cases have identical emissions inputs (Table 3.S3); the small difference in the dynamical d-s case from the other two cases for December is due to ~ 10% fewer matched model-observation pairs for this case in December. Statistical d-s, by a slim margin, has the largest SO_4 overprediction over the whole year among the three cases, with an average NMB of 65.3% and average NME of 78.2%

(Table 3.S3), because of the larger magnitude of wildfire PM emissions from which its SO_4 emissions contributions are estimated.

Due to the use of a common (NEI) speciation profile, both ammonia (NH_3) and gas-phase NO_3 from wildfires are allocated the same fractions of total $PM_{2.5}$ emissions in all three wildfire inventories, and across all seasons. Particulate NO_3 contribution to total $PM_{2.5}$ mass in the IMPROVE observations is between 2.5% in the summer, and ~ 8% on average in the spring and autumn (Figure 3.7), and as much as ~ 25% in winter (not shown). It has a positive MFB of 14% – 51% in the cooler months of the fire season over all three cases (Figure 3.S6, bottom row), but has an equally negative MFB in the warmer months; the monthly biases are more or less uniform across the three modeled cases. Once again, the statistical d-s case has the highest NMB (234%) for NO_3 among the three cases (Table 3.S5) in October. There is very little difference in the positive biases in the remainder of the year across the cases. On the other hand, ammonium (NH_4), a $PM_{2.5}$ constituent that partitions between SO_4 and NO_3, contributes a greater fraction to total $PM_{2.5}$ mass on average (12% - 17%) than does NO_3 throughout the year (Figure 3.7). Its bias is considerably less than that of NO_3 across the three cases, and comparable to that of SO_4.

Intermodel comparisons

(a) Daily-average $PM_{2.5}$

Our $PM_{2.5}$ model evaluation shows that although there is slightly more variability in the model simulation results for $PM_{2.5}$ than in those for ozone, these differences are much smaller than their differences from observations. Our intermodel comparisons of $PM_{2.5}$ are motivated by the need to better understand modeling uncertainties and compensating errors, and how they affect overall model performance. $PM_{2.5}$ concentrations summed over all constituent species are compared among the three cases over the whole fire season and inter-seasonally (Figure 3.8 and

Figure 3.9) at grid cells that contained both IMPROVE monitoring sites and wildfires, at the temporal frequency of the measurements. There is less statistical power in these results than in those for ozone due to relatively fewer monitors in IMPROVE than in AQS in the eastern U.S., in addition to the lower temporal frequency of the measurements (daily averages measured twice a week). As with ozone, however, the largest differences in $PM_{2.5}$ are in the statistical d-s case with respect to the other two cases (Figure 3.8, top and bottom rows). As with ozone, the smallest differences between cases occur in the spring, and the largest ones in autumn (Figure 3.9, bottom row). However, the dates of maximum intermodel differences do not coincide with those for ozone in most seasons, suggesting a different source contribution to these differences than that for ozone. This is explored in the next section.

(b) PM modeling uncertainties

The time frequency of $PM_{2.5}$ measurements is twice per week in IMPROVE among about 28 sites in the Southeast, and thus considerably less than in the AQS measurements for hourly and MDA8 ozone. Nevertheless, for all the days available in the fire season at all the locations showing large differences (i.e., > 50%) between the downscaling cases, we performed a similar analysis to that for ozone. Table 3.3 summarizes modeled and observed results for $PM_{2.5}$ at these outlier locations and their times of occurrence, which are somewhat different from those for ozone. The largest differences in $PM_{2.5}$ occur in the summer, particularly in August. With the exception of James River Face in coastal Virginia, which is a few grid cells to the northeast of AQS site 511611004, there is little agreement in the locations of these large differences in $PM_{2.5}$

with those in ozone, and none in their dates of occurrence. This lack of agreement suggests a different underlying source of these occurrences for $PM_{2.5}$ from that for ozone.

Despite the differences in the data of Tables 3.2 and 3.3, they do show some similarities. For all the 17 occurrences listed in Table 3.3 that show large differences in $PM_{2.5}$ between the two downscaling cases, the statistical d-s case once again has the larger biases with respect to observations, ranging from 0.42 to 14.26 $\mu g\ m^{-3}$. As with ozone, there is more negative bias (in 7 of the 17 occurrences) in the dynamical d-s case with respect to measurements, with the bias ranging from -3.52 to 7.81 $\mu g\ m^{-3}$. Also, as with ozone, the difference in $PM_{2.5}$ between the two cases in a given grid cell is not proportional to the differences in daily burned area within the cell, which is zero or negligible for both cases in most of the 17 occurrences. These large differences could be a result of the differences in daily fire activity in adjacent grid cells upwind, due to the larger burned area in the statistical d-s case than in the dynamical d-s case. This is true of each of the grid cells in Table 3.3 that had an adjacent grid cell with a fire on a given day.

As in the case of ozone, the domain-wide 24-hour trend (Figure 3.S10 in the Supplement) of absolute difference in $PM_{2.5}$ between the downscaling cases shows a very small median difference (on the order of 10^{-3} $\mu g\ m^{-3}$), but with even less variability than for ozone, and slightly more temporal variability at the upper end of the range than for ozone in Figure 3.S2. Primary emissions and their variability could contribute to a greater degree in these differences, as primary PM is a significant fraction (~ 23%) of these wildfire emissions excluding CO. The spatial distribution of the maximum absolute differences in $PM_{2.5}$ throughout the fire season in the lowest model layer (right panel of Figure 3.S11 in the Supplement) shows a similar pattern overall to the ozone differences in that it is appreciable mostly over the central and northeastern parts of the domain. However, the spatial pattern for $PM_{2.5}$ concentrations more closely

resembles that of the column-total point wildfire emissions of $PM_{2.5}$ (Figure 3.S11, left panel), than in the case of ozone, particularly in Southeastern Missouri and Appalachia. This indicates the greater role in the $PM_{2.5}$ concentration differences played by primary wildfire PM emissions than in the case of ozone.

Discussion

Across all three cases modeled, $PM_{2.5}$ shows an increasingly negative bias with respect to IMPROVE in the late spring through the summer, changing to a progressively more positive bias from autumn into winter, which has the largest MFE and MFB of 56.2% and 44.5%, respectively. The overall model performance for $PM_{2.5}$ is acceptable in all cases, but masks compensating errors in the PM constituents. Of these, the signature species for wildfires are EC and OC. Model performance for EC, which is primarily emitted in wildfires, is good-to-acceptable and mostly positively biased over the fire season. Taken alongside the poor performance for OC, which is mostly secondarily produced from precursors emitted from wildfires and other natural and anthropogenic sources, this indicates that wildfire EC emissions are not the driver of the pronounced negative biases seen in $PM_{2.5}$ in the summer months. The OC biases are mostly negative and most pronounced in the warmer months; they are smallest for statistical d-s and greatest for the NEI, which as noted previously, had an underestimation of emissions in the 2010 wildfire inventory due to the undercounting of fires below canopy by MODIS (Pouliot et al., 2008). This underestimate would be greatest in the months when the canopy cover is greatest, and could also account for EC being better predicted in June and August with the downscaled inventories than with the NEI inventory.

Another, and perhaps the biggest contribution to the low bias in $PM_{2.5}$ in summer comes from species other than the major organic and inorganic components (labelled “Other” in Figure 3.7).

Other PM is a larger fraction of the observed summer-average $PM_{2.5}$ concentration than even sulfate (Figure 3.7). Fine PM is the second largest component (~ 43%) after primary OC in wildfire PM emissions in all three inventories, and is the primary contributor to Other PM from wildfires in CMAQ. Given the uniform PM speciation profile across all seasons in all three wildfire inventories in this study, and the relatively good comparisons of Other PM with IMPROVE observations in spring and autumn, wildfire emissions are not the likely source of the poor summertime performance for this species. Fine dust episodes in the eastern U.S. and the Caribbean in the summer have been shown through satellite observations to be associated with long-range transport from the Sahel (Prospero, 1999; Prospero et al., 2014). The severe summertime underprediction of Other PM suggests a need to refine the eastern boundary conditions, which were the same across the three CMAQ simulations, specifically with respect to their intra-seasonal variability.

The large negative biases in OC predictions, which are seen across both rural and urban networks, are likely to be a result of underprediction in the CMAQ v5.0.2 secondary organic aerosol (SOA) mechanism rather than in the primary wildfire OC emissions. Some of the underestimation could come from the assumed NEI temporal profiles for emissions from smaller wildfires that are less than a full day in duration (Wilkins et al., 2018). Residential wood combustion has also been shown to be as a source of underestimation of carbonaceous PM in the NEI in a 2007 study over the Southeastern U.S. (Napelenok et al., 2014), and this possibility is supported by the better model performance for OC at CSN (urban) sites compared to IMPROVE (rural) sites. The potential role of residential wood combustion would need to be further

examined within the context of the spatial and temporal distribution of emissions from this source for our modeling domain in 2010.

The very good performance for OC in the winter that gradually degrades going from cool to warm months is an indication that temperature dependence of precursor emissions may not be well represented either in the fire emissions model, or in the SOA formation pathways in the CMAQ organic chemistry formulation. As the emission factors in the BlueSky fire emissions model do not adjust for the temperature dependence of individual PM species, the CMAQ SOA model is the most likely source of the seasonal variability of this bias. The underprediction of SOA in CMAQ is addressed somewhat by the volatility basis set (VBS--Donahue et al., 2013) implemented in a later version of CMAQ (CMAQ-VBS -- Koo et al., 2014) than the one used here. However, large uncertainties still remain in the representation of semi-volatile and intermediate VOCs (IVOCs), especially in the primary emission estimates, and in the SOA formation pathways according to Woody et al. (2016). These authors have argued for improving the CMAQ-VBS model further by including representations of semi-volatile organic compounds (SVOCs) in the form of primary organic aerosol (POA), and IVOCs.

In contrast to OC, EC has its highest MFB and MFE in winter for all the cases modeled. As EC is co-emitted with OC in biomass and biofuel combustion, this indicates that the emission factors, in particular, the OC/EC emission ratios used for non-wildfire combustion sources that are active in winter, e.g., biofuel, could account for the poor EC model performance. The monthly results for the EC and OC error metrics, which show a consistently higher MFB for EC than for OC indicate that the OC/EC emission ratios could also be an issue in wildfire emissions.

Our PM composition analyses show that the constituent driving total $PM_{2.5}$ performance is sulfate, due to its having the highest PM mass fraction. Wildfire emissions do not have a major

source contribution to the modeled sulfate concentration. Primary SO_x emissions constitute 1.8% of the total emissions from wildfires, as evidenced by the nearly constant concentration of SO_4 across the three modeled cases in every season. Thus, the sulfate overprediction (MFB > 30%) seen throughout the fire season is likely due to an overestimation in SO_x emissions from sources other than wildfires, or in the secondary sulfate production pathways in CMAQ, notably its cloud chemistry, rather than due to an overestimation of wildfire SO_4 emissions. In the other two major inorganic species, NO_3 and NH_4, there are large overpredictions for NO_3, most notably in autumn and winter, and largest (albeit by a small margin) in the statistical d-s case. Furthermore, the NH_4 overprediction is comparable to that of SO_4, and much smaller than that of NO_3 across all cases and seasons, suggesting that much of the NH_4 mass is associated with SO_4. The good-to-acceptable performance for NH_4, which has a significant contribution from wildfire-emitted NH_3, increases the likelihood that wildfire emissions, which are the only source of difference among the three inventories, are not the driver of the large positive bias in NO_3 in the cooler months, and clearly not in the winter. The overpredictions in SO_4 and NH_4, and to a lesser extent, in NO_3, offset the substantial underprediction in OC that persists throughout the fire season, leading to an acceptable aggregate $PM_{2.5}$ performance.

It is worth noting that in the NO_3 performance, the NMB values for NO_3 in Table 3.S5, as well as the seasonally averaged PM concentrations (Figure 3.7) show a uniformly positive bias for this constituent, while a number of the monthly MFB values in Figure 3.6 are negative (although on a seasonal-average basis, they are consistent with the results of Figure 3.7). The MFB metric is considered a better alternative to NMB at low concentrations (Boylan and Russell, 2006), as often occur in NO_3 over the Southeast. This is because MFB normalizes the bias with respect to the average of modeled and observed values, keeping it bounded (between -

200% and +200%), whereas NMB normalizes the bias with respect to observations, and can become very large at low concentrations. However, somewhat misleading results such as cited here for NO_3 are known to occur in using the MFB. Alternative metrics that avoid this issue while preserving its desirable features (boundedness and symmetry) have been proposed (Yu et al., 2006), but have not yet been adopted in standard AQ model evaluations. We have therefore based our performance evaluation on a variety of analyses.

The intermodel comparisons for $PM_{2.5}$ show similar difference patterns to those for ozone among the modeled cases in the scatterplots, but the largest differences are often not coincident spatially or temporally with those for ozone, indicating an alternative contributing source. While ozone is entirely produced in secondary chemical reactions from the primary emissions of NO_x and VOC, PM can have both primary and secondary components. It is likely that the PM concentration differences among the modeled cases are driven more by differences in their primary PM emissions. This is also supported by the similarity in the spatial patterns of maximum absolute difference over the fire season in $PM_{2.5}$ column emissions and surface concentrations between the two downscaled cases.

Conclusions

We have compared two wildfire emissions estimation methods that are both based on projections of AAB from a statistical model, to an empirically based benchmark inventory compiled by the U.S. EPA, by using them in AQ simulations of a historical period (2010). We compared the modeled ambient concentrations among the three cases simulated with these inventory methods, and between each case and air quality observations from various ground-

based networks for 1-h ozone, maximum daily 8-hour average ozone (MDA8), and for $PM_{2.5}$ and its constituents.

Our results show nearly identical performance for all three cases against AQS network observations for hourly ozone. The O_3 differences among the cases are 0.08% - 0.93%, but the biases are much larger for any of the cases with respect to AQS observations, being 13% - 25% over the entire year. Ozone has acceptable performance in spring through mid-summer, but degrades (MFE > 50%) in the cooler months, particularly in the fire-free winter. These results suggest that wildfire emissions are not a major contributor to the model errors in ozone. The statistical d-s has a significant high bias in O_3 with respect to the other two methods at specific locations in October, due to its larger AAB estimates. Large ozone differences between the two downscaling methods occur mostly in the northeastern quadrant of the domain, and downwind from peak differences in VOC and NO_x column emissions from wildfires in eastern Missouri and Appalachia. These results indicate that transport and secondary chemical transformations of precursor emissions from high fire activity areas to fire-free areas downwind drive the largest O_3 differences seen between the two downscaling methods.

The $PM_{2.5}$ model performance against observations from the IMPROVE network is acceptable throughout the year for all three methods, but is the result of compensating biases in SO_4 (positive) and OC (negative) in almost every month. Sulfate, with its highest PM mass fraction, drives the $PM_{2.5}$ bias, which is still within acceptable levels. The minimal contribution of SO_x to the total emissions from wildfires points to other anthropogenic SO_x sources or the CMAQ SO_4 production pathways as the main cause of this overprediction. EC and NH_4; which are key constituents in the primary emissions from wildfires also have good-to acceptable performance in almost all months. OC, which has a larger contribution from secondary chemical

reactions, has its largest underpredictions (beyond acceptable levels) in the summer, for the NEI. Given the good-to-acceptable performance for EC, which is co-emitted in wildfires, the likely cause of the OC biases is other VOC sources, or secondary chemical reactions in the CMAQ model. Future assessments with CMAQ-VBS (Koo et al., 2014) or even later enhancements to the SOA mechanism suggested by Pye et al. (2015) could help address the SOA underprediction and improve the OC model performance overall. The dramatically better OC model performance at urban sites compared to rural sites also indicates potential underestimates of residential wood combustion and biogenic emissions in rural areas.

Particulate NO_3, like much of OC, is formed through secondary processes. Its much lower concentrations in the summer than in the other seasons are correlated with that season's larger overpredictions of SO_4 and smaller overpredictions of NH_4, since less NH_3 is available for NO_3 formation. Kelly et al. (2014) cite gas-particle partitioning in the ISORROPIA II thermodynamics model as one of the factors contributing to the underprediction of NO_3 in CMAQ version 5.0; this may have some bearing on our summer NO_3 results. The severe overprediction of NO_3 in combination with larger overpredictions in NH_4 in the rest of the fire season indicates possible overestimates in the emissions of NH_3 or anthropogenic NO_x; the latter is more likely, as NH_4 performance is acceptable over these months.

As with ozone, the much smaller (1% - 8%) intermodel differences among the three wildfire emission methods for $PM_{2.5}$ than their individual biases with respect to observations (-14% - +51% at IMPROVE sites) during the fire season indicate that modeling uncertainties other than wildfire emissions contribute the larger part of the model bias. Differences in PM between the two downscaling cases also confirm our previous conclusions for ozone, that their biggest impact is in fire-free locations downwind from regions of high fire activity, but with a bigger

contribution from the transport of primary PM emissions. These analyses, however, do not clearly point to a superior candidate for estimating wildfire emissions, as all three methods have uncertainties. On average, the statistical d-s predicts $PM_{2.5}$ ~ 7% higher than the other methods in the summer when all methods underpredict observations, and ~ 4% higher in the remainder of the fire season when they all overpredict observations, as a direct result of its higher AAB estimates. To allow one-to-one comparisons of the two downscaling methods in their wildfire emissions estimates, Shankar et al. (2018) used a single GCM (CGCM31) for the statistically downscaled meteorological inputs in these AAB estimates, rather than the full ensemble of GCM results used in Prestemon et al. (2016). One avenue for future improvements could be the use of the statistical d-s emissions estimates from the full ensemble in future assessments. Multi-model ensembles are important for bracketing uncertainties in model results. Of the two downscaling methods, dynamical d-s compares more closely with the NEI, which has the smallest biases with respect to observations except in summer. Both these methods underpredict summertime $PM_{2.5}$, but for different reasons. In the case of dynamical d-s, which estimated much lower wildfire emissions than statistical d-s (Shankar et al., 2018), the underprediction is likely due to the overprediction of convective precipitation in summer by the WRF 3.4.1 model used in its AAB estimation inputs. This bias could be compounded by the propagation of similar bias in the WRFG model from which those WRF simulations were nested down. In the NEI's early versions of the SMARTFIRE system, the likely cause of underprediction is the undercounting of fires below canopy by MODIS in the summer. Later versions of WRF and SMARTFIRE have

addressed their respective underestimation issues, and could benefit such evaluations in the future.

In conclusion, both the downscaling methods are seen to perform comparably to the NEI wildfire inventory for ozone throughout the year, and better than the NEI for total $PM_{2.5}$ in the summer, in partial confirmation of our hypothesis. The good-to-acceptable performance for primarily emitted EC and NH_4 (from ammonia), especially by the downscaling methods, provides confidence in our overall methodology for estimating wildfire emissions, and in the likelihood that these emissions are not the major drivers of the biases in PM species dominated by secondary production (OC and NO_3). That the largest errors in PM occur in SO_4, which has a very small contribution from wildfires, and in the case of ozone in the fire-free winter months, point to chemical production pathways of these pollutants from non-wildfire sources as fruitful targets for future model improvements. Overall, the downscaling methods meet the criterion of being comparable to the NEI in simulating the air quality impacts of current-day wildfires while enabling assessment of those impacts much farther into the future.

Code Availability. CMAQ model code as well as the plotting and analysis software used in this paper are available to registered users of the Community Modeling and Analysis System through https://www.cmascenter.org.

Data Availability. Data used in the figures and tables are archived in the University of North Carolina at Chapel Hill mass storage system. They are available upon request from the corresponding author.

Author Contributions. US, DM, and JPP designed the research. AX and KT prepared all meteorological data used in the CMAQ and daily fire activity modeling. KT and US prepared the daily fire activity inputs for the wildfire emissions estimates. BHB and MO prepared the

emissions inputs to CMAQ. DY and US conducted the CMAQ simulations and the analysis of results. US, DM, JPP, and WV participated in the editing of the manuscript.

Acknowledgments

The authors thank Dr. George Pouliot, Dr. Joseph Wilkins and Dr. Matt Woody (U.S. EPA) for their helpful discussions regarding the NEI and CMAQ model performance. This research was supported entirely through funding provided by USDA Forest Service to the University of North Carolina at Chapel Hill under joint venture agreement 11-JV-11330143-080.

Table 3.1. Summary of cases simulated in modeling study

Case Name	Wildfire Inventory Method			Other Sector Emissions
	Annual Fire Activity Estimates	**Daily Fire Activity**	**Emissions Estimates**	
NEI Bench-mark	Empirical annual totals derived from the aggregation of acres burned in individual fire events	2010 MODIS fire counts matched to ground-based reports of areas burned per fire event using SMARTFIRE2[11]	BlueSky/ CONSUME[12]	NEI 2005
Statistical d-s	Meteorological inputs for the Annual Area Burned (AAB) estimation model[13] obtained from a Canadian General Circulation Model version 3.1 (CGCM31)/A2 greenhouse gas emissions scenario realization, statistically downscaled over the Southeastern domain at 12-km x 12-km resolution. County-level population and income, and land use inputs to the AAB estimation from census tracts and historical land use records.	Disaggregated from AAB by the Fire Scenario Builder (FSB) [14] using WRF meteorology	BlueSky/ CONSUME	NEI 2005
Dynamical d-s	Meteorological inputs for the AAB estimation model obtained from a simulation of the Weather Research and Forecasting (WRF) Model version 3.4.1 for the Southeastern domain at 12-km x 12-km resolution, which is nested down from a WRF simulation over North America dynamically downscaled from a CGCM3/A2 scenario realization [15]. County-level population, income, and land use inputs to the AAB estimation from census tracts and historical land use records.	Disaggregated from AAB by the FSB, using WRF meteorology	BlueSky/ CONSUME	NEI 2005

[11] Pouliot et al. (2008)

[12] Larkin et al. (2009)

[13] Prestemon et al. (2016)

[14] McKenzie et al. (2006)

[15] Mearns et al. (2009)

Table 3.2. Ozone at selected locations from statistical d-s, dynamical d-s and AQS✦ network observations

Date	Time (GMT)	AQS Site ID	O_3 (ppb)			O_3 Bias (ppb)		Daily burned area (ha)⋆	
			Obs.	Stat. d-s†	Dyn. d-s‡	Stat. d-s	Dyn. d-s	Stat. d-s	Dyn. d-s
10/9/2010	3:00	171170002[1]	30	3.0	0.36	-27	-30		
10/16/2010	14:00		53	90	43	37	-10		
10/30/2010	10:00		35	59	39	24	4		
10/8/2010	21:00	171193007[2]	1	7.2	0.034	6	-1		
10/16/2010	11:00		31	77	37	46	6		
10/29/2010	16:00		12	0.059	0.024	-12	-12	28.7 *	23.4 *
10/30/2010	10:00		24	54	31	30	7		
10/10/2010	20:00	210590005▲[,3]	16	4.3	2.7	-12	-13		
10/17/2010	21:00		9	10	3.6	1	-5		
10/30/2010	10:00		34	54	32	20	-2		
10/9/2010	18:00	210910012▲[,3]	42	0.97	0.13	-41	-42		
10/10/2010	21:00		21	0.067	0.048	-21	-21		
10/17/2010	21:00		15	1.5	0.14	-13	-15		
10/30/2010	11:00		38	60	37	22	-1		
10/8/2010	20:00	291831002⚑[,4]	8	0.29	0.0024	-8	-8		
10/16/2010	11:00		45	70	37	25	-8		
10/22/2010	17:00		37	20	10	-13	-23	201 *	176 *
10/29/2010	16:00		12	0.0048	0.000092	-12	-12	28.7 *	23.4 *
10/30/2010	10:00		42	60	35	18	-7		
10/16/2010	9:00	291860005[5]	38	72	44	34	6	393 *	
10/8/2010	18:00	295100085⚑[,4]	4	0.019	0.0026	-4	-4	212 *	
10/16/2010	16:00		30	64	32	34	2		
10/22/2010	16:00		27	23	12	-4	-15		
10/29/2010	16:00		20	5.6	0.028	-14	-20	28.7 *	23.4 *
10/30/2010	16:00		36	1.1	0.55	-35	-35		
9/6/2010	10:00	390490037[6]	45	69	42	24	-3		
9/6/2010	10:00	390490081[6]	42	64	39	22	-3		
10/10/2010	19:00	471650007[7]	35	0.76	0.47	-34	-35		
10/17/2010	18:00		40	1.4	0.71	-39	-39		
10/18/2010	16:00		66	7.1	3.8	-59	-62		
10/31/2010	17:00		49	13	7.9	-36	-41	22.6 *	
9/9/2010	20:00	511611004[8]	55	59	29	4	-26	391 *	
9/5/2010	20:00	540390010[9]	26	16	2.1	-10	-24	284 *	36.6 *
9/9/2010	11:00		33	66	35	33	2	323 *	

Symbols key: ✦Air Quality System. ⋆A blank in these columns indicates that there were no areas burned inside or within a few grid cells of the monitored cell. †Statistical d-s; ‡Dynamical d-s. *Denotes the area burned in an upwind location within 1-2 grid cells of the monitored cell. ▲KY-OH sites in Fig. 3.S3; ⚑MO-IL sites in Fig. 3.S3. AQS site key: [1]Nilwood, Illinois; [2]Wood River, Illinois; [3]Owensboro, Kentucky; [4]St. Louis, Missouri; [5]Bonne Terre, Missouri; [6]Columbus, Ohio; [7]Hendersonville, Tennessee; [8]Roanoke, Virginia; [9]Charleston, West Virginia.

Table 3.3. $PM_{2.5}$ at selected locations from statistical d-s, dynamical d-s and the IMPROVE✦ network

Date	IMPROVE Site Name and State	$PM_{2.5}$ (µg m^{-3})			$PM_{2.5}$ Bias (µg m^{-3})		Daily burned area (ha)⋆	
		Obs.	Stat. d-s	Dyn. d-s	Stat. d-s	Dyn. d-s	Stat. d-s	Dyn. d-s
9/5/2010	Brigantine NWR◈, NJ[1]	4.59	17.4	10.72	12.81	6.13	313 *	
8/27/2010	Cadiz, KY[2]	8.44	18.41	11.00	9.97	2.56		
8/27/2010	Cherokee Nation, OK[3]	9.48	13.34	8.62	3.86	-0.87		
8/21//2010	El Dorado Springs, MO[4]	8.88	19.08	16.69	10.2	7.81		
8/24/2010		12.27	14.40	9.09	2.13	-3.17		
9/5/2010		4.79	9.34	5.27	4.56	0.49		
9/23/2010		7.20	7.62	5.09	0.42	-2.11		
9/5/2010	Great Smoky Mountains NP×, TN[5]	3.99	12.5	7.25	8.51	3.26		
6/7/2010	Hercules Glades, MO	4.10	12.35	4.18	8.25	0.08	59.0 *	
6/19/2010		6.14	10.77	6.48	4.63	0.34		
8/6/2010	James River Face WA⊡, VA[6]	14.12	25.45	10.60	11.33	-3.52	48.0 *	
9/17/2010		7.38	11.59	7.01	4.21	-0.37		
11/10/2010	Lake Sugema, IA[7]	10.81	16.68	8.50	5.87	-2.31	162 *	106 *
6/7/2010	Linville Gorge, NC[8]	6.40	9.89	6.38	3.49	-0.02	20.3 *	
9/11/2010	Mingo, MO	3.63	12.86	6.28	9.23	2.65		
10/2/2010		5.03	19.29	8.56	14.26	3.53		
10/29/2010	Sikes, LA[9]	4.46	13.35	8.81	8.89	4.35		

Symbols key: ✦Interagency Monitoring of Protected Visual Environments network; ⋆a blank in these columns indicates that there were no areas burned inside or within a few grid cells of the monitored cell. * denotes the area burned in an upwind location within 1-2 grid cells of the monitored cell. Federal Class I Area designations: ◈National Wildlife Refuge; ×National Park; ⊡Wilderness Area. State abbreviations: [1]New Jersey; [2]Kentucky; [3]Oklahoma; [4]Missouri; [5]Tennessee; [6]Virginia; [7]Iowa; [8]North Carolina; [9]Louisiana.

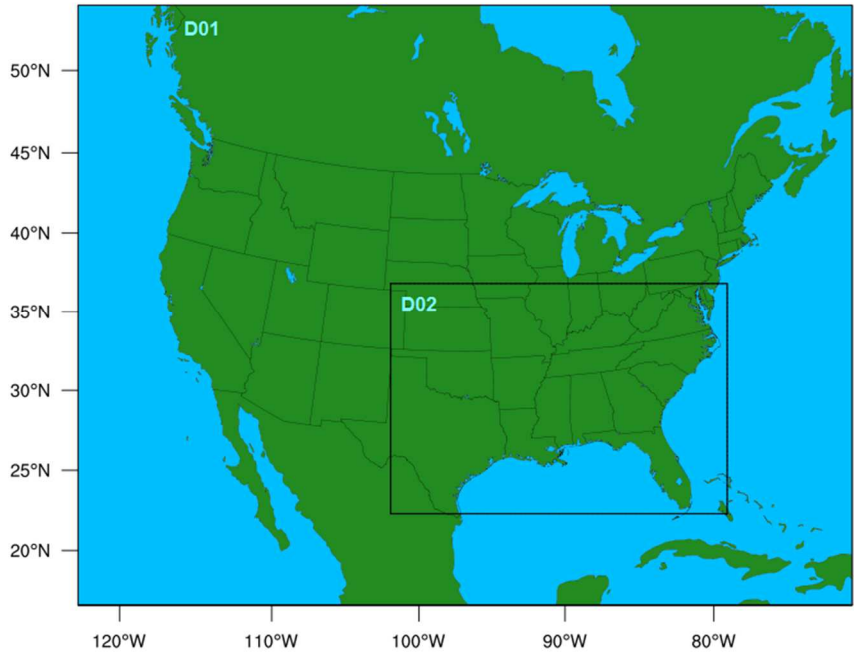

Figure 3.1. Modeling domains for the meteorological model: D01 at 50-km x 50-km grid spacing; D02 at 12-km x 12-km grid spacing

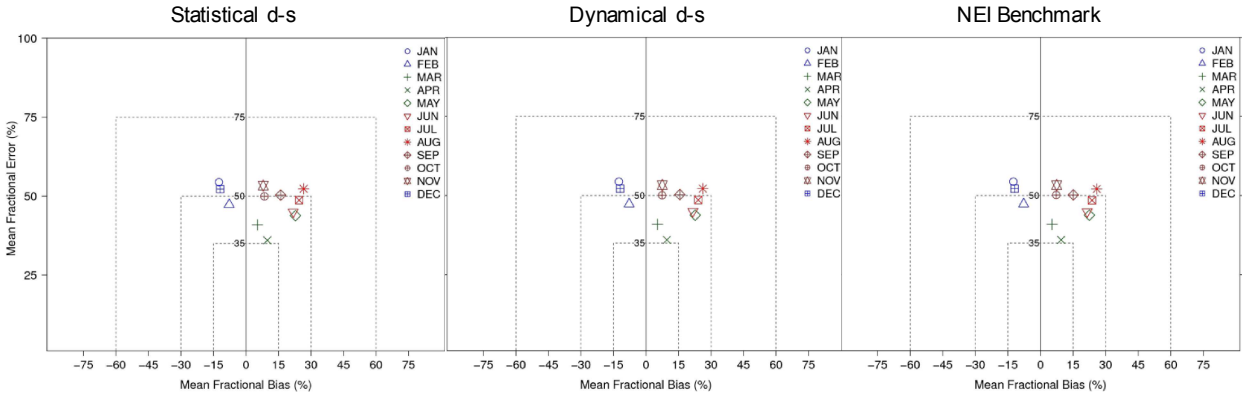

Figure 3.2. Monthly average performance for 1-h ozone: mean fractional error (%) on the vertical axis vs. mean fractional bias (%) relative to observations from the Air Quality System. L: statistical d-s; C: dynamical d-s; R: NEI benchmark.

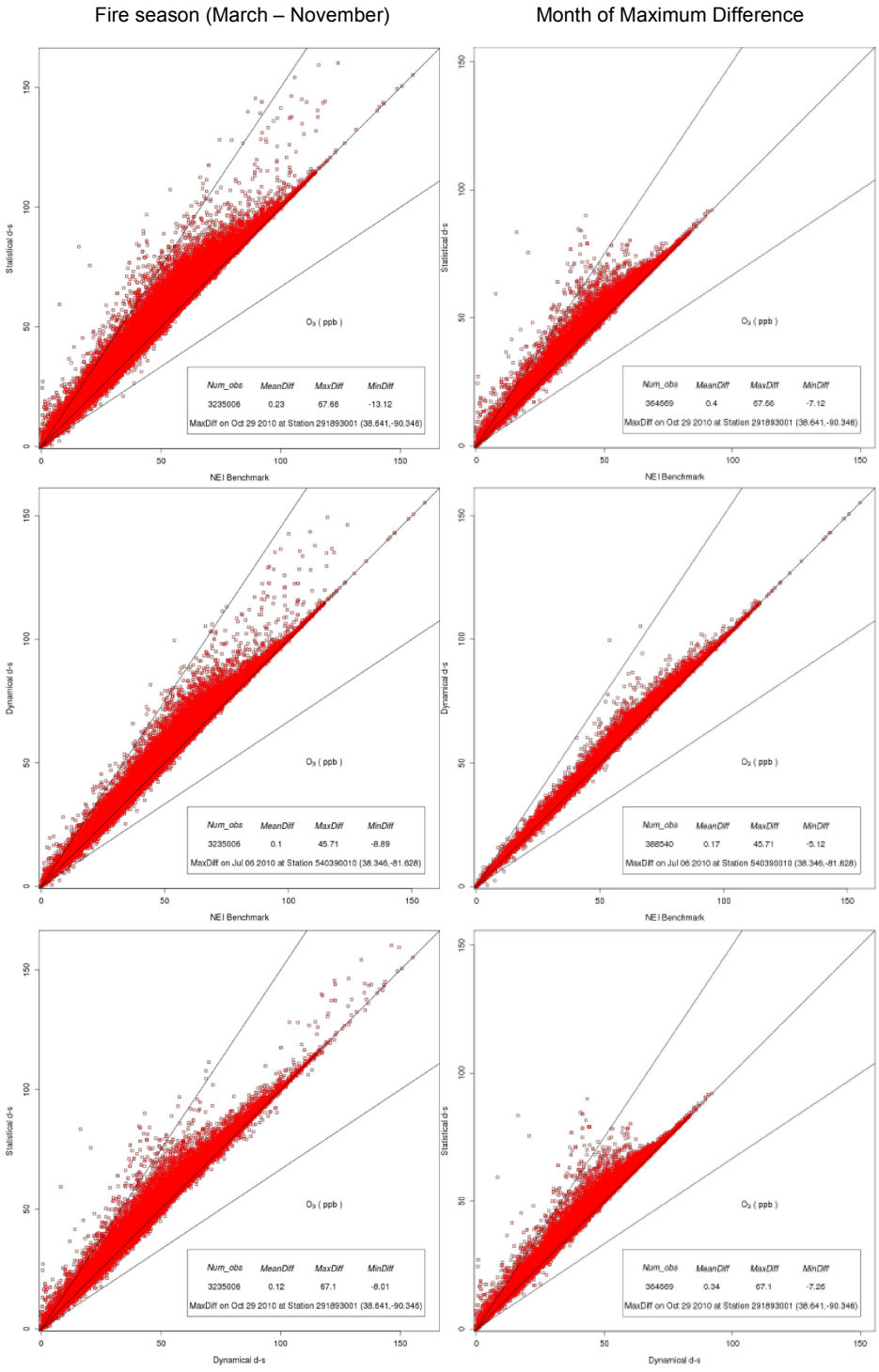

Figure 3.3. Comparisons of wildfire emissions methods for 1-h O_3 (ppb) predicted at grid cells containing Air Quality System (AQS) monitors and wildfires in 2010. L: fire season (March – November); R: top and bottom, October; middle, July. The mean, maximum and minimum intermodel difference (vertical axis variable – horizontal axis variable), denoted, respectively,

MeanDiff, MaxDiff and MinDiff, and the dates and coordinates of their occurrence are shown in the plot legend.

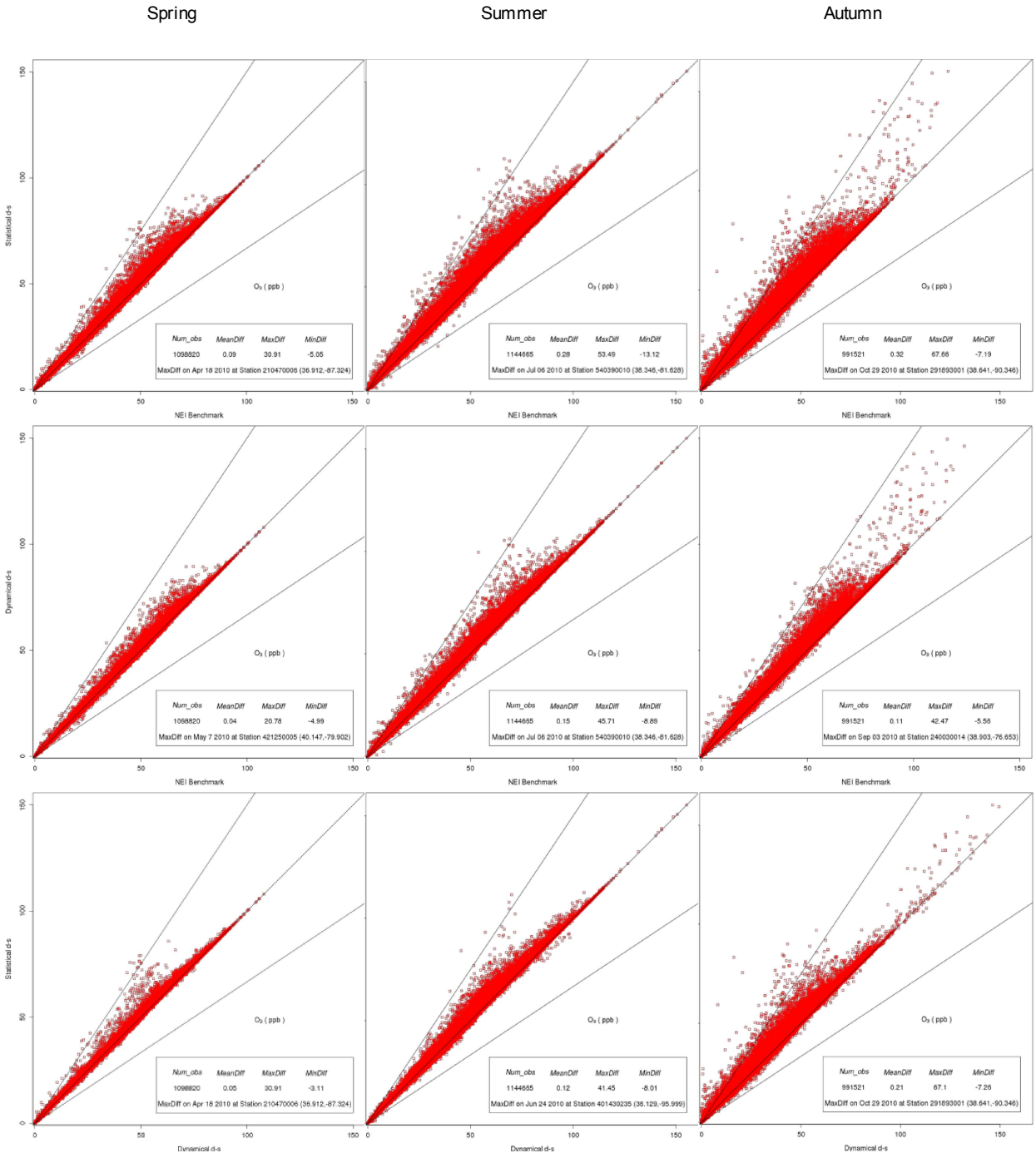

Figure 3.4. Seasonal comparisons of wildfire emissions methods for 1-h O_3 (ppb) predicted at grid cells containing both Air Quality System (AQS) monitors and wildfires in 2010. The mean, maximum and minimum intermodel difference (vertical axis variable – horizontal axis variable),

denoted, respectively, MeanDiff, MaxDiff and MinDiff, and the dates and coordinates of their occurrence are shown in the plot legend.

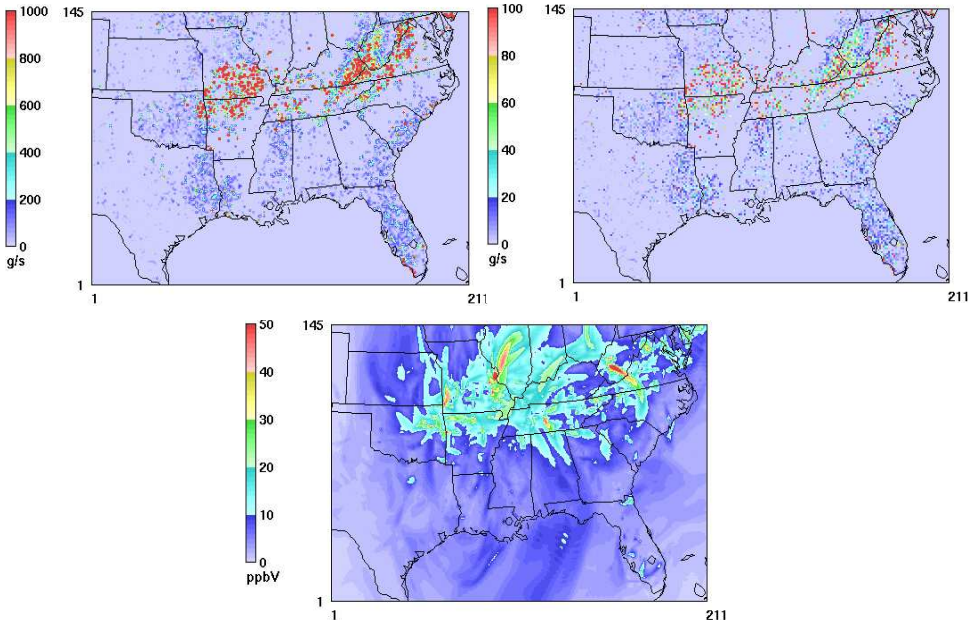

Figure 3.5. Maximum absolute difference between statistical d-s and dynamical d-s in each grid cell over the whole fire season in: Row 1, L – hourly VOC column emissions (g s^{-1}); Row 1, R – hourly NO_x column emissions (g s^{-1}); Row 2 – hourly O_3 mixing ratios (ppbV) in model layer 1. Here the fire season is defined as April 23 – November 30; almost all grid cell maxima in absolute difference in hourly O_3 occurred in this time period.

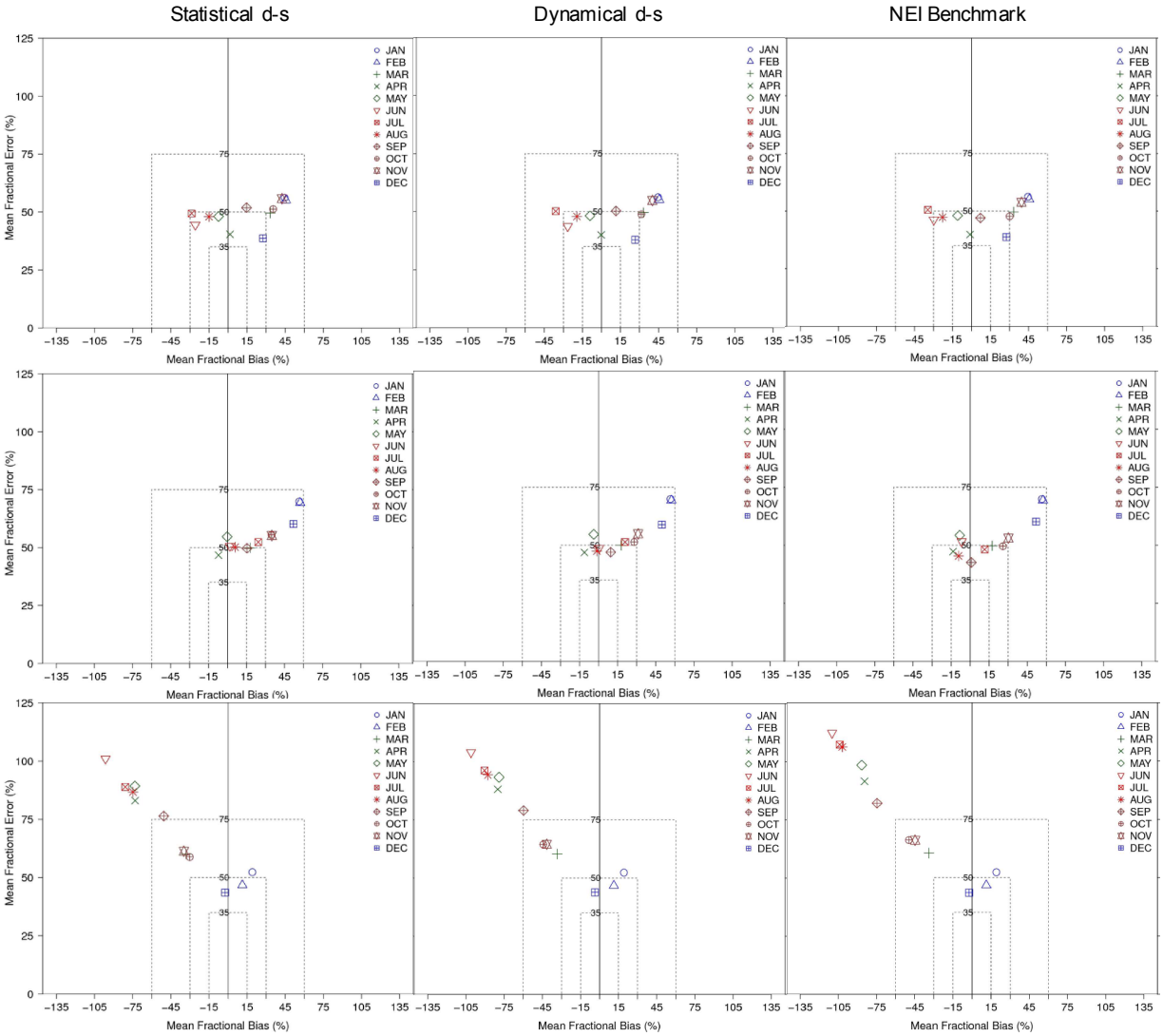

Figure 3.6. Monthly-averaged model performance for total $PM_{2.5}$ and key wildfire constituents relative to observations from the IMPROVE monitoring network. Row 1, $PM_{2.5}$; Row 2, elemental carbon (EC); Row 3, organic carbon (OC).

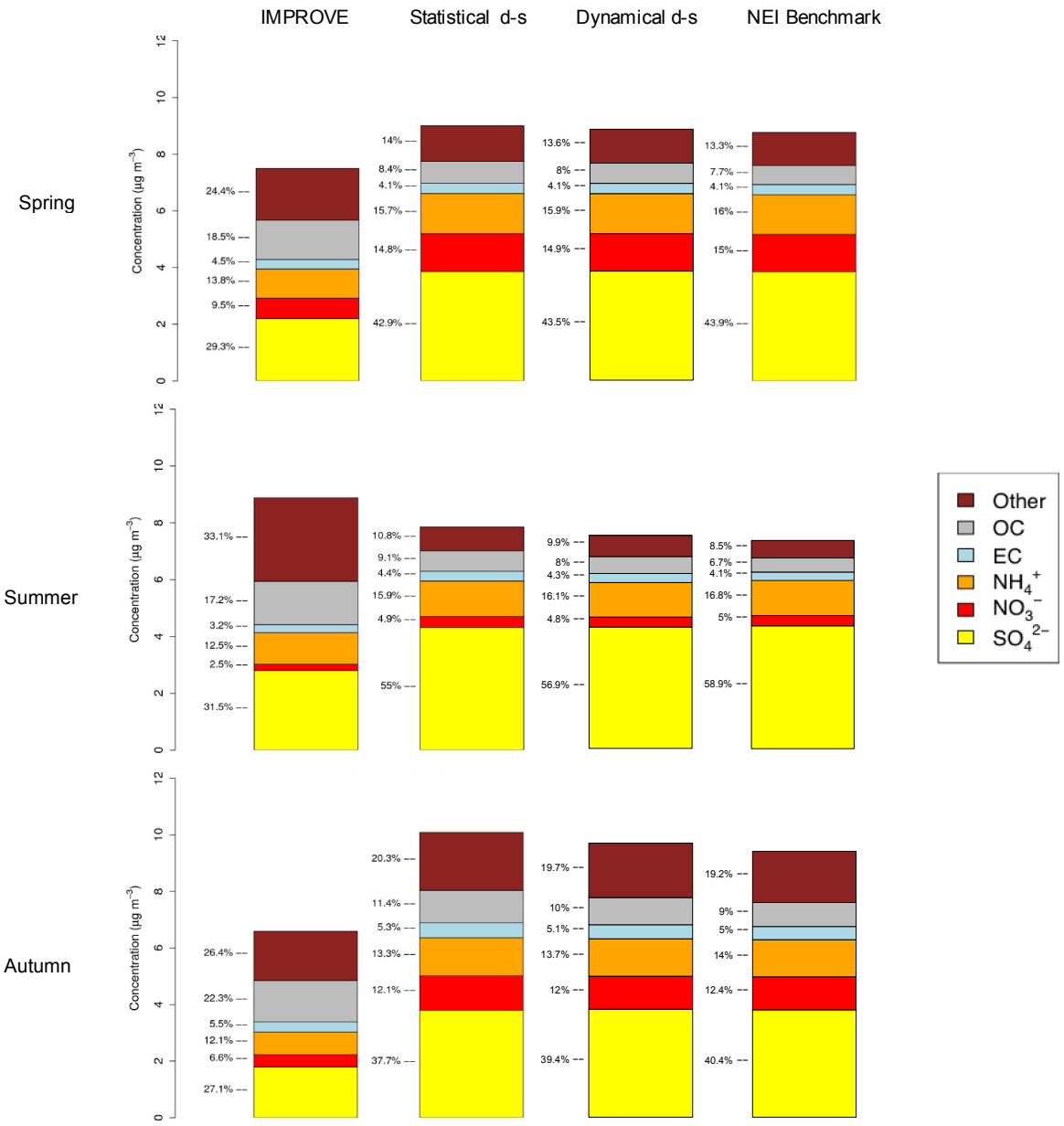

Figure 3.7. Domain-wide seasonally averaged total mass of $PM_{2.5}$ (µg m^{-3}) and fractional mass of major constituents during the fire season compared to observations from the IMPROVE monitoring network.

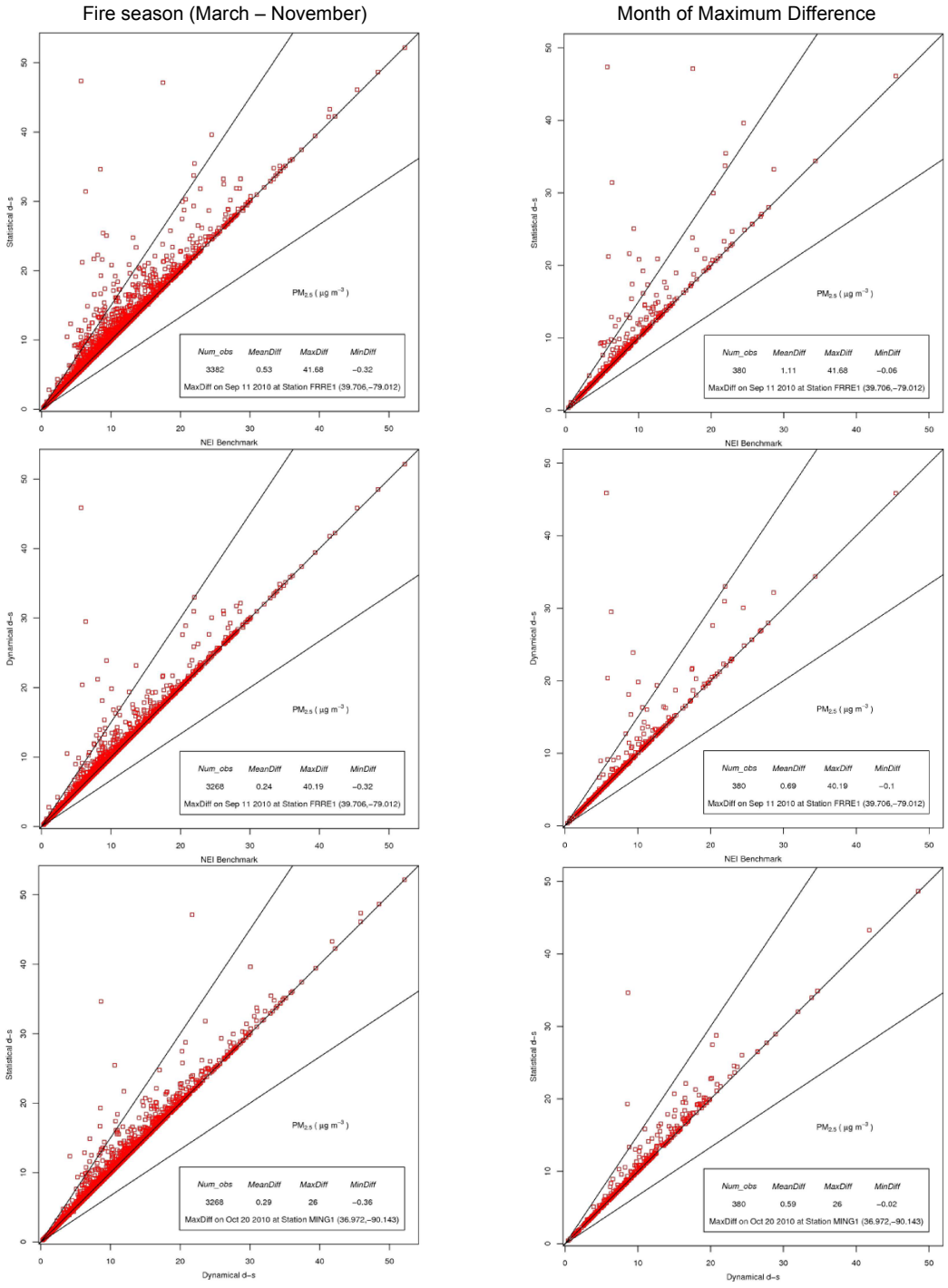

Figure 3.8. Comparisons of wildfire emissions methods for $PM_{2.5}$ (μg m^{-3}) predicted at grid cells containing both Interagency Monitoring of PROtected Visual Environments (IMPROVE) monitors and wildfires in 2010. The mean, maximum and minimum intermodel difference (vertical axis variable – horizontal axis variable), denoted, respectively, MeanDiff, MaxDiff and

MinDiff, and the dates and coordinates of their occurrence are shown in the plot legend. L: fire season (March – November); R: top and middle, September; bottom – October.

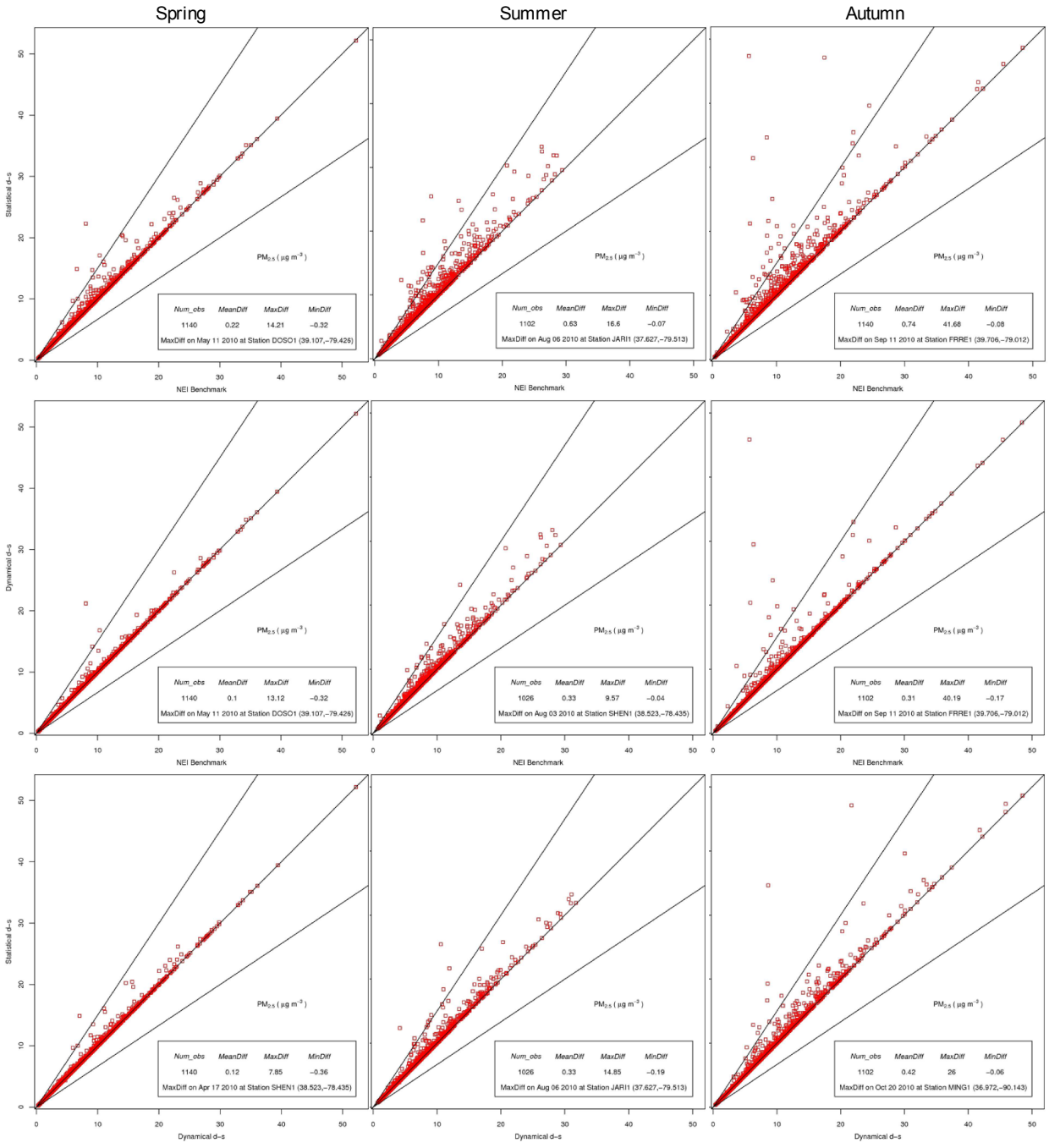

Figure 3.9. Seasonal comparisons of wildfire emissions methods for $PM_{2.5}$ (μg m^{-3}) predicted at grid cells containing Interagency Monitoring of PROtected Visual Environments (IMPROVE) monitors and wildfires in 2010. The mean, maximum and minimum intermodel difference

(vertical axis variable – horizontal axis variable), denoted, respectively, MeanDiff, MaxDiff and MinDiff, and the dates and coordinates of their occurrence are shown in the plot legend.

Supplemental Material for Chapter 3

Table 3.S1. Model performance statistics for monthly-averaged ozone vs. AQS✦ observations

	Ozone (ppb)				NME▲ (%)			NMB✖ (%)		
Month	AQS	Stat. d-s†	Dyn. d-s‡	NEI Bmrk*	Stat. d-s	Dyn. d-s	NEI Bmrk	Stat. d-s	Dyn. d-s	NEI Bmrk
Jan	24.4	25.3	25.3	25.3	38.4	38.4	38.4	3.6	3.6	3.6
Feb	28.2	28.9	28.9	28.9	33.3	33.3	33.3	2.4	2.4	2.4
Mar	34.0	37.1	37.1	37.1	31.5	31.5	31.5	9.0	9.0	9.1
Apr	38.4	41.9	41.8	41.8	28.4	28.4	28.4	9.2	9.0	8.8
May	32.9	40.3	40.3	40.2	39.1	39.1	39.0	22.7	22.6	22.4
Jun	30.6	37.5	37.4	37.4	38.6	38.5	38.4	22.7	22.5	22.3
Jul	29.0	36.5	36.3	36.2	41.9	41.7	41.5	25.5	25.0	24.5
Aug	30.7	39.1	39.0	38.7	45.5	45.3	45.0	27.3	26.8	26.2
Sep	30.0	34.8	34.6	34.4	40.0	39.9	39.6	16.0	15.5	14.8
Oct	30.2	32.6	32.3	32.2	37.7	37.8	37.8	8.0	6.8	6.7
Nov	25.0	29.3	29.2	29.2	43.3	43.2	43.2	17.2	16.8	16.7
Dec	24.0	24.4	24.4	24.4	35.3	35.3	35.3	1.8	1.8	1.8

Symbols key: ✦AQS: Air Quality System; ▲Normalized Mean Error; ✖Normalized Mean Bias; †Statistical d-s; ‡Dynamical d-s; *NEI Benchmark.

Table 3.S2. Model performance statistics for monthly-averaged total $PM_{2.5}$ vs. IMPROVE✦ observations

Month	Total $PM_{2.5}$ (μg m^{-3})				NME▲ (%)			NMB✖ (%)		
	IMPROVE	Stat. d-s†	Dyn. d-s‡	NEI Bmrk*	Stat. d-s	Dyn. d-s	NEI Bmrk*	Stat. d-s	Dyn. d-s	NEI Bmrk
Jan	7.0	11.5	11.5	11.5	75.9	75.9	75.9	65.1	65.1	65.1
Feb	8.4	13.7	13.7	13.7	71.7	71.7	71.7	63.1	63.1	63.1
Mar	7.2	10.8	10.8	10.8	64.7	64.8	64.7	50.0	49.9	49.9
Apr	8.5	9.3	9.1	9.0	43.4	42.2	41.7	9.2	6.6	5.3
May	7.6	7.4	7.2	7.1	47.5	47.1	46.0	-3.0	-4.9	-7.3
Jun	8.8	7.1	7.0	6.8	36.9	36.5	37.9	-19.8	-20.8	-23.4
Jul	9.8	8.2	7.5	7.6	41.2	40.0	40.2	-16.3	-23.7	-22.6
Aug	9.5	9.0	8.5	8.2	41.0	39.7	38.6	-5.2	-10.1	-13.3
Sep	7.6	9.9	9.5	8.7	61.6	57.2	48.8	30.6	24.8	15.2
Oct	6.9	10.8	10.2	10.1	69.0	63.0	61.1	56.2	47.9	45.7
Nov	6.5	10.9	10.5	10.5	79.4	78.3	74.9	67.3	64.4	61.6
Dec	8.0	10.9	11.3	10.9	46.6	45.7	46.6	36.4	35.5	36.4

Symbols key: ✦Interagency Monitoring of Protected Visual Environments network; ▲Normalized Mean Error; ✖Normalized Mean Bias; †Statistical d-s; ‡Dynamical d-s; *NEI Benchmark.

Table 3.S3. Model performance statistics for monthly-averaged sulfate (SO_4) vs. IMPROVE$^+$ observations

	SO_4 (μg m^{-3})				NME$^\blacktriangle$ (%)			NMB$^\blacktriangle$ (%)		
Month	IMPROVE	Stat. d-s†	Dyn. d-s‡	NEI Bmrk*	Stat. d-s	Dyn. d-s	NEI Bmrk	Stat. d-s	Dyn. d-s	NEI Bmrk
Jan	1.7	2.4	2.4	2.4	53.6	53.6	53.6	37.6	37.6	37.6
Feb	2.4	2.9	2.9	2.9	45.7	45.7	45.7	22.8	22.8	22.8
Mar	2.0	3.5	3.5	3.6	83.7	83.7	83.9	77.2	77.2	77.3
Apr	2.2	4.1	4.1	4.1	89.4	89.3	89.2	81.8	81.5	81.4
May	2.4	3.9	3.9	3.9	77.1	76.9	76.6	63.3	63.1	62.6
Jun	2.6	3.9	3.9	3.9	56.6	58.3	56.3	47.9	49.2	47.4
Jul	2.9	4.5	4.4	4.5	66.0	61.9	65.8	56.4	51.4	56.1
Aug	3.0	4.9	4.8	4.9	72.6	72.4	70.6	61.0	60.6	58.9
Sep	2.1	4.4	4.4	4.4	113.0	113.0	113.0	107.0	107.0	107.0
Oct	1.7	3.8	3.8	3.8	126.0	126.0	125.0	123.0	122.0	122.0
Nov	1.5	3.1	3.1	3.1	116.0	116.0	115.0	107.0	107.0	106.0
Dec	1.9	1.9	2.0	1.9	38.7	38.3	38.7	-1.4	0.6	-1.4

Symbols key: $^+$Interagency Monitoring of Protected Visual Environments network; $^\blacktriangle$Normalized Mean Error; $^\blacktriangleright$Normalized Mean Bias; †Statistical d-s; ‡Dynamical d-s; *NEI Benchmark.

Table 3.S4. Model performance statistics for monthly-averaged ammonium (NH_4) vs. IMPROVE[+] observations

	NH_4 (μg m^{-3})				NME[^] (%)			NMB[×] (%)		
Month	IMPROVE	Stat. d-s[†]	Dyn. d-s[‡]	NEI Bmrk*	Stat. d-s	Dyn. d-s	NEI Bmrk	Stat. d-s	Dyn. d-s	NEI Bmrk
Jan	1.2	1.3	1.3	1.3	40.4	40.4	40.4	8.6	8.6	8.6
Feb	1.6	2.0	2.0	2.0	44.8	44.8	44.8	25.6	25.6	25.6
Mar	1.1	1.7	1.7	1.7	68.0	68.0	68.1	53.7	53.7	53.7
Apr	1.0	1.5	1.4	1.4	67.7	67.0	66.3	42.2	41.1	40.4
May	1.0	1.1	1.1	1.1	57.0	56.6	56.2	7.4	6.6	5.5
Jun	1.1	1.1	1.1	1.1	47.1	48.0	47.2	7.4	8.0	6.4
Jul	1.2	1.3	1.3	1.3	49.7	45.7	48.9	15.0	7.8	11.7
Aug	1.2	1.3	1.3	1.3	54.7	54.6	53.5	9.3	8.0	7.3
Sep	0.9	1.3	1.3	1.2	75.0	73.3	69.1	48.7	46.8	42.2
Oct	0.7	1.3	1.3	1.3	93.8	92.2	91.8	80.0	78.2	77.6
Nov	0.8	1.4	1.4	1.4	97.4	97.2	95.8	81.2	79.4	79.4
Dec	1.3	1.1	1.1	1.1	31.7	31.5	31.7	-16.2	-16.8	-16.2

Symbols key: [+]Interagency Monitoring of Protected Visual Environments network; [^]Normalized Mean Error; [×]Normalized Mean Bias; [†]Statistical d-s; [‡]Dynamical d-s; *NEI Benchmark.

Table 3.S5. Model performance statistics for monthly-averaged nitrate (NO_3) vs. IMPROVE$^+$ observations

	NO_3 (μg m^{-3})				NME$^\blacktriangle$ (%)			NMB$^\blacktriangleright$ (%)		
Month	IMPROVE	Stat. d-s†	Dyn. d-s‡	NEI Bmrk*	Stat. d-s	Dyn. d-s	NEI Bmrk	Stat. d-s	Dyn. d-s	NEI Bmrk
Jan	1.8	2.4	2.4	2.4	77.4	77.4	77.4	36.2	36.2	36.2
Feb	2.3	3.9	3.9	3.9	87.8	87.8	87.8	68.2	68.2	68.2
Mar	1.2	2.4	2.4	2.4	132.0	132.0	132.0	109.0	109.0	109.0
Apr	0.6	1.0	1.0	1.0	134.0	132.0	130.0	66.1	63.0	61.1
May	0.4	0.5	0.5	0.5	123.0	121.0	118.0	35.0	32.2	28.7
Jun	0.2	0.3	0.3	0.3	140.0	141.0	139.0	44.9	41.3	41.6
Jul	0.2	0.4	0.3	0.4	168.0	146.0	164.0	59.5	31.7	52.2
Aug	0.2	0.4	0.4	0.4	207.0	200.0	198.0	110.0	102.0	95.3
Sep	0.2	0.5	0.5	0.5	238.0	232.0	216.0	154.0	146.0	128.0
Oct	0.3	1.1	1.1	1.1	278.0	270.0	267.0	234.0	223.0	220.0
Nov	0.8	2.0	2.0	2.0	189.0	182.0	185.0	165.0	157.0	160.0
Dec	1.8	2.2	2.2	2.2	55.5	52.6	55.5	18.4	14.2	18.4

Symbols key: $^+$Interagency Monitoring of Protected Visual Environments network; $^\blacktriangle$Normalized Mean Error; $^\blacktriangleright$Normalized Mean Bias; †Statistical d-s; ‡Dynamical d-s; *NEI Benchmark.

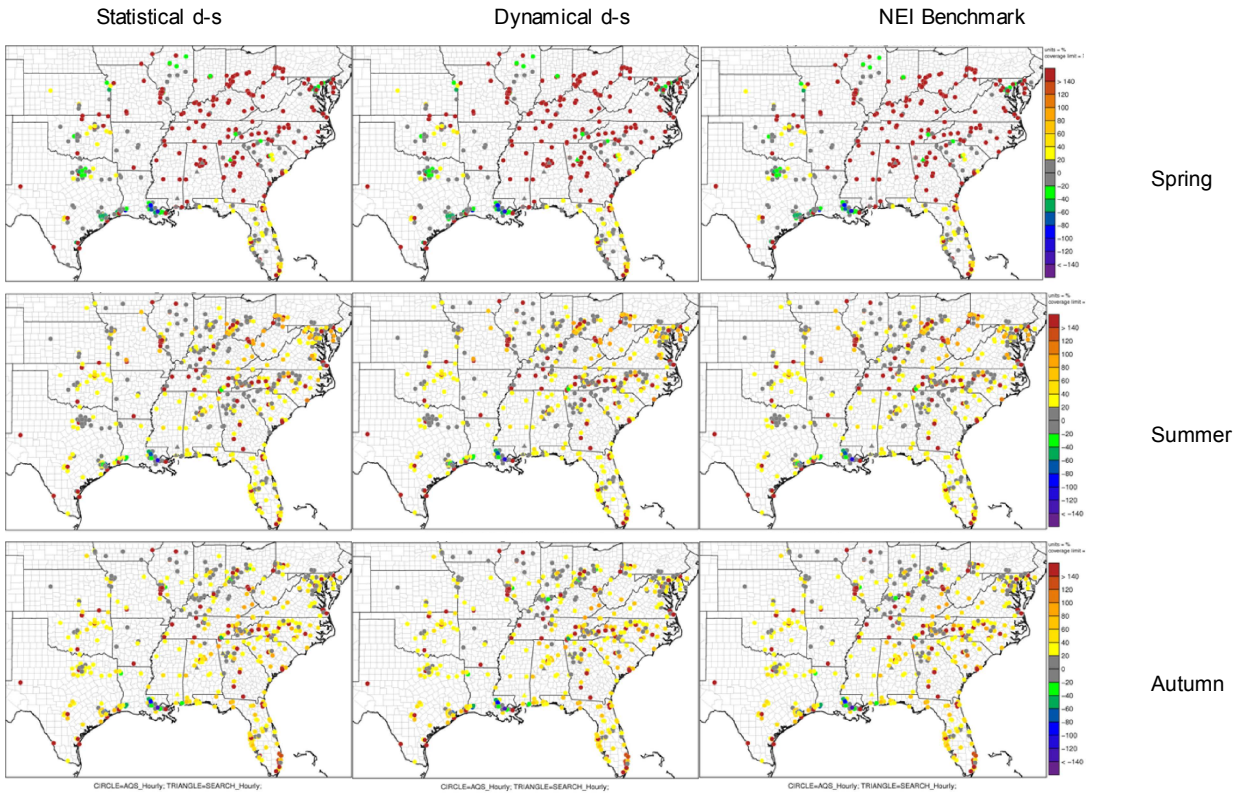

Figure 3.S1. Spatial distribution of hourly ozone Mean Fractional Bias with respect to AQS and SEARCH measurements in each season for each modeled case.

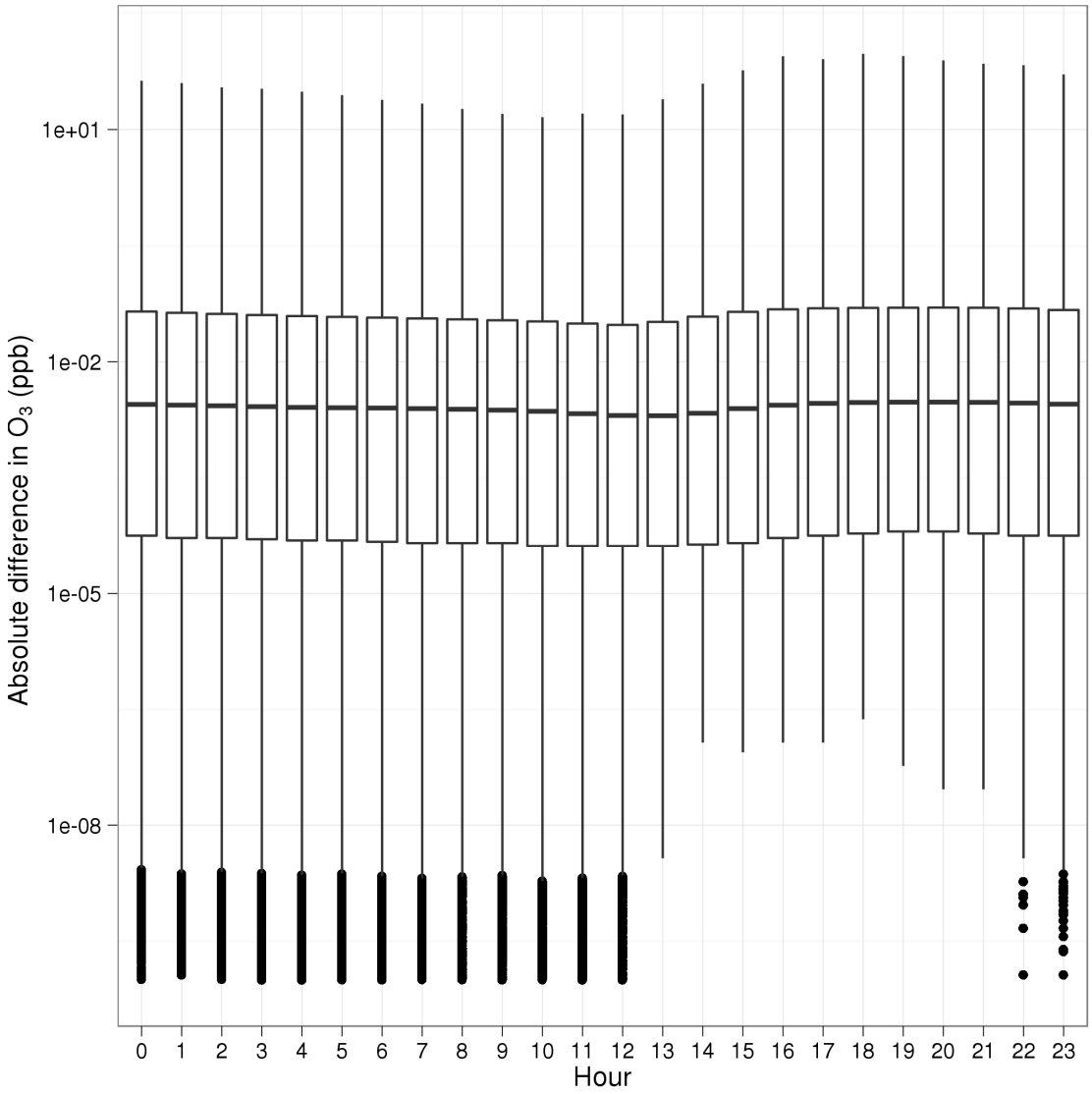

Figure 3.S2. Absolute difference between the statistical d-s and dynamical d-s cases in 1-h O_3 mixing ratios (ppb) from Hour 0 - 23 (local standard time) for the 2010 fire season (March 1 – November 30) over the whole domain (level 1).

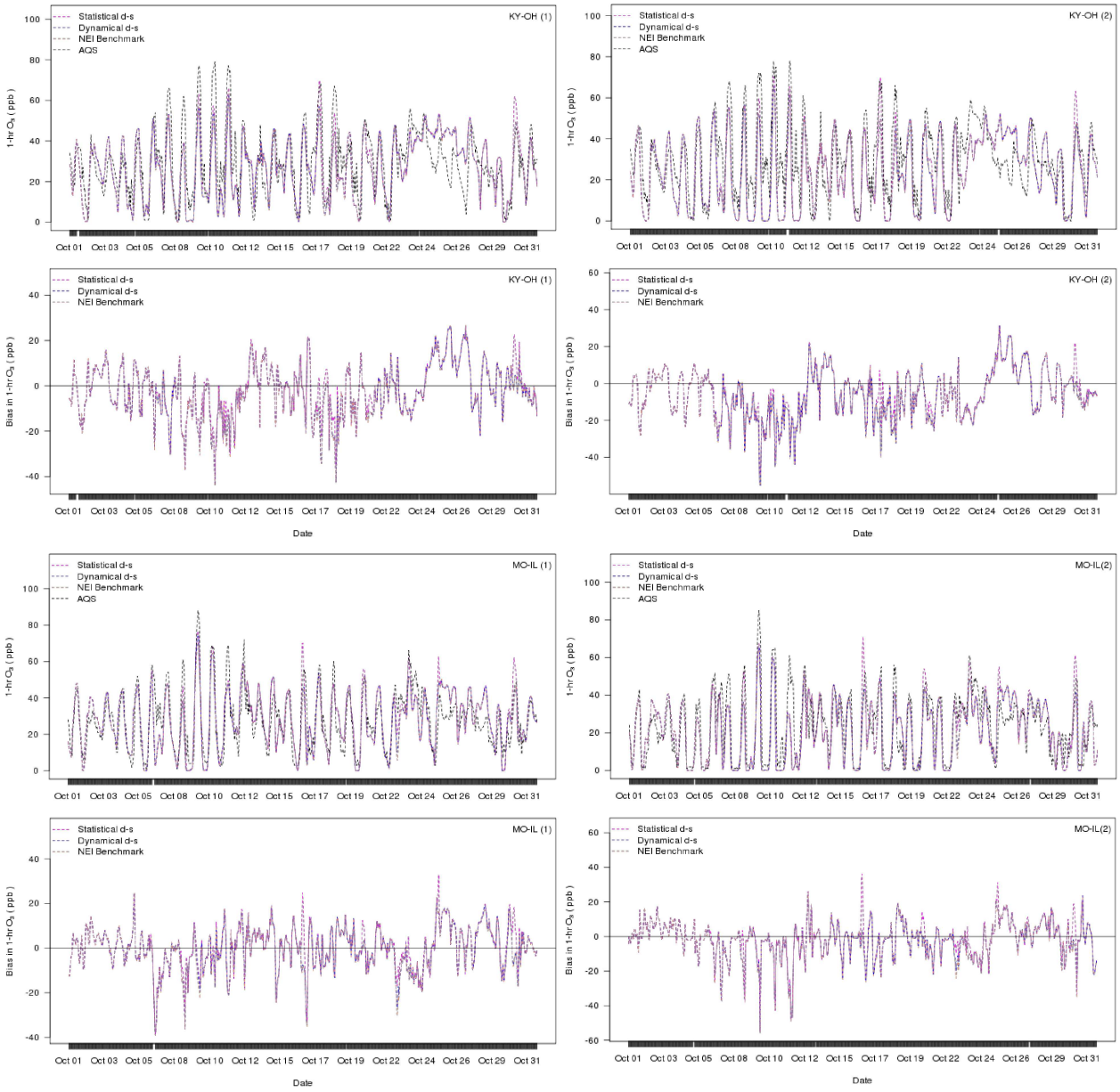

Figure 3.S3. 1-h ozone mixing ratios (ppb) and bias (ppb) relative to AQS observations at four sites in October 2010. UL – KY-OH (1): site 210590005, located on the KY-OH border; UR – KY-OH (2): site 210910012, located on the KY-OH border; LL – MO-IL (1): site 291831002 located on the MO-IL border; LR – MO-IL (2): site 295100085 located on the MO-IL border.

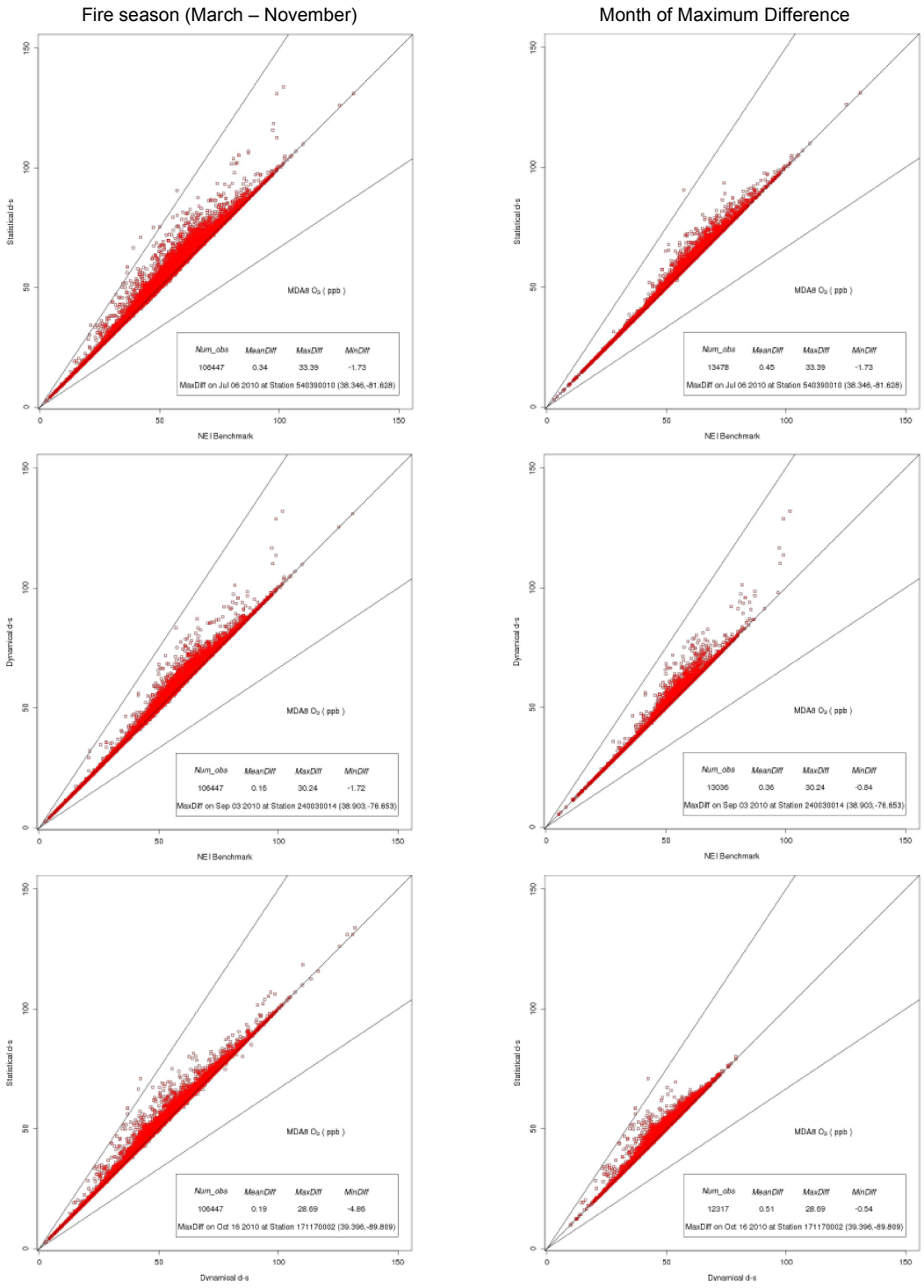

Figure 3.S4. Comparisons of wildfire emissions methods for maximum daily 8-h average (MDA8) O_3 (ppb) predicted at grid cells containing Air Quality System (AQS) monitors and wildfires in 2010. Mean, maximum and minimum intermodel difference (vertical axis variable –

horizontal axis variable), and the dates and coordinates of their occurrence are shown in the plot legend. L: fire season (March – November); R: top, July; middle, September; bottom, October.

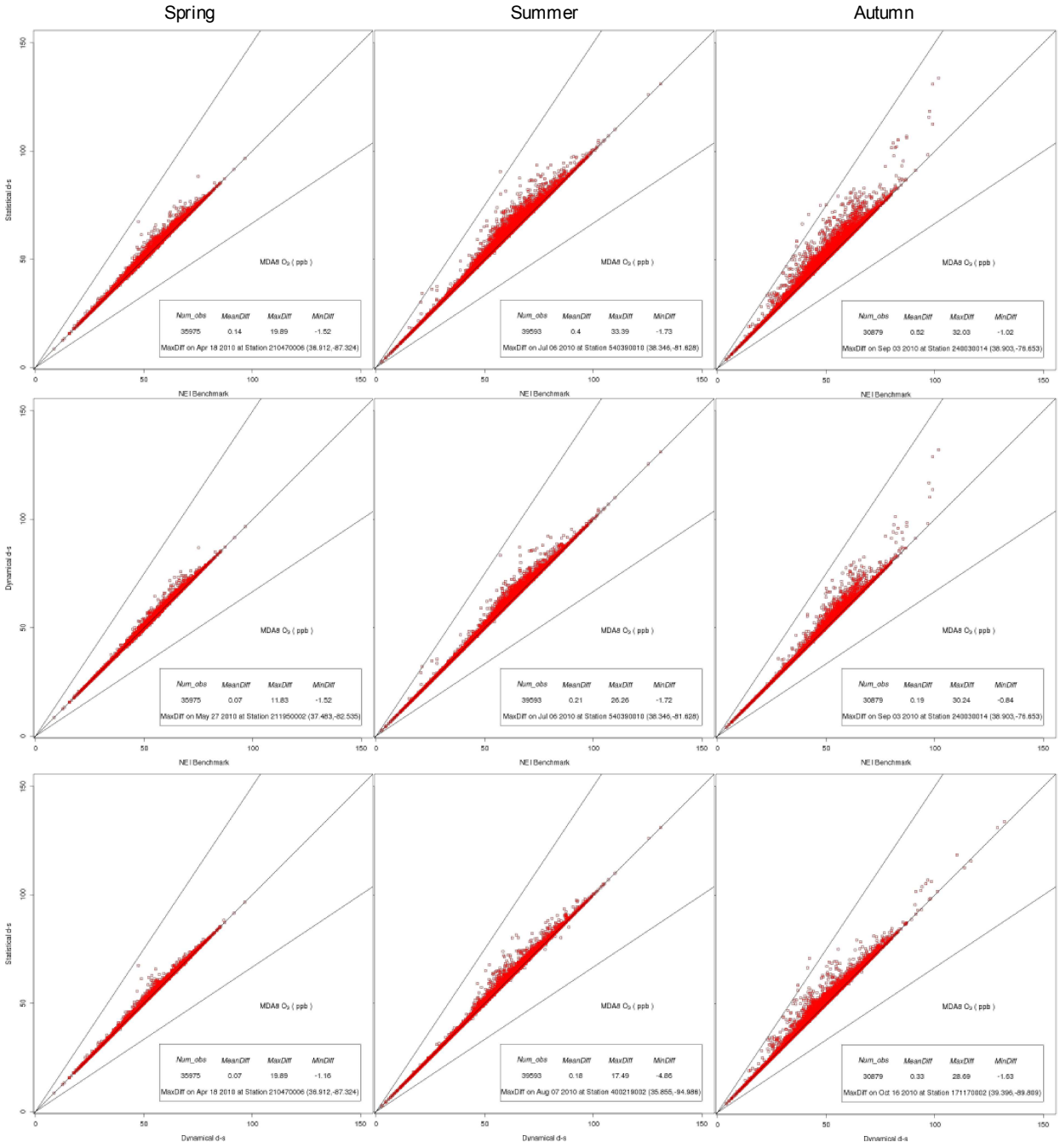

Figure 3.S5. Seasonal comparisons of wildfire emissions for maximum daily 8-h average (MDA8) O_3 (ppb) at grid cells containing both Air Quality System (AQS) monitors and wildfires in 2010. Mean, maximum and minimum intermodel difference (vertical axis variable –

horizontal axis variable), and the dates and coordinates of their occurrence are shown in the plot legend.

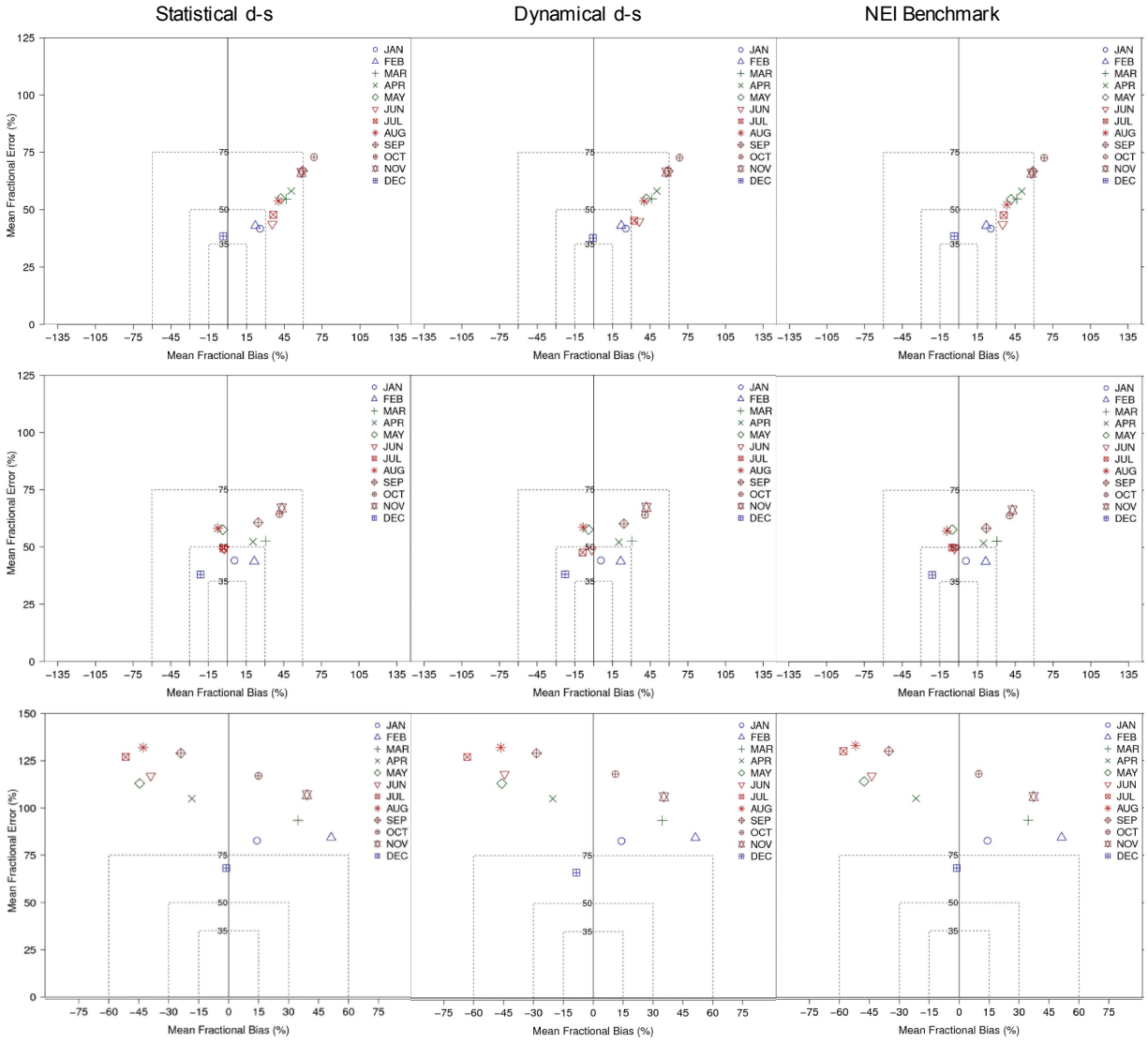

Figure 3.S6. Monthly-averaged model performance for inorganic PM constituents. Mean fractional error (%) vs. mean fractional bias (%) relative to observations from the IMPROVE monitoring network for: Row 1, sulfate (SO_4); Row 2, ammonium (NH_4); Row 3, nitrate (NO_3).

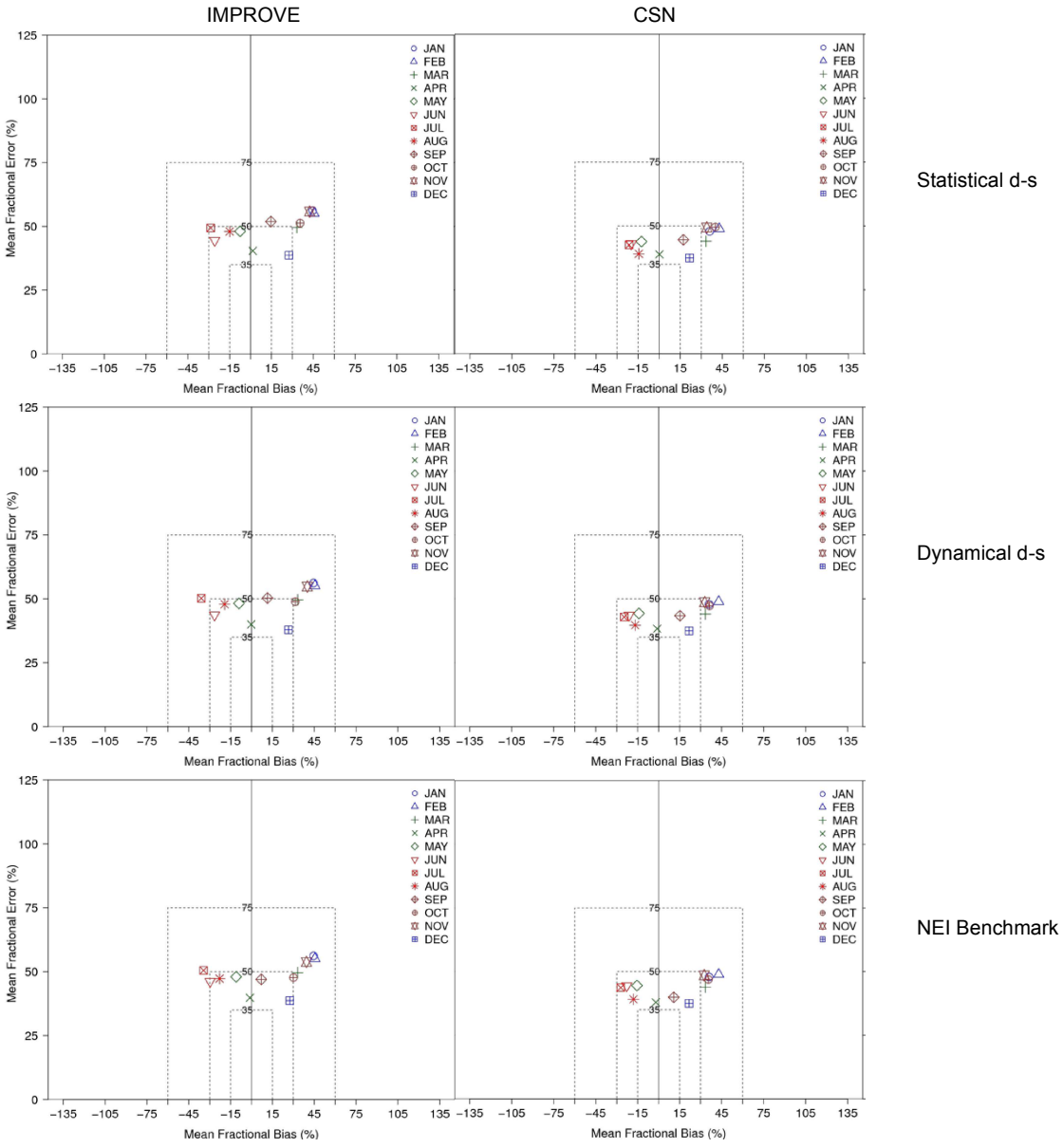

Figure 3.S7. Monthly-averaged model performance comparisons for total $PM_{2.5}$ between the IMPROVE and CSN monitoring networks.

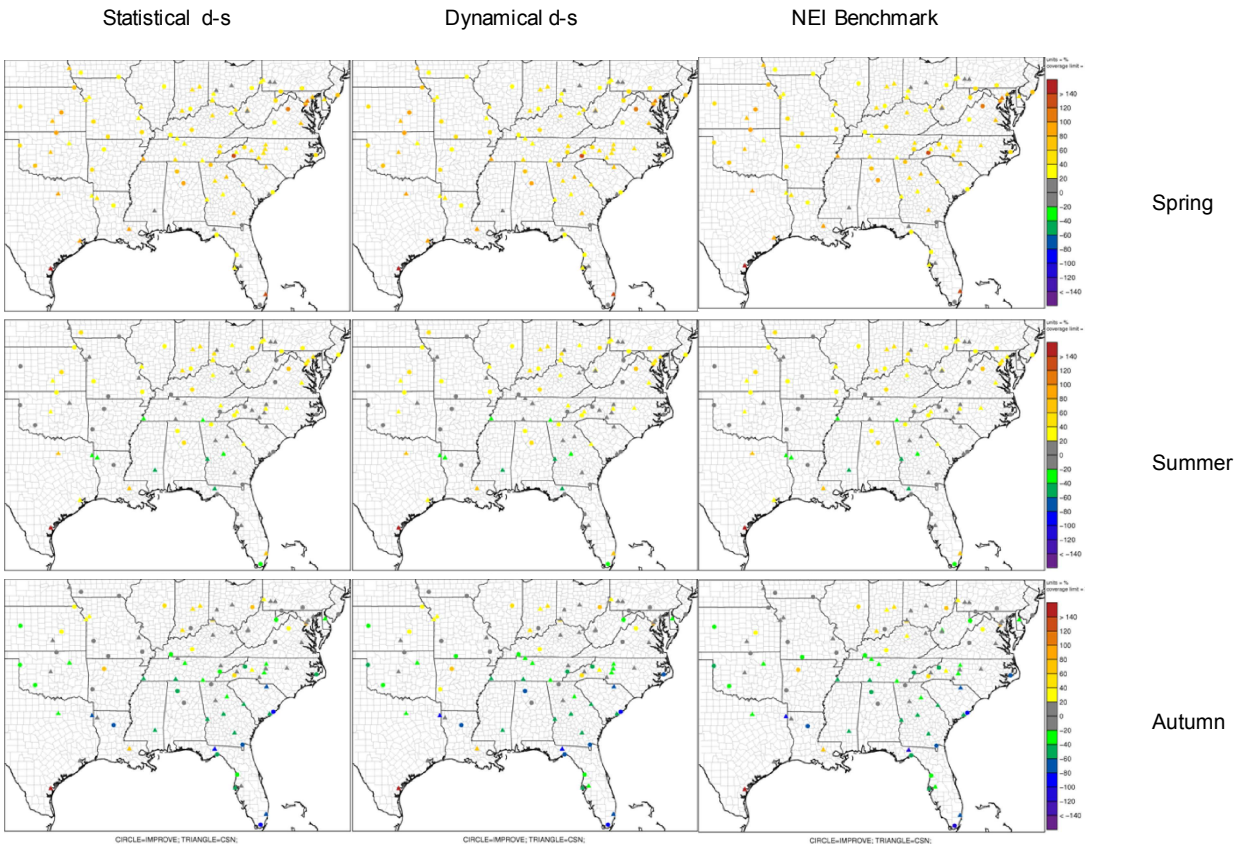

Figure 3.S8. Spatial distribution of total $PM_{2.5}$ Mean Fractional Bias (MFB) with respect to IMPROVE and CSN measurements in each season for each modeled case.

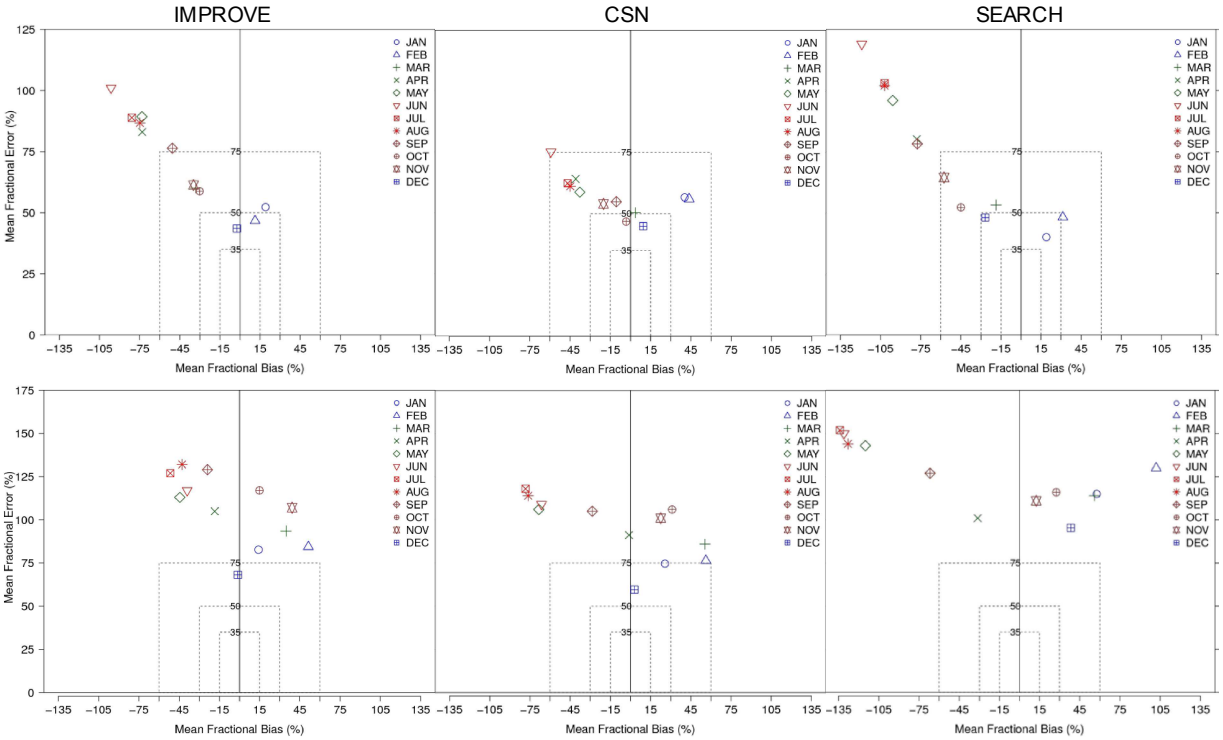

Figure 3.S9. Monthly-averaged model performance comparisons for PM constituents from statistical d-s against multiple monitoring networks. Mean fractional error (%) vs. mean fractional bias (%) relative to observations. Row 1, organic carbon (OC); Row 2, nitrate (NO_3).

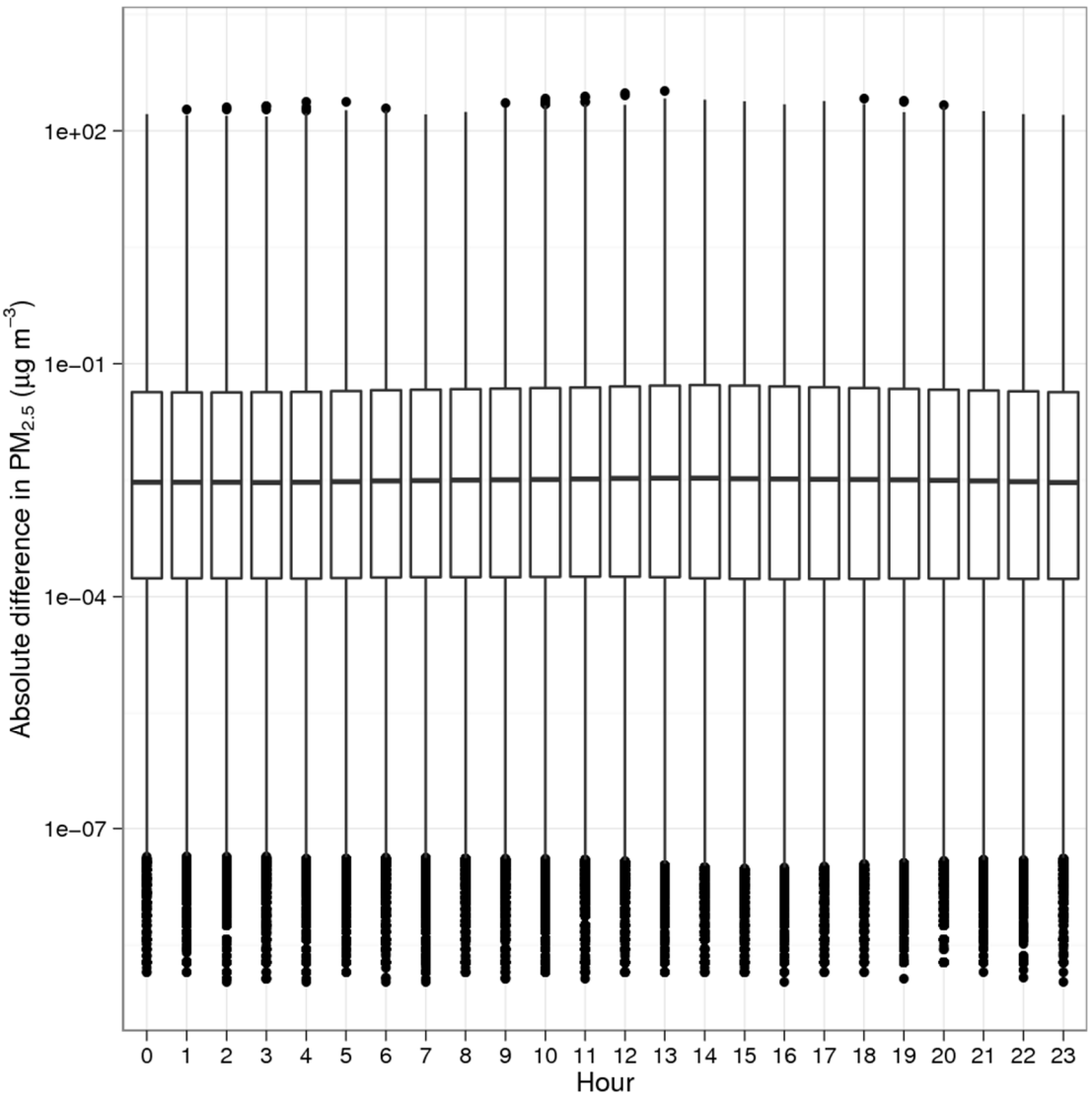

Figure 3.S10. Absolute difference between the statistical d-s and dynamical d-s cases in $PM_{2.5}$ concentrations (µg m^{-3}) from Hour 0 - 23 (local standard time) for the 2010 fire season (March 1 – November 30) over the whole domain (level 1).

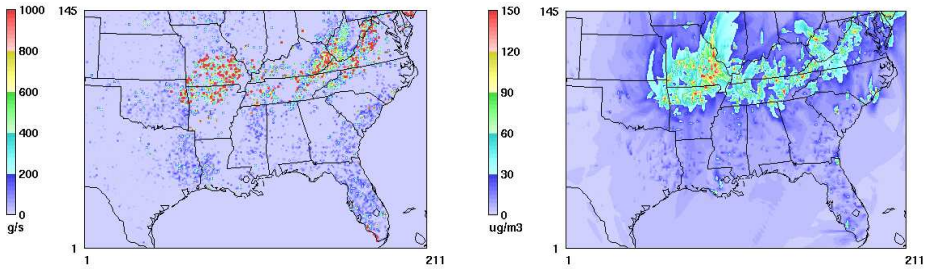

Figure 3.S11. Maximum absolute difference between statistical d-s and dynamical d-s in each grid cell over the fire season in: L – hourly $PM_{2.5}$ column emissions (g s^{-1}), and R – hourly $PM_{2.5}$ concentrations (µg m^{-3}) in model layer 1. Here the fire season is defined as April 23 – November 30; almost all grid cell maxima in absolute hourly $PM_{2.5}$ concentration differences occurred in this time period.

CHAPTER 4: ASSESSING THE IMPACTS OF PROJECTED WILDFIRE EMISSIONS ON FUTURE-YEAR AIR QUALITY

Introduction

The following is an excerpt from the Overview section of the recently released Summary Climate Change Report on the Fourth National Climate Assessment, Volume II (USGCRP, 2018):

> "…the assumption that current and future climate conditions will resemble the recent past is no longer valid".

The pace of climate change has been accelerating, signaled by an increasing number of catastrophic weather-driven events globally. Prominent in this category, wildfires have been experiencing a sharp rise over the past few decades in the U.S. and around the world. Five of the largest fires in California history occurred within the past 10 years (Cal Fire, 2018). In November 2018, the Camp Fire in Butte County, CA, and the Woolsey Fire in Ventura County, CA simultaneously became two of the most destructive fires in California history with a loss of nearly 21,000 structures, 18,000 of them, in the town of Paradise alone. With a death toll of 86, the Camp Fire was also the deadliest in California history. The Southeastern U.S. also experienced very large fires in November 2016 over a four-state area in the Smoky Mountains (Georgia, South Carolina, North Carolina and Tennessee). These late-year megafires, and the gradual disappearance of a distinct fire season (USGCRP, 2018), are increasingly attributed to

climate change (Coumou and Rahmstorf, 2012; McKenzie et al., 2014; Stavros et al., 2014; Barbero et al., 2015; Littell et al., 2010, 2016).

Wildfires can also have adverse health consequences for vulnerable populations through exposure to the emitted pollutants, notably $PM_{2.5}$, and ozone, with associated economic costs far beyond those of fire suppression. Fann et al. (2018) estimated the economic impacts of wildfires in the form of additional premature deaths and hospital admissions between 2008 and 2012 over the Southeastern and Northwestern U.S. to be $11B - $20B (2010$) per year. Rappold et al. (2014) estimated the long-term health care costs of the 2008 Pocosin Swamp wildfires in eastern North Carolina at ~ 48 times those associated with acute ailments from smoke exposure (~ $1M).

In the face of the escalating ecological, human, and economic costs of wildfires, a number of wildfire projections have been developed to better prepare the firefighting community, forest managers and populations living in fire-prone areas for future fire events (Abatzoglou and Kolden, 2011, 2013; Westerling et al., 2011ab; Liu et al., 2013, Littell et al., 2018). These methods focus mostly on the impacts of climate change on fire activity, and on very large fires in the Western U. S. In the Southeastern U. S., however, considered to be one of the fastest growing regions of the country (U.S. Census Bureau, 2018), human factors are a major driver of wildfires (Prestemon et al., 2002, Mercer and Prestemon, 2005; Syphard et al., 2017). Humans both ignite and suppress the majority of wildfires (Prestemon et al., 2013; Balch et al., 2017). The wide geographic variability and rapid evolution of climate and socioeconomic drivers of wildfires in the U.S. and elsewhere (Syphard et al., 2017; Viedma et al., 2018) call for region-specific methods to investigate how wildfires may respond to expected changes in their primary drivers.

Besides supporting resource planning and land management, region-specific AAB projections provide a critical input for estimating wildfire emissions that drive air-quality (AQ)

simulations to inform exposure assessments and calculate health risks in future fire regimes. Current AAB projection methods, however, lack the ability to estimate daily wildfire emissions, because AAB are, by definition, annual estimates of fire extent, not emissions. For example, studies of wildfires in the Western and even the continental U.S. are either at a relatively coarse spatial resolution greater than the 12-km x 12-km grid spacing typically used in regional air-quality simulations (e.g., Abatzoglou and Kolden, 2011; Liu et al., 2013, 2014; Yue et al., 2103, 2015; Liu et al., 2016), or over a limited area, e.g., California, as in Westerling et al. (2011 ab), because they are mainly intended for understanding the impacts of climate drivers of wildfires on annual areas burned (AAB). The challenge, then, is to develop methods to translate AAB and similar measures into emissions, thereby helping quantify the impacts of future wildfires on air quality and health. To date, there are no known investigations over the Southeast that examine not only the long-term impacts of wildfire on air quality, but also the influences of climate change and other important drivers (population and income growth) on wildfire at spatiotemporal resolutions appropriate for AQ studies over this region.

Shankar et al. (2018) developed such a method leveraging AAB projections by Prestemon et al. (2016) to estimate wildfire emissions over a Southeastern modeling grid at 12-km x 12-km spatial resolution for 2010 and four selected years around mid-21st century. These include, for the first time over this region, the influence of both climate and socioeconomic changes at a spatial and temporal resolution suitable for AQ impact assessments. The AAB projections are made by multilinear regression models (Prestemon et al. 2016) over 13 Southeastern states, with input county-level projections of the major wildfire drivers in the region (climate, population and income, and land use) based on the Intergovernmental Panel on Climate Change greenhouse gas (GHG) emissions scenarios (Nakicenovic and Steward, 2000). Shankar et al. (2018) compared

wildfire emissions for 2010, and the four future years using two sets of these AAB projections, made with two different methods of downscaling the climate inputs, to emissions estimated with 19-year historical mean AAB. Their AAB projections were lower (by 7% to 38%) on average in the selected future years than the historical mean AAB. Thus, the wildfire emissions that were estimated from them were also lower by 13% - 62% than those using the historical mean AAB (Shankar et al., 2018). The analyses of Prestemon et al. (2016) find that human-caused ignitions burn five times the area of lightning-caused ignitions annually in the Southeast. Human-caused AAB, which were found to be strongly correlated with socioeconomic variables, were projected to decrease by 6% on average over the region from 2011 to 2060, while lightning-caused AAB, which were strongly correlated with climate variables, were projected to increase by 34% on average; this results in a net median increase of 4% in AAB in 2011-2060 over the Southeast (Prestemon et al., 2016). These offsetting climate and socioeconomic influences, combined with the temporal variability of the climate system (Prestemon et al., 2016) explain the substantially lower AAB and emissions projected for the four arbitrarily selected future years (2043, 2048, 2053 and 2058), compared to those based on the historical mean AAB (Shankar et al., 2018).

A subsequent study (Shankar et al., 2019), included as Chapter 3 in this document, evaluated these two wildfire emissions projection methods by using their respective estimates of 2010 wildfire emissions in AQ simulations, and by comparing the results to those using EPA's empirical National Emissions Inventory (NEI) for 2010 wildfires, and to ground-based air-quality observations. The AQ results using the two projection methods are within 0.08% - 0.93% and 1% - 8% of those using the NEI for O_3 and $PM_{2.5}$ respectively. Their biases compared to observations are, in fact, smaller than those for the NEI for two key primary wildfire PM species, elemental carbon (EC), and ammonium (NH_4). But all three wildfire emissions estimates have

larger biases with respect to observations for other secondary PM species and ozone. These are found attributable mainly to emissions underestimates from non-wildfire sectors, or to the secondary aerosol models for organic carbon (OC) and particulate NO_3. These results partially confirm the study hypothesis that these wildfire emissions projection methods would yield AQ model results for the criteria pollutants that are within published criteria for acceptable model performance, and comparable to those using the standard (NEI) inventory. They thus show that these methods can be used in present-day AQ studies while providing contemporaneous emissions for future-year AQ assessments that are not possible with empirical inventories.

The study described in this chapter extends the application of the projected wildfire emissions to AQ assessments of selected future years. Its hypothesis is that the dynamic wildfire emissions projection methods will result in considerably different ozone and $PM_{2.5}$ spatial distributions and seasonal-average concentrations by mid-century from their 2010 levels. This hypothesis is tested in AQ simulations using the projected wildfire emissions in the future years, and comparisons of simulated ozone and $PM_{2.5}$ between past and future years.

Methods

Emissions inputs

Chapter 2 described in detail the estimation of emissions from wildfires for the statistical d-s and the dynamical d-s methods of projecting wildfire AAB (summarized in Table 2.1) for four years around mid-21st century. These provided two sets of wildfire emissions inputs for the corresponding AQ simulation cases for each year (Table 3.1).

The simulations in this study and in 2010 are not zero-out studies that examine the impacts of wildfire emissions in isolation by removing all other sources (e.g., Wilkins et al., 2018). Rather, they are designed to examine the AQ impacts of wildfire emissions in the context of changes in

climate and society over time, including those in the anthropogenic emissions sectors. To account for how anthropogenic emissions and their AQ impacts might change along with those of wildfires in the future, projections of anthropogenic sector emissions were obtained from the U. S. EPA (Loughlin, D., personal communication). These consisted of emissions projections for fuel combustion in electricity generation, industry, residential, commercial, and transportation sectors, commercial marine vehicles, aviation, and agricultural emissions (crop and animal production, forestry and logging) from 2005 to 2055. They were made at 5-year intervals for the Representative Concentration Pathway 4.5 (RCP4.5), under the assumption of stabilization of the anthropogenic components of radiative forcing to 4.5 W m^{-2} by 2100 using the Global Change Assessment Model (GCAM – Moss et al., 2010; Thomson et al., 2011, and references therein).

In addition to projected emissions of six greenhouse gases, emissions were estimated in GCAM as speciated national-scale projection factors for the criteria air pollutants (CAPs) NO_x, SO_x, non-methane Volatile Organic Compounds (VOCs), CO, particulate NH_4, SO_4, NO_3, EC and OC, and could therefore be used in this study. They were applied to the 2005 emissions for the relevant anthropogenic sectors in the NEI and processed in the Sparse Matrix Operations Kernel Emissions (SMOKE) processing system (Baek and Seppanen, 2018) for the four future-year simulations. As there were no exact matches between the simulation years and those in the GCAM projection package, the years in GCAM that most closely matched the simulation years were used for the projected emissions: thus, SMOKE processing of 2043 CMAQ-ready emissions used the 2045 projected inventory; 2048 emissions processing used the 2050 inventory, and 2053 and 2058 emissions, the 2055 inventory. The levels of control and growth for the various pollutant species are provided for major emission sectors in Table 4.S1. All other

non-wildfire sector emissions were as specified in the 2010 simulations. Specifically, VOC from solvents, and biogenic emissions were kept at 2010 levels.

Meteorological inputs

The meteorological inputs for the AQ simulations for the four future years were the ones generated for the dynamical d-s AAB projections in the Chapter 2 study using the Weather Research and Forecasting (WRF) model v3.4.1 (Skamarock et al., 2008). They were processed in version 4.2 of the Meteorology-Chemistry Interface Processor (MCIP -- https://www.cmascenter.org/help/model_docs/mcip/4.2/ReleaseNotes) to produce model-ready inputs to the AQ simulations.

Other simulation inputs

Simulation inputs other than emissions and meteorology include initial and boundary conditions. To avoid potential artifacts introduced by inter-year changes in the boundary conditions, the same initial and boundary input data were used in all future years and for both the simulation cases as in 2010. As the simulations are compared only to each other in this study, and not to observations, the 2010 chemical boundary inputs serve as a hypothetical set of hourly varying concentrations transported into and out of the domain.

Air-quality simulations

Air-quality simulations for the future years were performed for the statistically and dynamically downscaled cases as for 2010 over the Southeastern U. S. domain shown in Figure 3.1 (D02) at a 12-km x 12-km horizontal grid spacing. The same model configuration of the Community Multiscale Air Quality (CMAQ) model version 5.0.2 (Byun and Schere, 2006) was used as in the 2010 simulations (Shankar et al., 2019). In addition, the future year simulations also included a sensitivity case for each year wherein wildfire emissions were not included. This

allows an examination of the impact of future wildfire emissions on air quality, and is similar to the approach of Wilkins et al. (2018) and Koplitz et al. (2018) in their retrospective analyses for 2008-2012.

Analysis tools and data

The analyses for this study focus on intermodel and inter-year comparisons of simulated ozone and PM. To keep the statistics of mean and maximum differences comparable between the cases in all modeled years, the intermodel comparisons in the future years are made at the same locations used in the 2010 evaluations described in Chapter 3. The impacts of wildfire emissions on future air quality, however, are examined domain-wide, and compared to published estimates of these impacts in 2010 from retrospective studies (Wilkins et al., 2018; Koplitz et al., 2018).

Results

Hourly ozone over the fire season

The model results shown in Figures 4.1, 4.2, and 4.3 were filtered as in the 2010 analyses (Shankar et al., 2019) to compare the modeled ozone at grid cells that contained AQS monitor sites and also had wildfires, i.e., grid cells with non-zero AAB as estimated for the statistical d-s case. Domain-wide results of the sensitivity of hourly ozone to wildfire emissions are presented later in this section. As the downscaled simulations are not driven by wildfire emissions in isolation, the impacts of those emissions on atmospheric constituents are inferred in Figures 4.1 – 4.3 by examining the difference between the predictions of the modeled cases due to the differences in their wildfire emissions. As all other inputs are identical between these cases in any given year, intermodel comparisons in each year do provide insights into the sensitivity of the air quality metrics to the wildfire emission differences, and their causes, and can shed light on the relative merits of the wildfire emission estimation methods (Koplitz et al., 2018). On the

other hand, inter-yearly comparisons for either modeled case show the impacts of changes across years in meteorology and anthropogenic emissions, because both cases use same hourly meteorology, and non-wildfire sector emissions in each year.

Hourly ozone mixing ratios compared at the AQS sites between the statistical d-s and dynamical d-s over the fire season in each modeled year (Figure 4.1 and Table 4.1) show a significant drop in the maximum difference (statistical d-s – dynamical d-s) from the 2010 value of 67.1 ppb, to values ranging from 23.2 ppb in 2043 to 38.8 ppb in 2053. Relative to 2010, the ozone values at the upper end of the range are somewhat lower in the future years in both modeled cases; this decrease in peak ozone is likely due to emission reductions relative to 2010 from wildfire and non-wildfire sources. This is further explained in "Discussion".

In all years, the statistical d-s ozone mixing ratios are higher on average than dynamical d-s as indicated by the positive mean intermodel differences (statistical d-s – dynamical d-s) over all sites; these fire season statistics are displayed in the plot legends in Figure 4.1. The average of these mean differences is ~ 0.07 ppb in the future years, but is ~ 42% lower than the 2010 value of 0.12 ppb, indicating closer agreement between the cases in projected ozone.

In all future years, Table 4.2 shows a temporal shift in the month of maximum intermodel difference, from October 2010 to much earlier in the fire season. The table also shows the projected shift in the location of the maximum intermodel difference over the whole fire season from Chesterfield, MO at the Missouri-Illinois border in 2010 to locations farther east and/or south. These results indicate a change from 2010 in the projected ozone spatial and temporal characteristics due to changes in the wildfire emissions, but also due to the inter-year variability

introduced by the meteorology, and the anthropogenic emissions. Possible explanations for these trends are explored under “Discussion”.

Hourly ozone seasonal variability

Tables 4.1 and 4.2 and the seasonal intermodel comparisons (Figure 4.2) confirm that the trends shown in Figure 4.1 over the entire fire season are also repeated within each season of each future year: that is, the maximum intermodel differences in ozone in spring and summer occur between late May and mid-August, while the autumn maximum difference is projected in early September. There is a shift in autumn in the future years to the warmer part of the season (early September) from late October, the period when the seasonal maximum difference occurs in 2010. Autumn is also projected to have the smallest intermodel differences in the future years, especially in 2058, with nearly identical values between the simulations; the maximum intermodel difference in autumn 2058 is 0.2 ppb, compared to 67.1 ppb in the autumn of 2010). This is a substantial shift from the 2010 ozone characteristics.

Ozone time series

To better understand the changes among 2010 and the future years in the intermodel differences in ozone over the whole fire season, and inter-seasonally (Tables 4.1 and 4.2, and Figures 4.1 and 4.2) from the perspective of daily fire activity, ozone time series are examined for the month and the location of maximum intermodel difference in each year (Figure 4.3). The ozone time series for 2010 over selected AQS sites (Figure 3.S3) showed that in the locations and months that had large intermodel differences, there were sporadic but sharp differences throughout the month, coinciding with intermodel differences in daily fire activity upwind due to differences in the AAB estimates between the two modeled cases. The time series of Figure 4.3 show that there are smaller and fewer such sharp differences in the future-year locations and

months of maximum intermodel difference than in that of 2010, in October at the Missouri-Illinois (MO-IL) border (Figure 4.3, top panel). This is indicative of lower fire activity, and/or less sensitivity of ozone levels to fire activity. The mean monthly intermodel difference averaged over the four future-year locations in Figure 4.3 is ~ 0.12 ppb, less than a tenth of the October 2010 mean monthly value of 1.3 ppb at the MO-IL site (Table 4.S2). This is partly due to the lower projected AAB for both modeled cases in at least two out of the four future years than in 2010 (Figure 2.3), leading to lower ozone precursor emissions in these years, and also due to 2010 having the largest AAB difference among all the years between the two cases.

Another pronounced difference from 2010 in each future year is that the average monthly ozone level at these sites in the future years is higher than in October 2010 by ~ 20 ppb. Specifically, the monthly mean 2010 ozone mixing ratio for October from the dynamical d-s simulation at the MO-IL site (Figure 4.3, top panel and Table 4.S2) is 22.2 ppb (1.3 ppb lower than the monthly mean from statistical d-s); it ranges from 39.3 ppb – 44.8 ppb in the future-year locations shown in this figure. These results at individual locations are consistent with the findings over all AQS sites in Figures 4.1 and 4.2 and Tables 4.1 and 4.2, that the ozone levels in the dynamical d-s case are higher over all seasons at the locations of maximum intermodel difference, while the mean intermodel difference over all seasons is smaller. Likely explanations of these features are explored further in "Discussion".

Ozone impact of wildfire emissions

These analyses examine the difference in ozone of the statistical simulation from the no-wildfire baseline simulation. Of the two downscaled simulations, statistical d-s is the one driven by the highest wildfire emissions due to having largest estimates of AAB in all the future years.

It thus provides an upper bound on the impact of wildfire emissions on future air quality estimated by the downscaling methods.

Analysis of the seasonal-average ozone impact of wildfire emissions within the fire season in each of the future years (Figure 4.4) confirms the findings of the foregoing analyses. In all years, the highest ozone mixing ratios occur in the spring, but the highest wildfire impacts are in the summer. This is expected as summertime is not only the season of relatively high ozone production, but also the season of highest fire activity. The ozone impact is not large, with a domain-wide maximum value of 1.48 ppb in 2043 summer, and < 0.01 ppb in autumn in 2048 and 2058; the domain-wide maximum changes in ozone due to wildfires in each season and year, as well as the region of the impact are summarized in Table 4.3. Spatially, the biggest impact of wildfire on ozone is in the Appalachian region around West Virginia, the southern tip of Florida and along the Gulf Coast, and in the western part of the domain around eastern Oklahoma and Missouri. The maximum impact is projected to be ≈ 1.5% – 3% in the spring and summer, and as low as 0.4% in autumn (Figure 4.4), discounting the negligible impacts domain-wide projected in autumn 2048 and 2058. This is in the expected range compared to the average impact in 2008-2012 of 0.41% nation-wide reported by Wilkins et al. (2018), since future wildfire emissions are projected as much as 62% lower than in 2010 (Shankar et al., 2018); our results are consistent with those lower wildfire emissions and their spatial patterns. Besides the high impact in the summer, there is a small to negligible impact on ozone in autumn in almost all years. Even 2053,

with the highest AAB estimates among the future years has a maximum impact in autumn of only 0.3 ppb. Probable causes of these seasonal trends are explored in "Discussion".

$PM_{2.5}$ over the fire season

Comparisons of $PM_{2.5}$ intermodel differences among the years over the fire season (Figure 4.5 and Tables 4.4 and 4.5) show decreases similar to ozone in the ambient PM levels and their intermodel differences in the future years relative to 2010. This would be expected from the decrease in AAB in the future years compared to 2010, as well as its temporal variability. The peak differences over the fire season range from 10.6 $\mu g\ m^{-3}$ in 2048 to 16.8 $\mu g\ m^{-3}$ in 2043, compared to 26.0 $\mu g\ m^{-3}$ in 2010; this is somewhat consistent with the differences in AAB between the two cases in these years, as 2048 had the smallest AAB difference, and 2043, the second highest (Figure 2.3). $PM_{2.5}$ predictions from the two simulations are in better agreement in the future years than in 2010 (Figure 4.5). The mean differences (0.14 $\mu g\ m^{-3}$ – 0.19 $\mu g\ m^{-3}$) are also smaller over the fire season than in 2010 (0.29 $\mu g\ m^{-3}$) as shown in the legends in each panel of Figure 4.5, and have little inter-year variability.

As in the case of ozone, maximum differences in $PM_{2.5}$ over the fire season are also projected to shift from their 2010 location near the Mingo National Wildlife Refuge (NWR) in southeastern Missouri in late October (Figure 4.5, 4.10, and Tables 4.4 and 4.5), to warmer locations and periods, i.e., farther east and south in future summers. These are Quaker City, OH in Appalachia in July 2043 and August 2048, and James River Wilderness in Virginia in July 2053 and July 2058. These future-year characteristics are further examined in "Discussion".

$PM_{2.5}$ seasonal trends

Table 4.4 summarizes the results of the seasonal mean and maximum intermodel differences in $PM_{2.5}$ in the future years, and Table 4.5 provides the locations and periods of their occurrence.

The mean intermodel differences are highest in summer and lowest in autumn, being almost negligible in that season in 2043 and 2058. For a given season, the shift in the location of the maximum intermodel differences (Figure 4.S1 and Table 4.5) to the south and east is most apparent in the spring in three of four future years, from Shenandoah National Park (NP), VA in the spring of 2010 to the Everglades NP (spring 2043), St. Marks, FL on the Gulf Coast (spring 2048), and Chassahowitzka NWR, FL (spring 2053). Unlike ozone, the summertime maximum differences are not projected to change much spatially from 2010, occurring in the same location and month as in 2010 (James River Wilderness) in two out of four future years. Among the future years, 2053 has an outlier location in autumn with the largest maximum intermodel difference for that season of 14.7 $\mu g\ m^{-3}$ in early September. It also has a large intermodel difference (16.2 $\mu g\ m^{-3}$) in the summer, the highest over the fire season among all future years. This would be expected, as this year has the largest AAB difference between the simulations.

$PM_{2.5}$ impacts of wildfire emissions

Similar analyses to those displayed in Figure 4.4 were also performed for $PM_{2.5}$ to examine the domain-wide and seasonally averaged impact of wildfire emissions on its ambient concentrations (Figure 4.6). The maximum impacts and their locations are summarized in Table 4.6. The impact of wildfires on $PM_{2.5}$ is considerably greater than those on ozone, even though many of the maximum impact locations are the same as for ozone. Once again, the greatest impacts are in the summer in all years, with 2058 being an outlier year (nearly 200% impact). Allowing for the decreases in emissions projected by mid-century by the statistical d-s methodology (Shankar et al., 2018), these projected impacts are in the range of both the percentage increase (275%) estimated by Wilkins et al. (2018) across the U.S., and the magnitude of the impact seen in some locations (4 $\mu g\ m^{-3}$) by Koplitz et al. (2018) in their

retrospective studies. The smallest impacts are in 2048, which had the lowest wildfire emissions projected by the statistical d-s method. Autumn is again the season with the least impacts on $PM_{2.5}$, but even with that, the domain-wide maximum impact is over 50% in two out of four autumns. Spatially, the maximum impacts occur farther north than with ozone, in the Midwest, as well as in the high wildfire emission region in Appalachia.

$PM_{2.5}$ compositional variability

All future years for both the modeled cases have lower values of $PM_{2.5}$ in each season than in 2010 because of large projected emissions reductions in the energy and transportation sectors (see "Methods"). In the data provided by EPA for the future-year emissions projections for non-wildfire sectors, sulfur emissions, the biggest contributor to $PM_{2.5}$ in the Southeast, are reduced to 25.6%, and NO_x, to 33.7% of their respective 2005 values from the energy sector by 2045. EC and OC emissions from this sector are reduced to 63.2% and 76.9% of their 2005 values by 2045. Also by 2045, EC emissions from transportation are reduced to 73.1%, and EC and OC emissions, respectively, to 76.4% and 60.9% of their 2005 values from commercial marine vehicles. There are, however, some emission increases, e.g., an increase of 4% in NO_x and primary NO_3 emissions, and ~ 20 % in EC and OC emissions from the aviation sector, and increases of 25% - 30% in nitrate, ammonia/ammonium, and VOC emissions from agriculture.

The $PM_{2.5}$ compositions for dynamical d-s and statistical d-s (Figure 4.7) compare more closely in the future years than in 2010, but they have more inter-year variability than might be expected from the large and monotonic emissions reductions in the major components (sulfate and nitrate) from 2005 to mid-century. The variability in the $PM_{2.5}$ constituent concentrations resembles, and is likely due to the variability in the AAB projections, but also to the seasonal

variability in the WRF meteorology underlying the daily fire activity projections in both simulations. This variability is especially noticeable in the later years.

Seasonally, the $PM_{2.5}$ trends in Figure 4.7 follow those seen in Figure 4.S1. Summer shows the biggest difference between the two cases in the $PM_{2.5}$ constituent mass fractions; the differences are greater than 0.5% for most constituents. Spring and autumn have the smallest differences between the cases in total $PM_{2.5}$ and its components, and the dynamical d-s results are higher than statistical d-s in 2048 autumn. The smallest AAB difference between the cases are in that year. As in Figure 4.S1, autumn 2058 has the smallest intermodel differences for all species.

To better interpret the results of Figures 4.7, especially for PM constituents with small mass fractions of total $PM_{2.5}$, such as OC and EC, the differences in concentrations between the simulation cases are shown as trend plots for each constituent by season in Figure 4.8, and as percent differences (statistical d-s – dynamical d-s) in Table 4.7. Yearly trends for the concentrations of each constituent and total $PM_{2.5}$ are also shown in Figure 4.S2. The maximum difference in $PM_{2.5}$ (0.41 ug m^{-3}) between the cases over all the modeled years is in 2010 autumn (Figure 4.8, Row 1), as discussed in the previous figures for ozone and PM, while the largest differences inter-seasonally in $PM_{2.5}$ in the future years are in the summer. These show a slightly increasing trend ranging from ~ 0.32 to 0.38 μg m^{-3}. These differences are largely driven by OC and Other PM, a composite species that represents unspeciated PM, e.g., dust, from multiple sources including wildfires. Table 4.7 shows that OC differences are as high as 28.7% between the cases, with 2053 being the year of greatest difference, and 2048, the least. The large

summertime differences in this species are due to that being the season of largest projected differences in AAB and wildfire emissions, and are further examined in "Discussion".

Other PM has an appreciable mass fraction of $PM_{2.5}$ (~ 19% - 27 %) as seen in Figure 4.7, and the difference in the projected values of this constituent in the summer between the modeled cases is 0.06 - 0.14 μg m^{-3} (Figure 4.8). As this is a primary species, these intermodel differences are directly attributable to wildfires; all other emission sources contribute equally to its ambient concentration in both modeled cases. There is an increasing trend of ~ 4.5% in these differences in the future summers, but it is more than offset by the much more negative trend in autumn due to lower fire activity.

Another notable feature of the $PM_{2.5}$ difference trends in Figure 4.8 is the value of -0.09 μg m^{-3} in autumn 2048; this is the amount by which the dynamical d-s $PM_{2.5}$ prediction exceeds that of the statistical d-s. This is the season and year in which almost all PM constituents are higher in the dynamical d-s case than in the statistical d-s. This is also the year with the smallest difference in domain-wide AAB between the cases (Figures 2.3). The negative difference in $PM_{2.5}$ is almost entirely due to that of SO_4, the constituent with the highest mass fraction (~ 31% - 50%). The difference in SO_4 also drives the negative differences in the semivolatile inorganic species NH_4 and NO_3, through the thermodynamics (-0.03 μg m^{-3} and -0.01 μg m^{-3} respectively in 2048).

Discussion

Ozone projections

The smaller intermodel differences in hourly ozone in all years and all seasons compared to their 2010 values are as expected from the smaller intermodel differences in AAB in all the future years than in 2010; the exception is 2053 (Figure 2.3). Accordingly, among all the future

years 2053 does have the largest fire-season maximum intermodel difference in ozone (38.8 ppb), as well as the largest mean intermodel difference (0.08 ppb).

To understand these temporal and spatial changes in the intermodel differences, some of the meteorological drivers of fire activity from selected months in 2010 and the future years are compared. In a comparison of monthly precipitation in the future years in the WRF model output, the summertime precipitation is much lower in all of the future years than in 2010 (Figure 4.9), and temperatures are much higher (Figure 4.10); Figure 4.9 (Row 6) also shows the relatively dry October in 2010 that had the highest intermodel difference in ozone in that year, for comparison with a future summer month (August 2043). Recalling that the WRF model is used in the calculation of the daily fire weather index to estimate daily area burned for both modeled cases, a warmer and drier summer would increase the daily fire activity in this season, when ozone levels are driven up by temperature (see, e.g., Dawson et al., 2006), while the statistical d-s case would still predict higher ozone than the dynamical d-s due to its higher AAB and precursor emissions.

Potential evapotranspiration (PET), a composite temperature-based indicator of fuel aridity and one of the regression variables in the AAB estimates, is also higher in the future years than in 2010, higher for the statistical d-s than for the dynamical d-s, and highest in mid-summer among all seasons (Figures 4.S3 – 4.S5). Spatially, the higher AAB values are along the eastern seaboard and to the south along the Gulf Coast and Florida, and somewhat concentrated in Appalachia and the Ohio valley in all future years, and are also the locations of most of the maximum air quality impacts from wildfires (Figures 4.4 and 4.6). These meteorological trends explain the shift to the warmer months and to the south and east in future fire activity, and the resulting higher wildfire emissions in these months and locations, as well as the consistently

lower ozone values in the dynamical d-s compared to statistical d-s, albeit by smaller margins in the future. The shift of peak fire activity to the warmer months means higher ambient ozone compared to 2010 in both modeled cases, while the difference in the climate downscaling underlying their AAB difference, explains the difference between the cases in ozone in a given year and location.

A potential contribution to the increases in projected ozone (Figure 4.3) is from the anthropogenic sector emissions. In the projected emissions (Table 4.S1) used in the future-year simulations, VOC emissions are reduced in the mobile emissions sector to 37.5% of their 2005 levels by 2045. Over the same period, NO_x emissions are reduced to 27.6% of 2005 levels from this sector, and to 33.7% from electrical generation; these are the biggest NO_x emission sectors. On the other hand, VOC emissions from the energy sector are projected to increase by 52.4% from their 2005 values by 2045 due to increased oil and gas activity. Furthermore, VOC from agricultural production is projected to increase by 29.7% by 2045. In NO_x-rich regimes, these VOC increases could explain the increases in ambient ozone levels in both modeled cases. This combined with the lower AAB and wildfire emissions compared to 2010 explain the features seen in the time series of Figure 4. 3, that in the months of maximum intermodel differences, (a) the two cases have nearly identical ozone; (b) the differences due to increased wildfire activity become appreciable less frequently and by smaller amounts than in 2010.

PM projections

The same arguments apply as for ozone in explaining the total $PM_{2.5}$ intermodel differences over the fire season, and inter-seasonally. That is, the meteorological drivers of both seasonal and yearly wildfire activity that best explain the differences in the AQ predictions of the modeled cases are precipitation and PET in the future years. In contrast to 2010, warmer and drier

conditions earlier in the year lead to increased summer fire activity in both modeled cases, but statistical d-s has the higher $PM_{2.5}$ concentrations in the years with the larger AAB estimates.

The variability of $PM_{2.5}$ composition across the years shows an increasing contribution to the total PM mass in OC and unspeciated other PM, and slight increases in the other constituents; the exception is EC, which shows a steady decrease consistent with decreases of 24% - 60% in EC emissions from the major emission sectors (commercial marine vessels, energy, and transportation). The reduction in anthropogenic emissions reduces sulfate, nitrate, and total PM mass relative to 2010. In combination with wildfire $PM_{2.5}$ emissions that are projected to be nearly constant or slightly increasing in the later years (2053 and 2058) as shown in Figure 2.6, this leads to the higher mass fractions in those years for the PM constituents with significant contributions from wildfire (Figure 4.7). For example, PM nitrate has some of its highest seasonal average values in the spring and autumn in the later years despite the large reduction in the anthropogenic emissions of NO_x, suggesting an increasing contribution from wildfire emissions in these years. On the other hand, the projected emission increases in VOC in some anthropogenic sectors (Table 4.S1) explain the increase in OC contributions to total PM in both modeled cases through secondary organic aerosol (SOA) formation. The projected summertime ozone increases could also contribute to enhancing the SOA formation. Overall, these results indicate that wildfire emissions contribute a significant fraction to the total PM mass concentration averaged over the whole fire season, and their proportional contribution is

projected to increase as anthropogenic $PM_{2.5}$ emissions decrease, under the assumed anthropogenic emissions scenario.

Conclusions

This study assesses the projected impacts of wildfire emissions from two different emissions estimation methods that are both based on projections of AAB from a statistical model, in AQ simulations of four future years. The analyses of differences between the wildfire emissions projections find that there is likely to be less difference between them in the hourly ozone impacts from wildfire emissions in the future years than in 2010. Warmer and drier summers are projected in the future years by the WRF model, resulting in a shift in the season of maximum ozone differences between the wildfire projection methods from late autumn in 2010 to summertime, the high fire activity season in the future. Consequently, there are higher ambient ozone levels in the locations of these maximum differences. The lower AAB and AAB difference between the cases in the future years compared to 2010 (see Figure 2.3) also lead to a reduction in the maximum differences between the projection methods in the future, compared to those in 2010. Spatially, the impact of fire activity on ozone and PM in the future years is projected to be higher along the Atlantic seaboard and the Gulf coast in Texas and Florida, consistent with the spatial patterns of the AAB projected by the two methods (Shankar et al., 2018). The maximum impacts of wildfire on AQ are projected to occur in the summer, and to be as much as 1.5 ppb for ozone in 2043, and 14 $\mu g\ m^{-3}$ for $PM_{2.5}$.

As with ozone, the locations of maximum intermodel difference in $PM_{2.5}$ in future years shift east and south to Virginia and Florida in July and August, from the 2010 location in the Midwest in autumn, due to the warmer, drier conditions projected in the summers and the higher projected AAB in these areas. The total $PM_{2.5}$ concentration variability over the future years and seasons

more or less follows that of the $PM_{2.5}$ emissions projections (Figure 2.8). Projected concentrations of key wildfire PM species (OC and unspeciated Other PM) remain constant or increase slightly, offsetting the reductions by up to 84% and 76% in SO_x and NO_x from the energy and transportation sectors by 2055, the final anthropogenic inventory year used in these simulations. These results indicate that wildfire emissions will have a greater proportional impact on future PM levels as emission controls on major anthropogenic constituents such as sulfur and NO_x are implemented, and will increase the contributions of constituents that have projected increases in their anthropogenic emissions. An important caveat is that this is one of several possible future emission scenarios for the anthropogenic sectors, and does not take into account changes in other sectors, e.g., biogenics, or policy shifts in the near future regarding the use of fossil fuels, which will have a bearing on the significance of these wildfire emissions.

Another caveat is that these wildfire emissions projections were made with no changes to fuel loads. The AAB projections do not explicitly include fuel load changes and would therefore not need correcting for this omission. However, calculations of wildfire emissions in BlueSky may need to be corrected for future changes in their fuel load inputs, which are based on current FCCS fuel loads (McKenzie et al., 2007). Thus, the projected wildfire emissions could be an underestimate at least in those areas of the domain where intensive fuel management practices are not expected to be implemented. The removal of fuel by fires in the future will somewhat offset this impact, as it is also not included in these estimates.

In conclusion, both the downscaling methods perform comparably, and differ spatially and temporally from 2010 in the locations of maximum difference in the wildfire projection methods for ozone and $PM_{2.5}$. Despite the anthropogenic emission reductions, and the resulting drop in concentrations in 2043 relative to 2010, constituent concentrations of wildfire PM (OC and Other

PM) remain at that level, or even increase in future years; this results in as much as a 50% increase in the case of Other PM in the summer from 2010 to 2058. As the emissions of most of the PM constituents are reduced in the anthropogenic sectors (maximum decrease of 84% by 2058), but less so from wildfires (maximum decrease of 40 % in 2048), these constituent mass fraction increases can be inferred as the net contribution of wildfire PM, both primary and secondary, to the total ambient $PM_{2.5}$ concentration. The net increase in wildfire-driven $PM_{2.5}$ is estimated to be ~ 4.5% in the summers, based on the average increase projected by the modeled cases in $PM_{2.5}$ from 2043 to 2058 (Figure 4.S2), and is consistent with the projected median increase in AAB over this period. The impact assessment done by subtracting the baseline no-fire simulation from the statistical d-s simulation estimates much larger increases than this at specific locations due to wildfires. However, equivalent or larger decreases in $PM_{2.5}$ are projected in the spring and autumn over the same period. Overall, the projected $PM_{2.5}$ concentrations capture the inter-year variability of the wildfire emissions that would not be possible to represent with empirically based inventories. This confirms the study hypothesis that the projected wildfire emissions will lead to ozone and $PM_{2.5}$ spatial distributions and seasonal-average concentrations that significantly deviate from 2010 levels by mid-century.

Acknowledgments

This research was supported entirely through funding provided by USDA Forest Service to the University of North Carolina at Chapel Hill under joint venture agreement 11-JV-11330143-080. The author[16] thanks Dr. J. P. Prestemon (USDA Forest Service) for his support of this

[16] Author Contributions. The author designed the research described in collaboration with Dr. D. McKenzie and

study, in particular, the use of his annual area burned projections, and his insights into the socioeconomic scenarios represented in those data. She thanks Dr. D. McKenzie (USDA Forest Service) for his insights into the role of wildfire emissions in these analyses. The author is grateful for the editorial comments that he and Dr. W. Vizuete provided on this chapter. The author thanks Dr. D. Loughlin (U. S. Environmental Protection Agency) for his assistance in obtaining the anthropogenic emissions projections used in this study. The contributions of Ms. D. Yang, Dr. B. Baek, Dr. M. Omary, Mr. K. Talgo, Dr. A. Xiu to the modeling, and the timely software support by Ms. E. A. Adams on the VERDI visualization tool are gratefully acknowledged.

.

Dr. J. P. Prestemon, and directed all aspects of the modeling. Dr. A. Xiu and Mr. K. Talgo prepared all meteorological data used in the CMAQ modeling. The author directed and participated in the CMAQ modeling and performed all analysis of the model results presented here, with assistance from Ms. D. Yang. She prepared all drafts of the chapter manuscript, and participated in the editing of the manuscript in coordination with Dr. D. McKenzie, Dr. W. Vizuete and Dr. J. P. Prestemon.

Table 4.1. Seasonal mean and maximum differences in hourly O_3 between wildfire emissions methods in each modeled year.

Note: Differences are calculated over grid cells containing Air Quality System (AQS) monitors and wildfires. Max. Δ-O_3, maximum difference (statistical d-s – dynamical d-s) in hourly O_3 mixing ratios; Dyn. d-s O_3, O_3 mixing ratio from dynamical d-s simulation. $^+$ Denotes maximum difference over the entire fire season in a given year.

	Mean Δ-O_3 (ppb)			Spring		Summer		Autumn	
Year	Spring	Summer	Autumn	Max. Δ-O_3 (ppb)	Dyn. d-s O_3 at max. Δ-O_3 (ppb)	Max. Δ-O_3 (ppb)	Dyn. d-s O_3 at max. Δ-O_3 (ppb)	Max. Δ-O_3 (ppb)	Dyn. d-s O_3 at max. Δ-O_3 (ppb)
2010	0.05	0.12	0.21	30.9	44.9	41.5	70.0	67.1$^+$	16.3
2043	0.02	0.18	0.00	18.6	48.3	23.2$^+$	52.6	5.9	59.2
2048	0.01	0.11	0.04	18.3	47.5	25.2$^+$	44.5	24.0	58.5
2053	0.01	0.19	0.02	38.8$^+$	40.4	22.5	54.2	22.0	57.3
2058	0.02	0.17	0.00	14.0	66.0	37.6$^+$	47.9	0.2	38.9

Table 4.2. Locations and times of seasonal maximum differences in hourly O_3 between wildfire emissions methods in each modeled year.

Note: Differences are calculated over grid cells containing Air Quality System (AQS) monitors and wildfires. Lat-lon, latitude-longitude; Max. Δ-O_3, maximum difference (statistical d-s – dynamical d-s) in hourly O_3 mixing ratios. $^+$ Denotes location of maximum difference over the fire season in a given year. These are Chesterfield, MO in 2010; Moundsville, WV in 2043; two proximal locations in Middlesboro, KY in 2048 and 2058, and Seabrook, TX in 2053.

	Spring		Summer		Autumn	
Year	Lat-lon of max. Δ-O_3	Month/day of max. Δ-O_3	Lat-lon of max. Δ-O_3	Month/day of max. Δ-O_3	Lat-lon of max. Δ-O_3	Month/day of max. Δ-O_3
2010	36.91, -87.32	April 18	36.13, -96.00	June 24	38.64, -90.35$^+$	October 29
2043	30.39, -89.05	May 16	39.92, -80.73$^+$	August 27	40.51, -81.64	September 1
2048	26.27, -80.30	May 14	36.67, -83.53$^+$	July 18	37.48, -82.53	September 8
2053	29.58, -95.02$^+$	May 17	29.94, -89.92	August 19	37.91, -80.63	September 6
2058	37.28, -83.21	April 20	36.61, -83.74$^+$	July 19	37.30, -79.96	September 1

Table 4.3. Domain-wide maxima and locations of the seasonal average impacts of wildfire emissions on hourly ozone (ppbV) projected by the statistical d-s method

Note: Wildfire impact is defined as the ozone mixing ratio difference (statistical d-s – baseline no-wildfire).

Year → Season↓	2043	2048	2053	2058
Spring	0.80 South Florida	0.13 South Florida	0.16 KY-OH border	0.17 KY-OH border
Summer	1.48 KY-OH border	0.57 KY-OH border	0.85 KY-OH border	1.11 Appalachia
Autumn	0.08 Ohio Valley	< 0.01	0.32 Eastern Oklahoma	< 0.01

Table 4.4. Seasonal mean and maximum differences in daily-average $PM_{2.5}$ between wildfire emissions methods in each modeled year.

Note: Differences are calculated at grid cells containing Interagency Monitoring for PROtected Visual Environments (IMPROVE) monitors and wildfires. Max. Δ-$PM_{2.5}$, maximum difference (statistical d-s – dynamical d-s) in daily-average $PM_{2.5}$ concentrations; Dyn. d-s $PM_{2.5}$, $PM_{2.5}$ concentration from dynamical d-s simulation. + Denotes maximum difference over the fire season in a given year.

	Mean Δ-$PM_{2.5}$ (μg m^{-3})			Spring		Summer		Autumn	
Year	Spring	Summer	Autumn	Max. Δ-$PM_{2.5}$ (μg m^{-3})	Dyn. d-s $PM_{2.5}$ at maximum (μg m^{-3})	Max. Δ-$PM_{2.5}$ (μg m^{-3})	Dyn. d-s $PM_{2.5}$ at maximum (μg m^{-3})	Max. Δ-$PM_{2.5}$ (μg m^{-3})	Dyn. d-s $PM_{2.5}$ at maximum (μg m^{-3})
2010	0.12	0.33	0.42	7.85	7.04	14.9	10.6	26.0+	8.64
2043	0.04	0.41	0.00	7.46	6.04	16.8+	8.04	3.01	4.27
2048	0.04	0.28	0.12	4.64	5.86	10.6+	11.2	9.55	11.2
2053	0.06	0.45	0.07	5.58	4.52	16.1+	9.56	14.7	11.8
2058	0.08	0.38	0.00	8.94	9.66	13.1+	6.16	0.10	12.0

Table 4.5. Locations and times of seasonal maximum differences in daily-average $PM_{2.5}$ between wildfire emissions methods in each modeled year.

Note: Differences are calculated over grid cells containing Interagency Monitoring for PROtected Visual Environments (IMPROVE) monitors and wildfires. Lat-lon, latitude-longitude; Max. Δ-$PM_{2.5}$, maximum difference (statistical d-s – dynamical d-s) in daily-average $PM_{2.5}$ concentrations; + Denotes location of maximum difference over the fire season in a given year. These are Mingo National Wildlife Refuge, MO in 2010; Quaker City, OH in 2043 and 2048, and James River Wilderness, VA in 2053 and 2058.

	Spring		Summer		Autumn	
Year	Lat-lon of max. Δ- $PM_{2.5}$	Month/day of max. Δ- $PM_{2.5}$	Lat-lon of max. Δ- $PM_{2.5}$	Month/day of max. Δ- $PM_{2.5}$	Lat-lon of max. Δ- $PM_{2.5}$	Month/day of max. Δ- $PM_{2.5}$
2010	38.52, -78.43	April 17	37.63, -79.51	August 6	36.97, -90.14+	October 20
2043	25.39, -80.68	May 17	39.94, -81.34+	July 28	35.97, -81.93	September 8
2048	30.09, -84.16	May 29	39.94, -81.34+	August 15	39.94, -81.34	September 2
2053	28.75, -82.55	May 23	37.63, -79.51+	July 28	39.94, -81.34	September 8
2058	39.94, -81.34	April 26	37.63, -79.51+	July 22	39.71, -79.01	November 10

Table 4.6. Domain-wide maxima and locations of the seasonal average impacts of wildfire emissions on hourly $PM_{2.5}$ ($\mu g\ m^{-3}$) projected by the statistical d-s method

Note: Wildfire impact is defined as the $PM_{2.5}$ concentration difference (statistical d-s – baseline no-wildfire).

Year → Season↓	2043	2048	2053	2058
Spring	5.6 South Florida	3.8 South Florida	4.3 KY-OH border	3.0 Ohio valley
Summer	7.9 KY-OH border	3.4 KY-OH border	4.6 Appalachia	14.0 Appalachia
Autumn	1.5 Northern Ohio	4.3 Central Missouri	4.6 Eastern Oklahoma	< 0.01

Table 4.7. Difference (%) between statistical d-s and dynamical d-s in $PM_{2.5}$ and constituents by season and year.

Note: % difference = (statistical d-s – dynamical d-s) / (statistical d-s + dynamical d-s) x 200.

		Difference (%) Between Modeled Cases						
Season	Year	SO_4	NO_3	NH_4	EC	OC	OTHER	Total $PM_{2.5}$
Spring	2010	0.10	0.79	0.47	2.56	6.36	4.68	1.51
	2043	0.06	0.11	0.09	1.26	2.71	1.17	0.60
	2048	0.06	0.19	0.13	0.99	2.04	1.39	0.62
	2053	0.10	0.38	0.20	2.22	3.77	1.62	0.86
	2058	0.15	0.53	0.18	3.62	6.12	1.36	1.18
Summer	2010	0.66	7.04	2.36	7.46	17.11	12.58	4.18
	2043	0.62	5.48	0.26	12.57	24.89	8.66	6.16
	2048	0.40	2.91	0.70	8.32	18.54	5.54	3.65
	2053	0.66	6.54	0.47	17.81	28.67	12.65	6.85
	2058	0.61	3.63	0.39	16.27	25.50	11.43	6.12
Autumn	2010	-0.30	4.27	1.22	7.71	16.78	7.14	4.19
	2043	0.02	0.03	0.04	0.28	0.62	0.76	0.31
	2048	-3.77	-1.35	-3.31	1.02	4.38	-0.81	-1.44
	2053	0.12	0.29	0.18	2.11	3.63	1.46	0.96
	2058	0.00	0.00	0.00	0.01	0.02	0.00	0.00

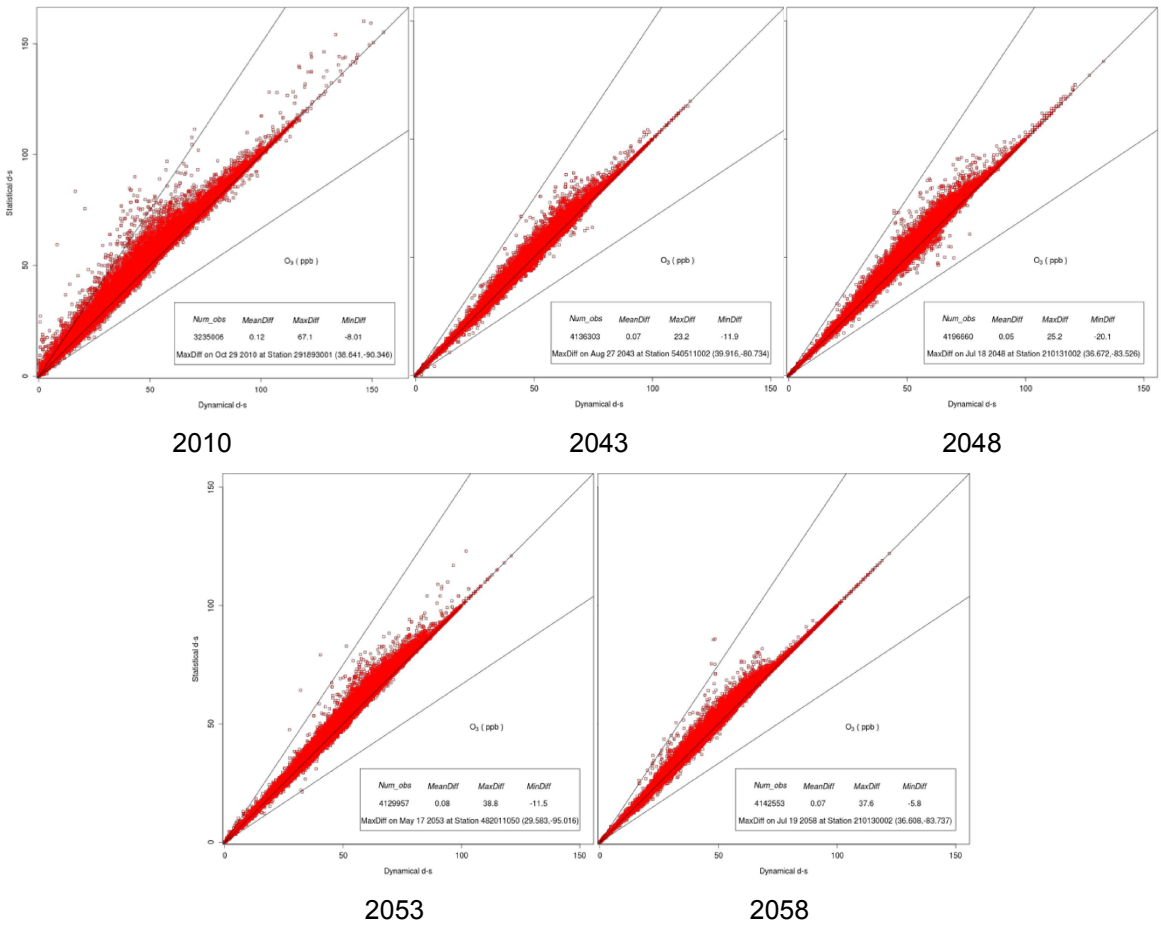

Figure 4.1. Comparisons of wildfire emissions methods over the fire season for 1-hr O_3 (ppb) predicted at grid cells containing Air Quality System (AQS) monitors and wildfires in each modeled year. The mean, maximum and minimum intermodel difference (statistical d-s – dynamical d-s), denoted, respectively, MeanDiff, MaxDiff and MinDiff, and the dates and coordinates of their occurrence are shown in the plot legend.

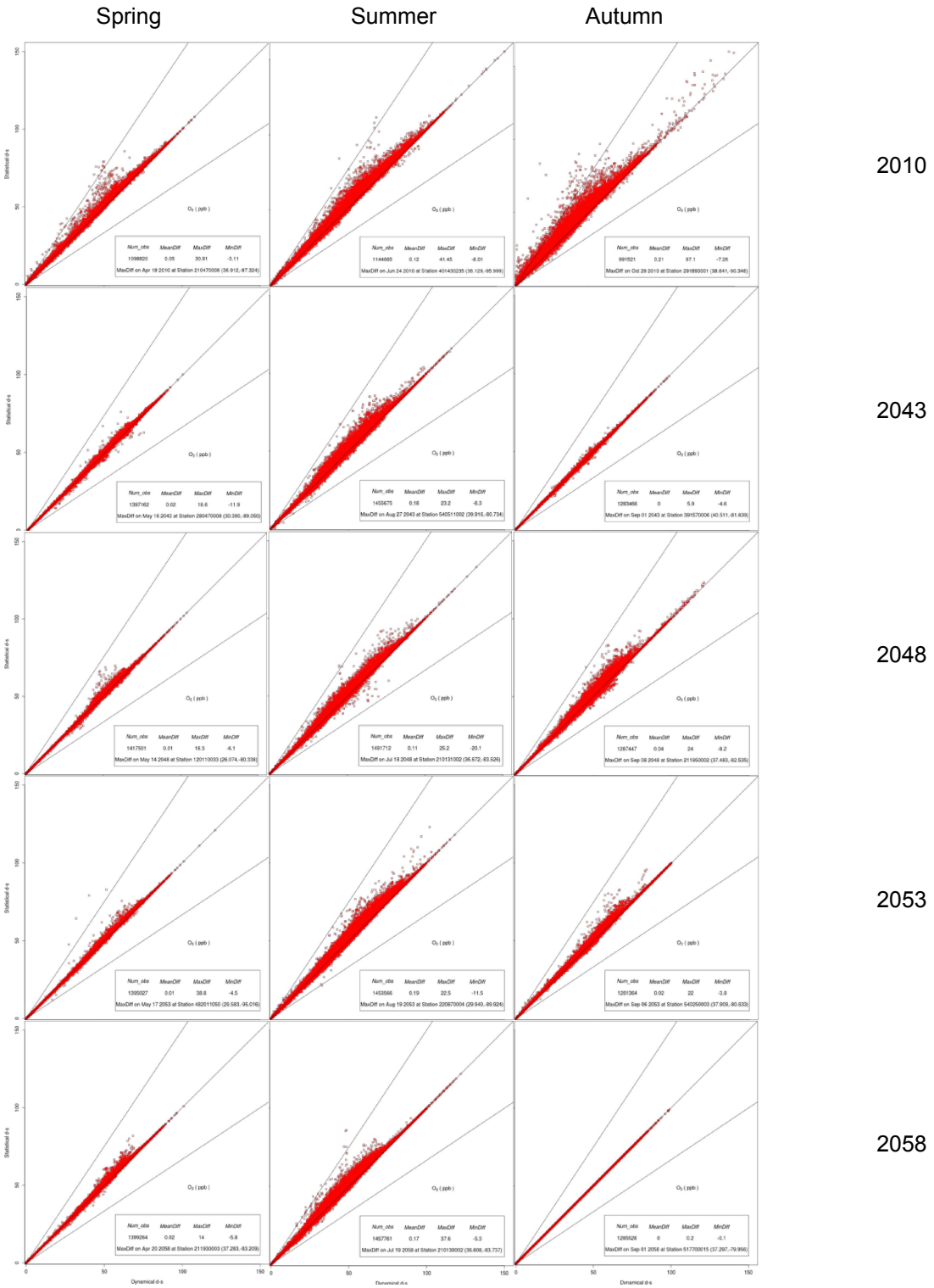

Figure 4.2. Seasonal comparisons of wildfire emissions methods for 1-hr O_3 (ppb) predicted at grid cells containing Air Quality System (AQS) monitors and wildfires in each modeled year. The mean, maximum and minimum intermodel difference (statistical d-s – dynamical d-s), denoted, respectively, MeanDiff, MaxDiff and MinDiff, and the dates and coordinates of their occurrence are shown in the plot legend.

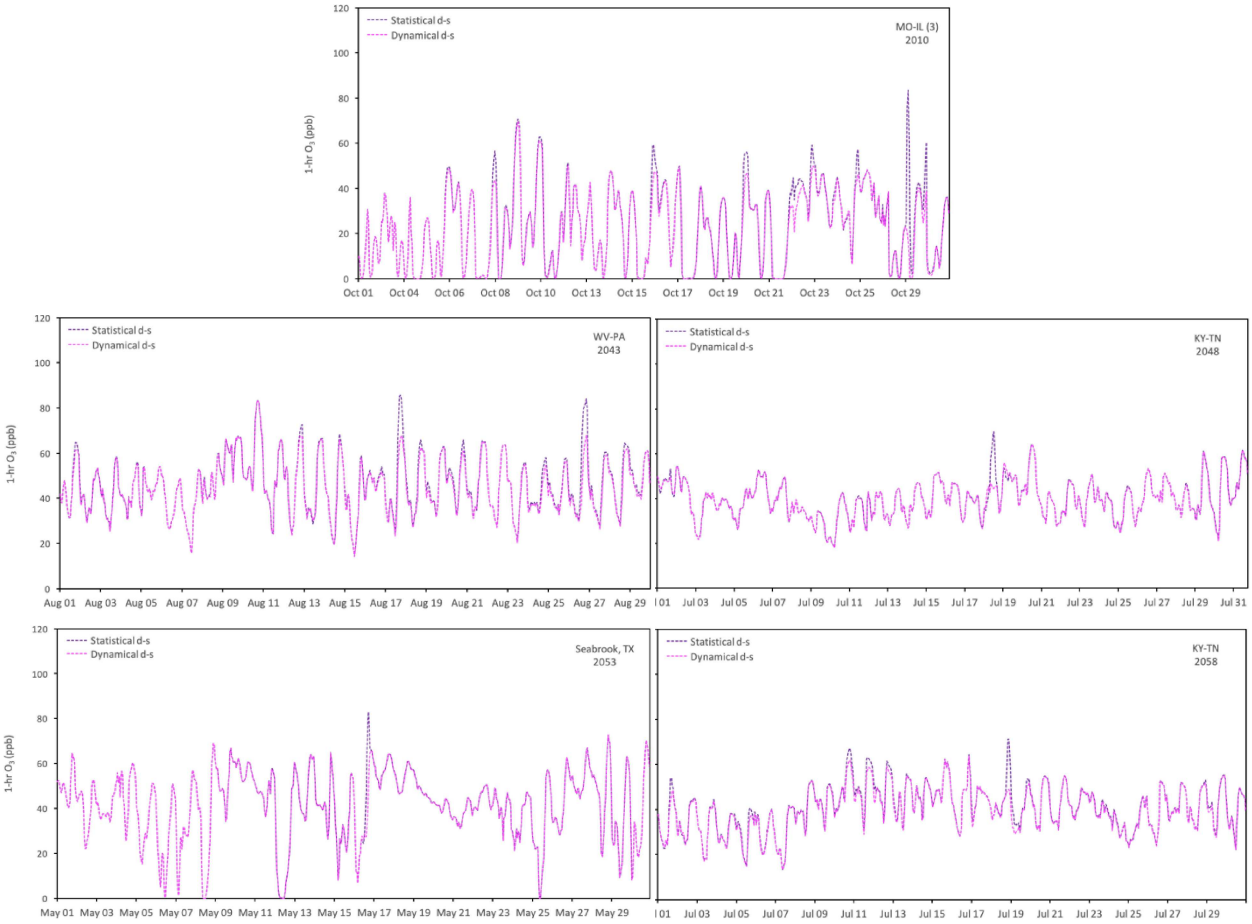

Figure 4.3. Hourly ozone time series in the months and locations of maximum difference in ozone (statistical d-s – dynamical d-s) identified in Table 4.2 over the fire season in each modeled year. Top: Chesterfield, MO, on the MO-IL border; Middle: L – Moundsville, WV, near the WV-PA border; R – Middlesboro, KY, near the KY-TN border; Bottom: L – Seabrook, TX, on the Gulf Coast; R – Middlesboro, KY.

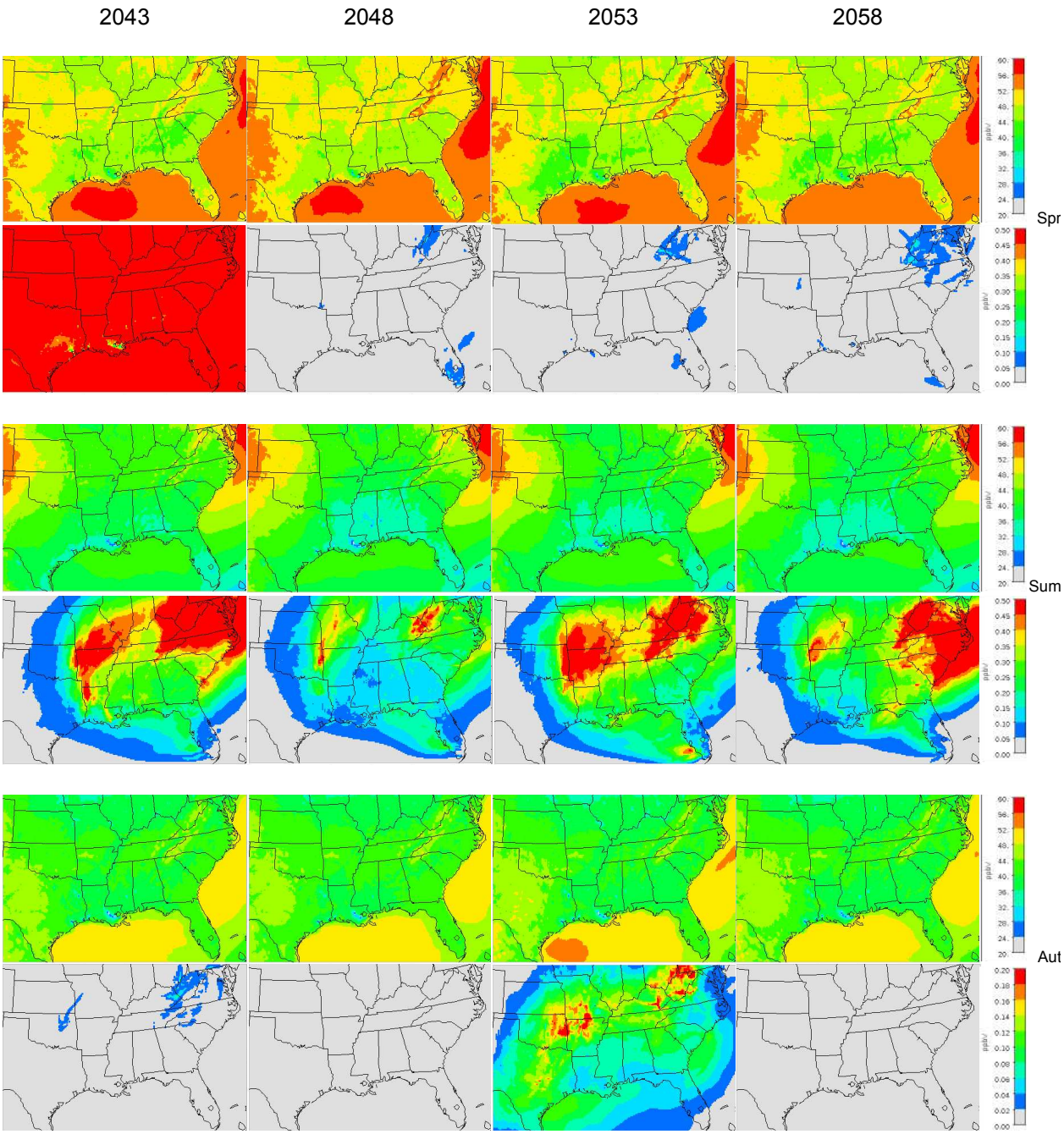

Figure 4.4. Seasonal-average spatial distribution of hourly ozone mixing ratios (ppbV) from a no-wildfire baseline simulation (Rows 1, 3 and 4) and difference in ozone (statistical d-s - baseline no-wildfire) simulations (Rows 2, 4, and 6) in each future year. Note the scale change in Row 6 to display the spatial pattern. Spr, Spring; Sum, Summer; Aut, Autumn.

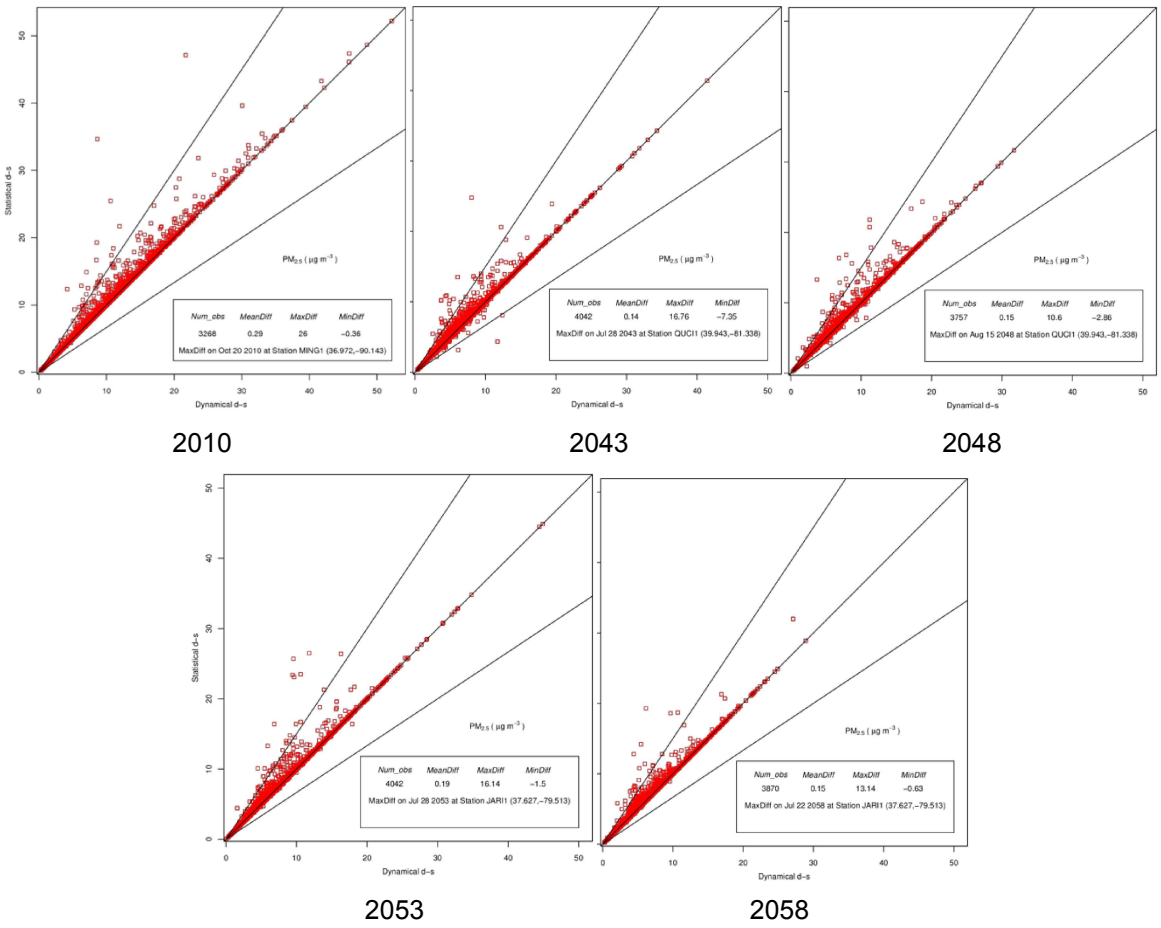

Figure 4.5. Comparisons of wildfire emissions methods over the fire season for $PM_{2.5}$ (μg m^{-3}) predicted at grid cells containing both Interagency Monitoring of PROtected Visual Environments (IMPROVE) monitors and wildfires in each modeled year. The mean, maximum and minimum intermodel difference (statistical d-s – dynamical d-s), denoted, respectively, MeanDiff, MaxDiff and MinDiff, and the dates and coordinates of their occurrence are shown in the plot legend.

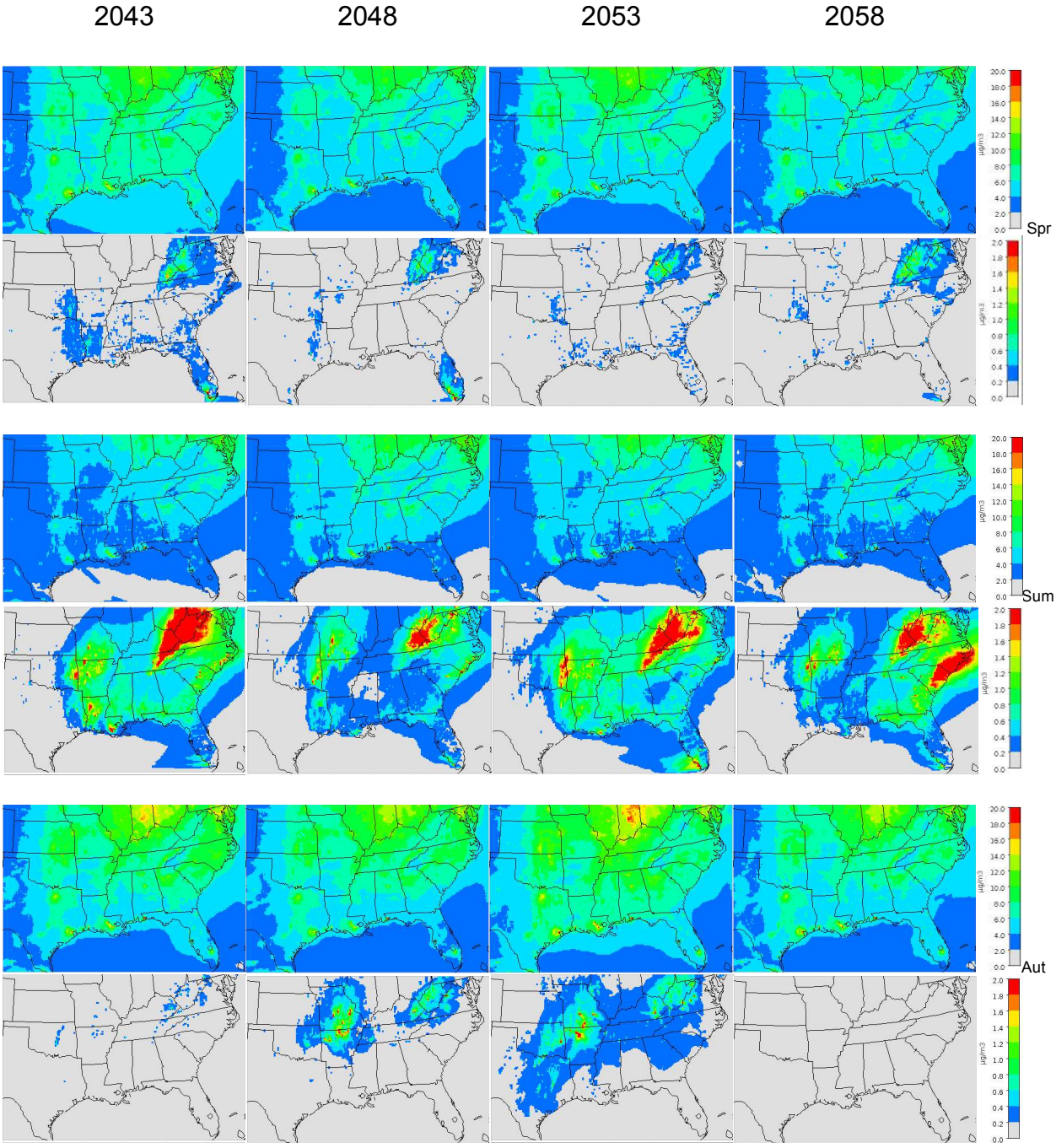

Figure 4.6. Seasonal-average hourly $PM_{2.5}$ (µg m^{-3}) from a no-wildfire baseline simulation (Rows 1, 3 and 4) and difference in $PM_{2.5}$ (statistical d-s - baseline no-wildfire) simulations (Rows 2, 4, and 6) in each future year. Spr, Spring; Sum, Summer; Aut, Autumn.

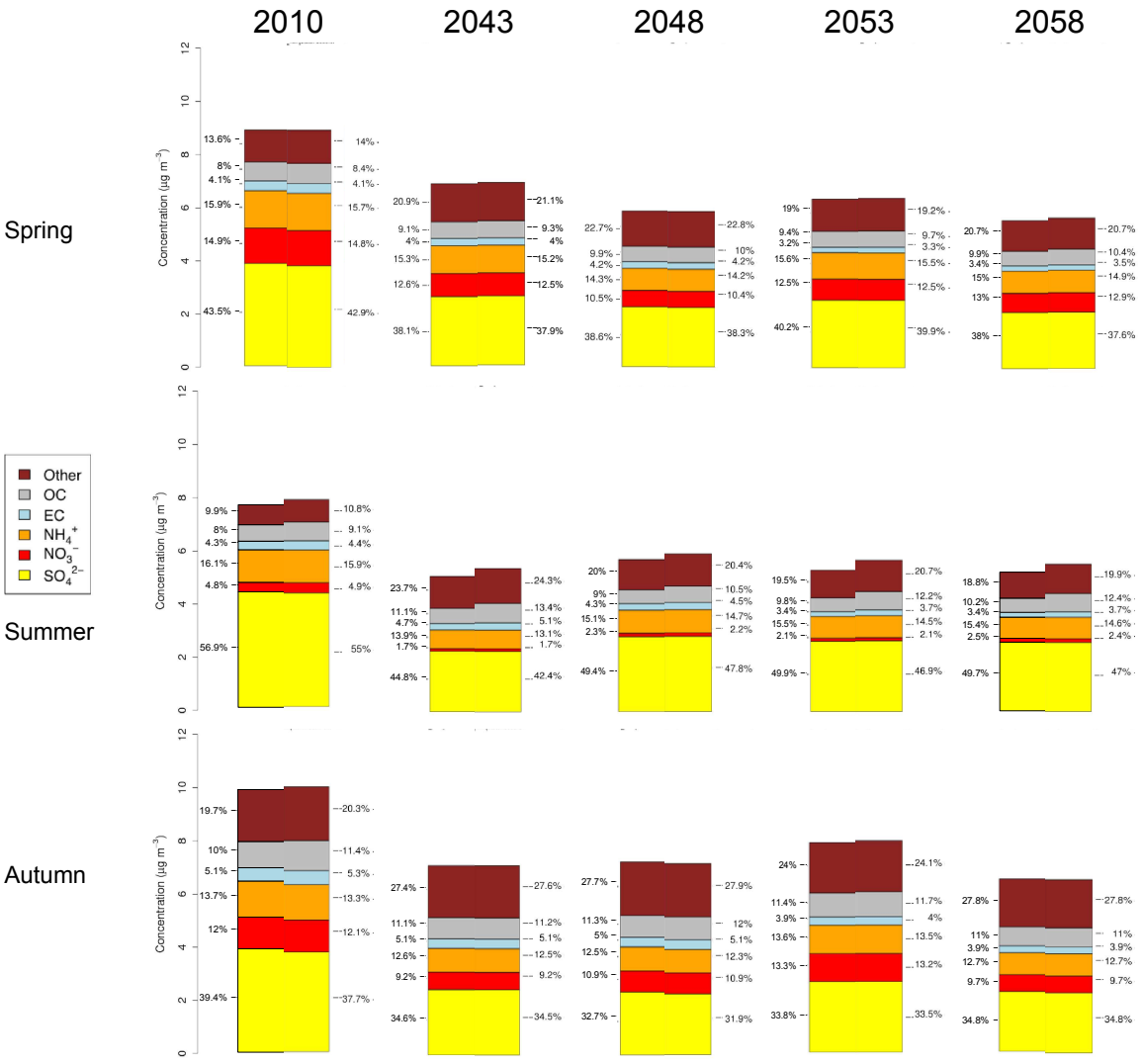

Figure 4.7. $PM_{2.5}$ composition (μg m^{-3}) averaged over IMPROVE sites in each season in each modeled year from the dynamical d-s simulation (L) and the statistical d-s simulation (R).

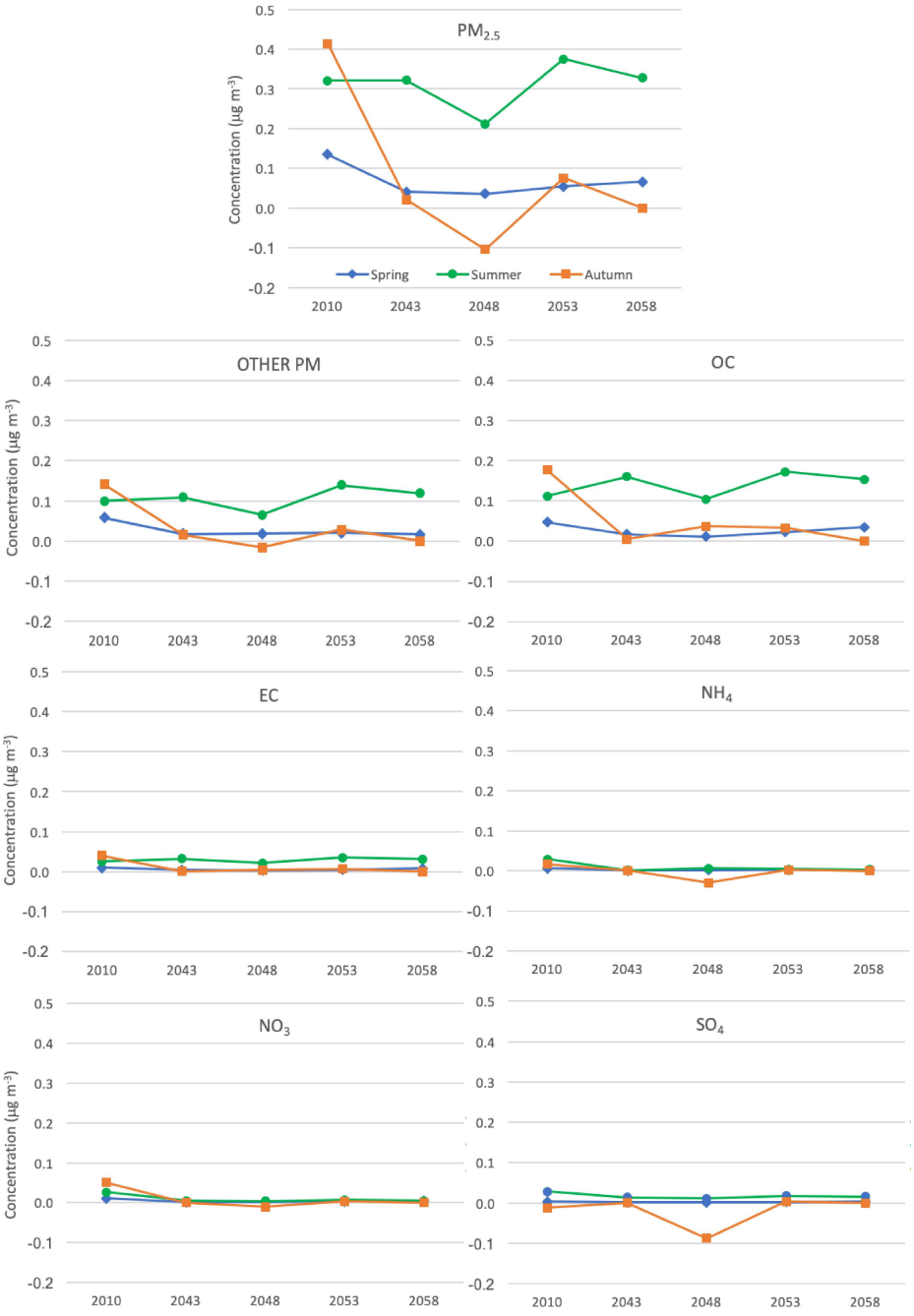

Figure 4.8. Seasonal average intermodel differences (statistical d-s – dynamical d-s) in $PM_{2.5}$ and constituents (µg m^{-3}) in the years simulated.

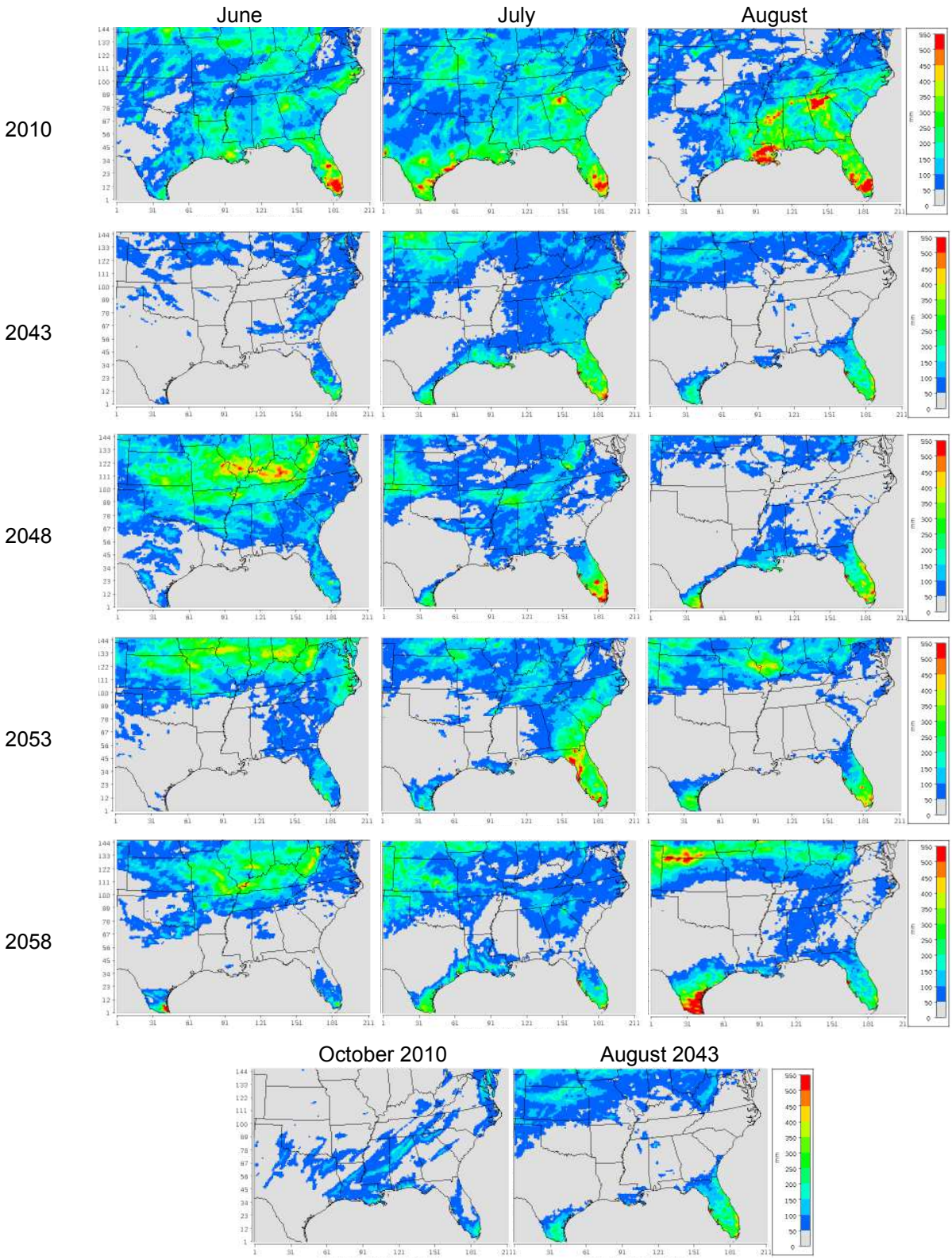

Figure 4.9. Monthly total precipitation predicted by the WRF model in the summer months. Row 1 – 5: 2010, 2043, 2048, 2053 and 2058; Row 6: October 2010 and August 2043, the months of maximum intermodel difference in ozone over the fire season in those years.

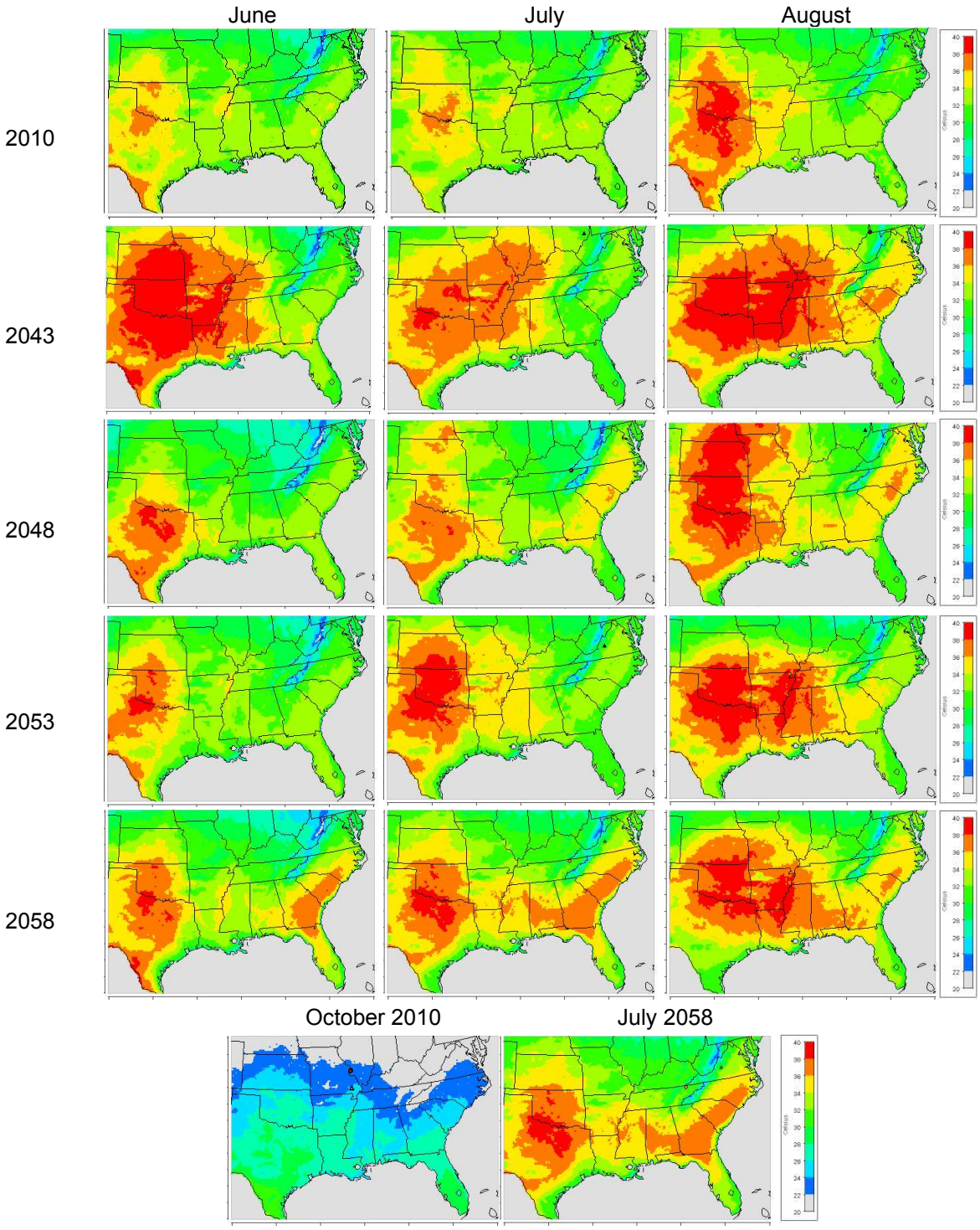

Figure 4.10. Monthly average daily maximum temperature (°C) predicted by the WRF model in in the summer months. Rows 1-5: 2010, 2043, 2048, 2053 and 2058; Row 6: October 2010 and July 2058, the months of maximum intermodel difference in both ozone and $PM_{2.5}$ over the fire season in those years. The locations of their occurrence, also provided in Tables 4.2 and 4.4, are denoted by circles for ozone, and triangles for $PM_{2.5}$.

Supplemental Material for Chapter 4

Table 4.S1. Emission growth /control factors for pollutant emissions by anthropogenic source sector used in the Sparse Matrix Operator Kernel Emissions (SMOKE) processing system for the future-year simulations.

Note: These factors are multipliers applied to 2005 emissions to estimate the emissions in 2045. Anthropogenic emissions in RCP4.5 are projected to decrease in most of these sectors from 2045 to 2055 by 2% - 5% every 5 years, depending on the pollutant and the source sector, but increases in emissions, shown here as multipliers greater than 1, are projected in some sectors, e.g., aviation and agriculture. NO_x, oxides of nitrogen; PNO_3, particulate nitrate; SO_2, sulfur dioxide; PSO_4, particulate sulfate; CO, carbon monoxide; VOC, volatile organic compounds; NH_3, ammonia; PNH_4, particulate ammonium; CH_4, methane; BC, black carbon; OC, organic carbon.

Emission Sector	NO_x	PNO_3	SO_2	PSO_4	CO	VOC	NH_3	PNH_4	CH_4	EC	OC
Rail, truck, transit and passenger transport	0.28	0.28	0.52	0.52	0.23	0.38	0.66	0.66	0.66	0.73	1.03
Deep sea freight	0.47	0.47	0.18	0.18	0.47	0.68			0.97	0.76	0.61
Aviation	1.04	1.04	0.93	0.93	0.51	0.74			1.07	1.20	1.19
Energy conversion, extraction and distribution	0.34	0.34	0.26	0.26	0.63	1.52	0.52	0.52	0.86	0.63	0.77
Industry (combustion and processing)	0.53	0.53	0.51	0.51	0.44	0.61	0.79	0.79	0.95	0.40	0.00
Agricultural production	1.25	1.25				1.30	1.26	1.26	1.17		
Commercial and institutional fuel combustion	0.69	0.69	0.63	0.63	0.37	0.54	0.68	0.68	0.77	0.47	0.52

Table 4.S2. Monthly mean values and differences in hourly O_3 in the months and locations of maximum intermodel difference in each modeled year.

Note: Δ-O_3, hourly ozone difference (statistical d-s – dynamical d-s)

Year	Month	Location	Monthly Mean Hourly O_3 (ppb)		Monthly Mean Δ-O_3 (ppb)
			Statistical d-s	Dynamical d-s	
2010	October	Centerfield, MO	23.50	22.18	1.32
2043	August	Moundsville, WV	45.94	44.84	1.10
2048	July	Middlesboro, KY	39.68	39.60	0.08
2053	May	Seabrook, TX	42.59	41.38	0.21
2058	July	Middlesboro, KY	39.59	39.34	0.25

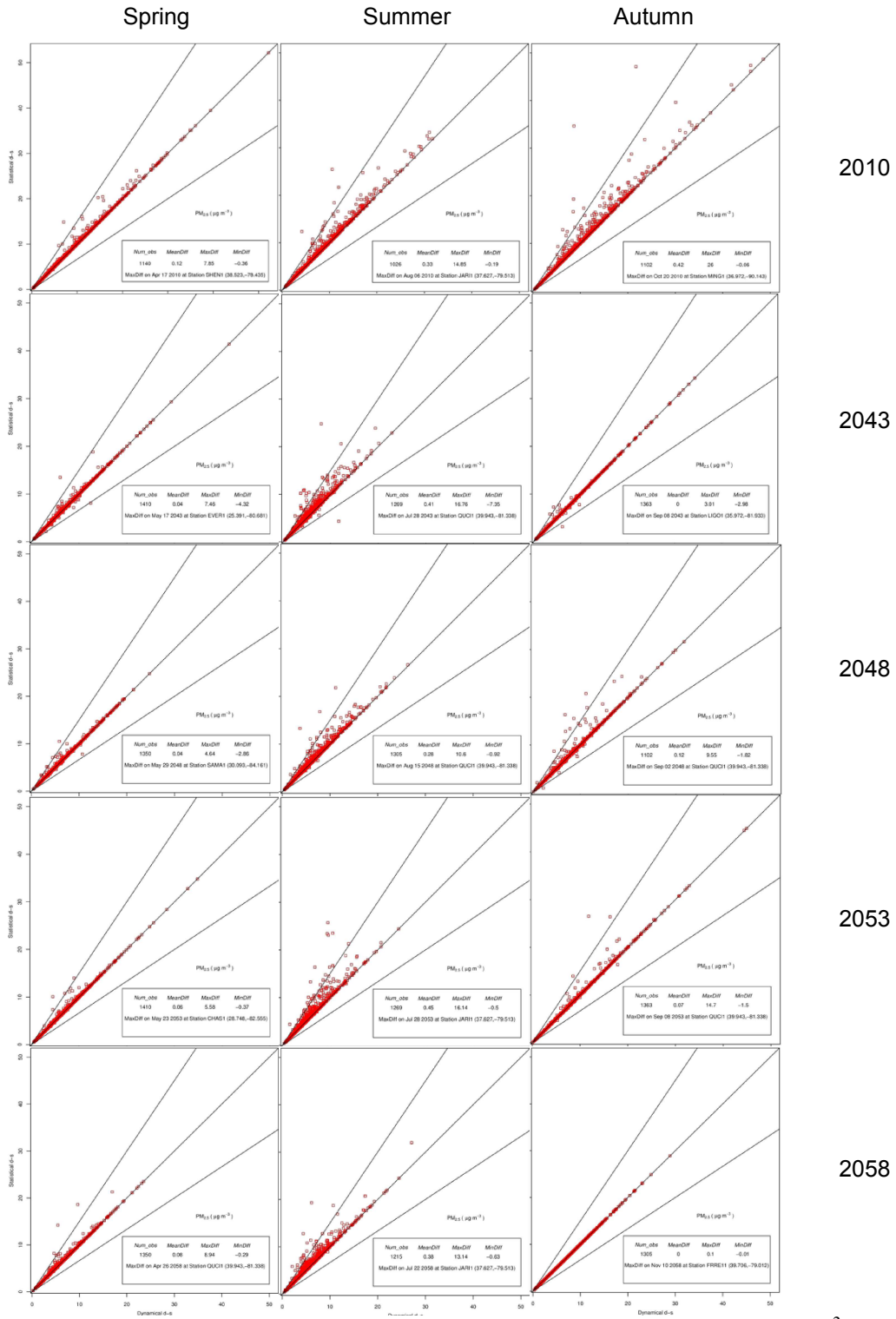

Figure 4.S1. Seasonal comparisons of wildfire emissions methods for $PM_{2.5}$ (μg m^{-3}) predicted at grid cells containing Interagency Monitoring for PROtected Visual Environments (IMPROVE) monitors and wildfires in each modeled year. The mean, maximum and minimum intermodel difference (statistical d-s – dynamical d-s), denoted, respectively, MeanDiff, MaxDiff and MinDiff, and the dates and coordinates of their occurrence are shown in the plot legend.

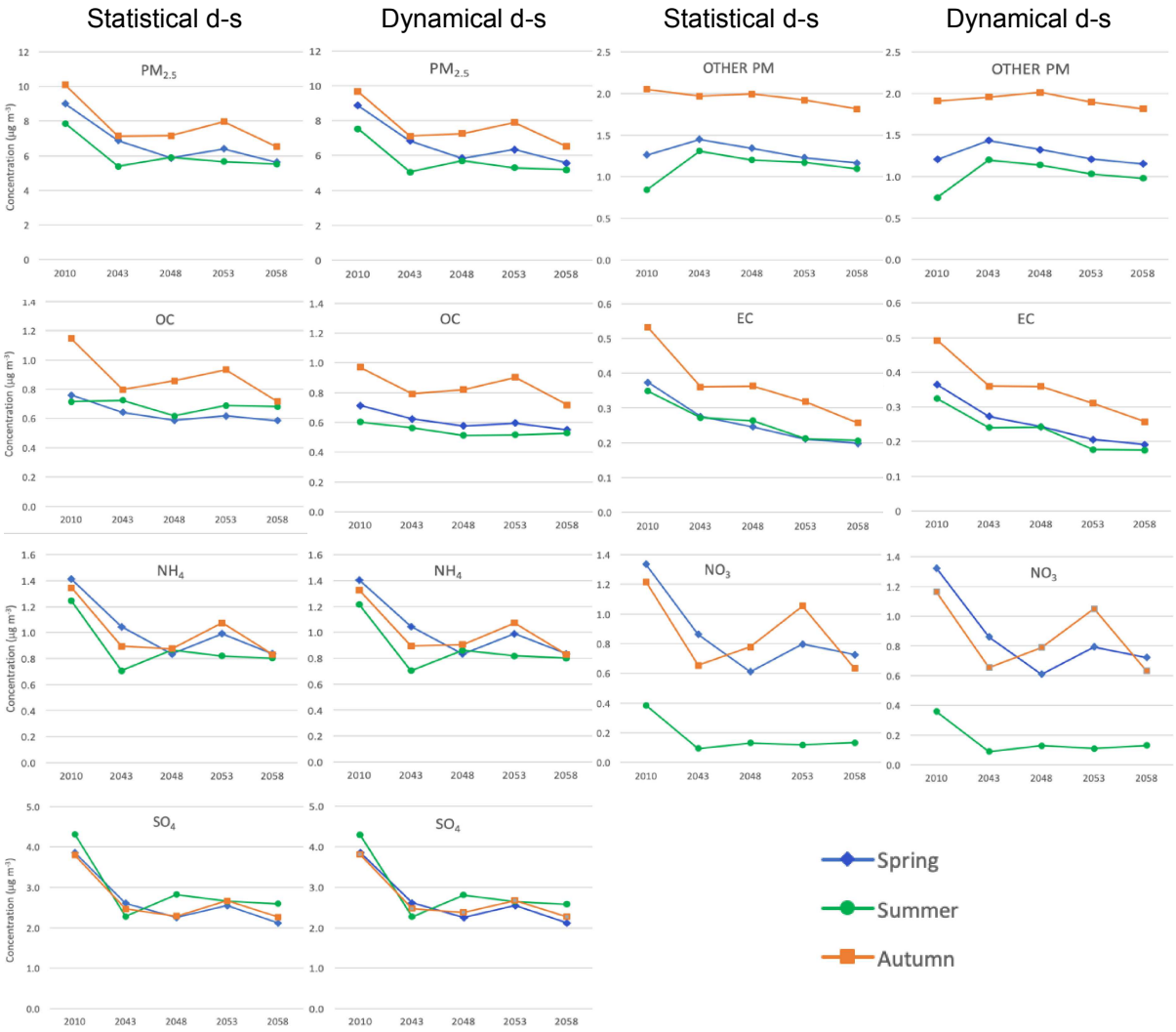

Figure 4.S2. Seasonal-average concentrations (µg m^{-3}) of $PM_{2.5}$ and constituents over all grid cells containing Interagency Monitoring for PROtected Visual Environments (IMPROVE) monitors and wildfires in each modeled year from each modeled case.

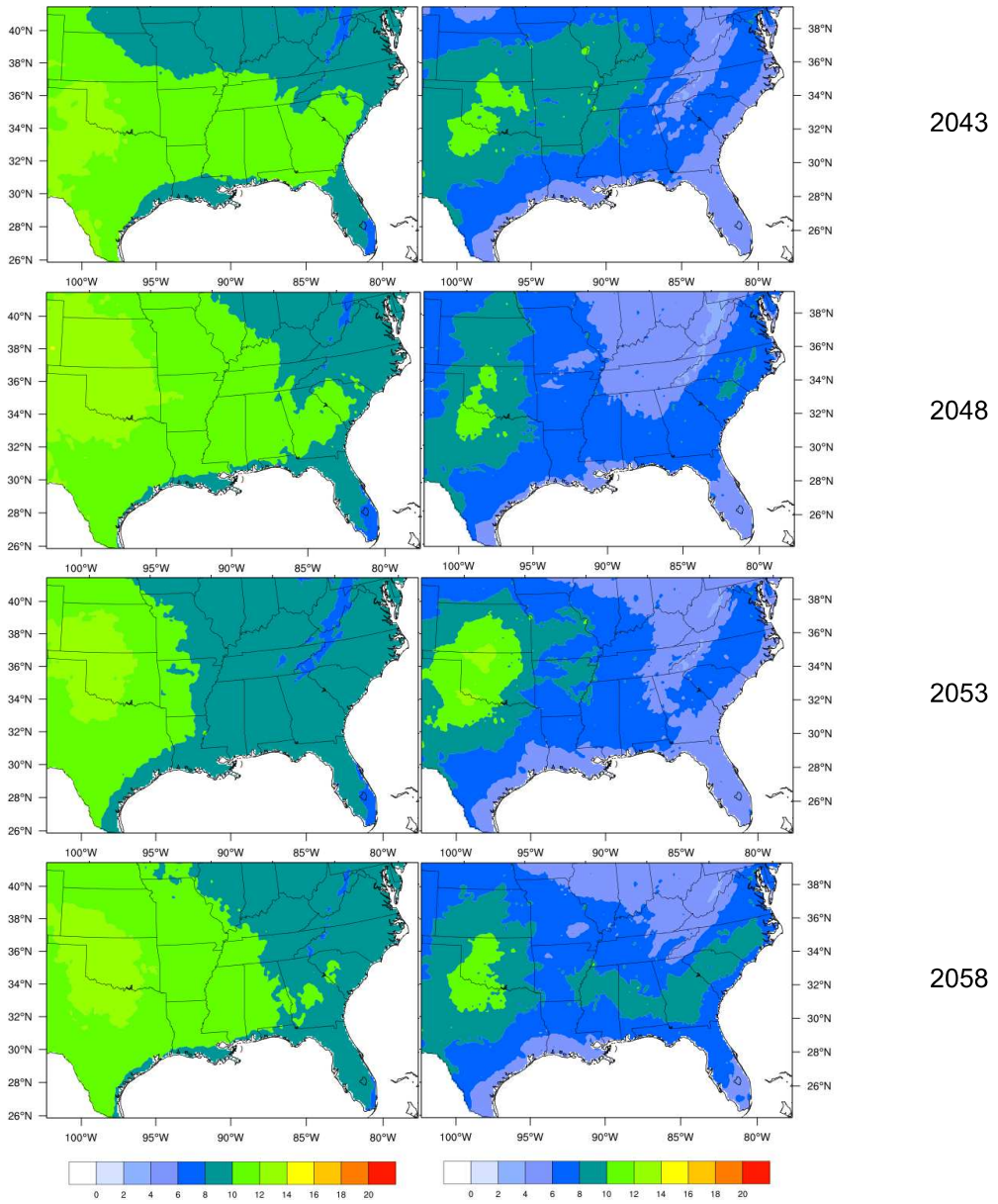

Figure 4.S3. Potential evapotranspiration (PET – mm) used in the AAB estimates in July of each future year, calculated from statistical downscaling (L), and dynamical downscaling (R) of the meteorological inputs.

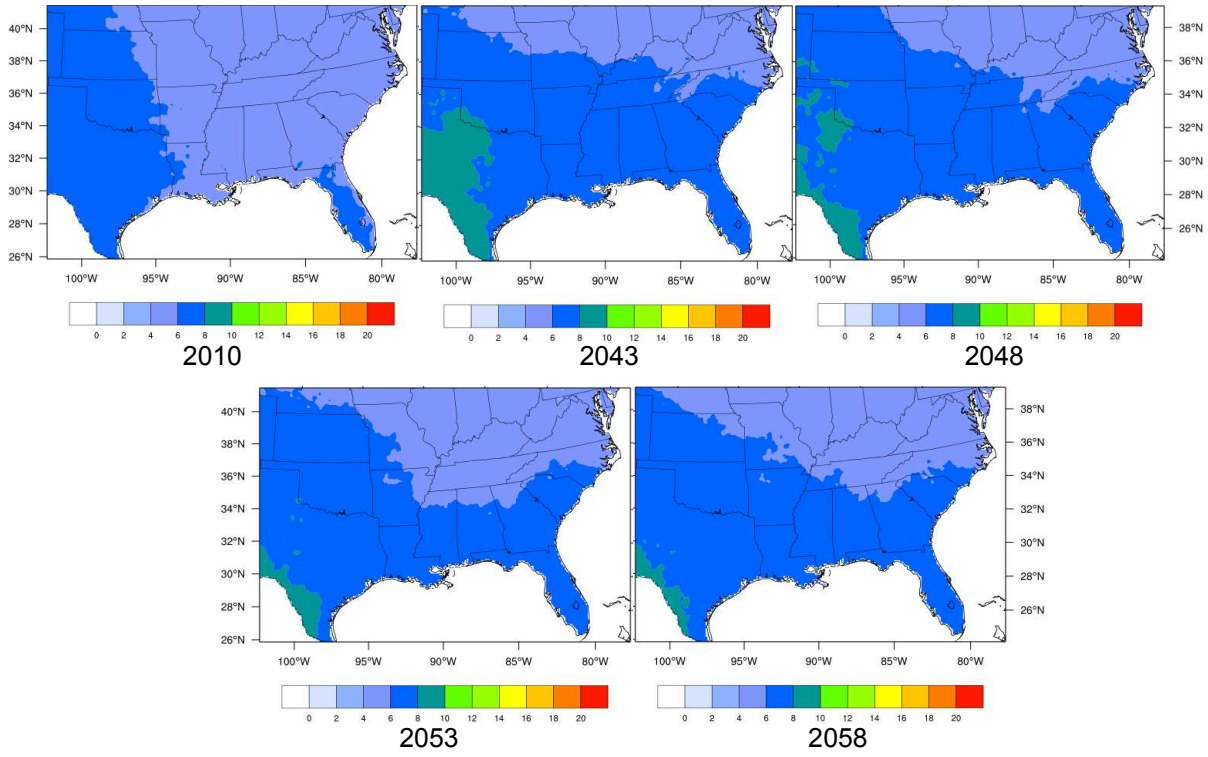

Figure 4.S4. Potential evapotranspiration (PET – mm) from statistical downscaling averaged yearly in each of the modeled years.

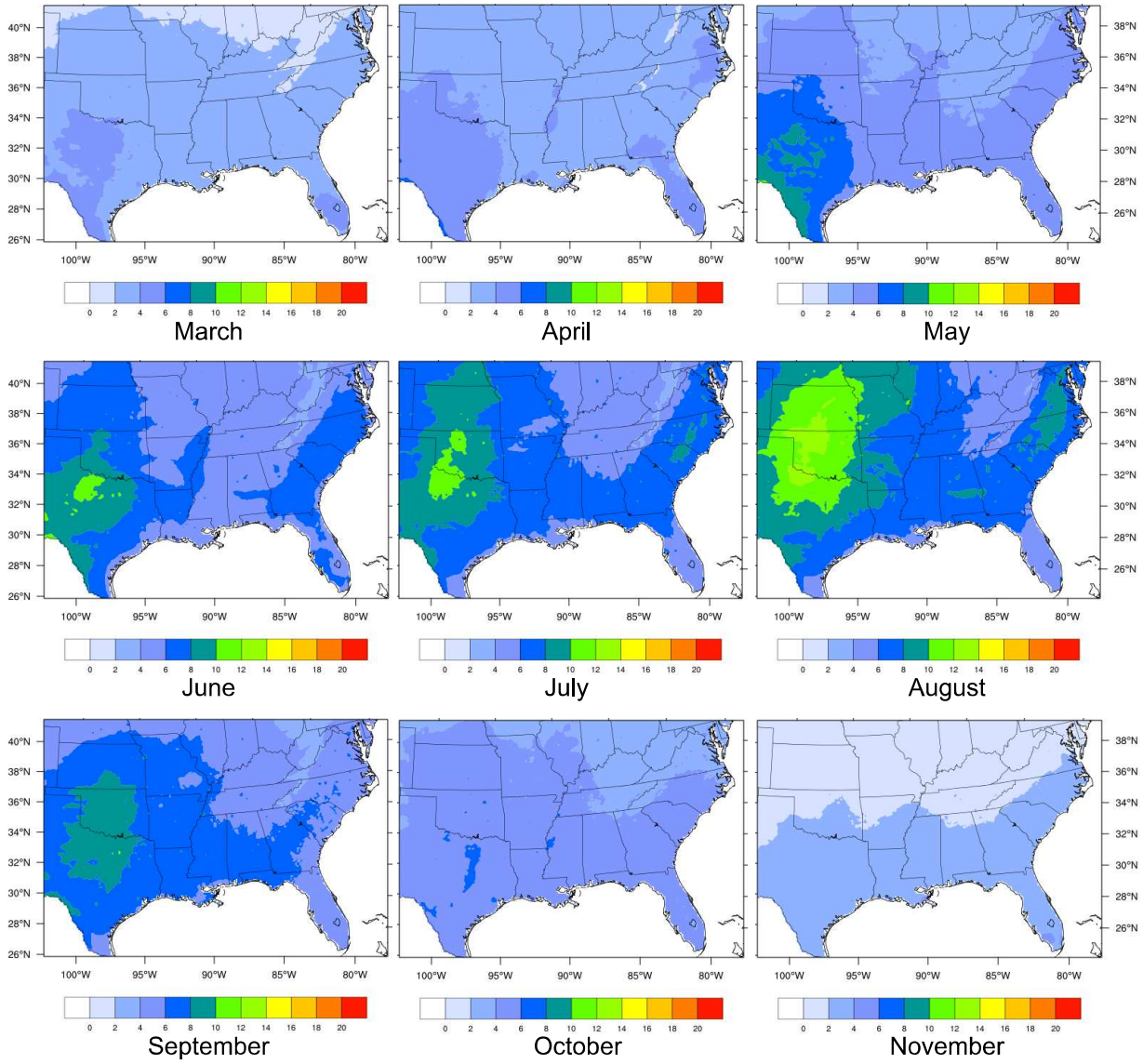

Figure 4.S5. Monthly-averaged potential evapotranspiration (PET – mm) from statistical downscaling in 2048. Top: spring; middle – summer; bottom – autumn.

CHAPTER 5: CONCLUSIONS

Introduction

This chapter summarizes the conclusions of the three studies undertaken in this research to understand the impacts of wildfires on air quality in the Southeastern U. S. by mid-21st century. These modeling studies compare two different approaches to estimating wildfire emissions, and the resulting air quality predictions. They examine the wildfire contribution to overall air quality in the context of other anthropogenic emissions, and not in isolation. As such, the comparisons of these two approaches cannot draw definitive conclusions about future AQ impacts of wildfires in the Southeast, e.g., "an X % increase in wildfire emissions will result in a Y% increase in $PM_{2.5}$", although they do provide insights into differences in the current and future AQ predictions of these methods. To examine the impacts on future-year air quality of wildfire emissions, therefore, the third study includes a modeling sensitivity comparing the results from one of these two approaches against a baseline simulation zeroing out the wildfires. The conclusions from each study are enumerated in the following sections.

Study 1

This study compared wildfire emissions estimated over the Southeastern U. S. from three methods: (a) using AAB projected with meteorological inputs from statistical downscaling of a climate realization with the CGCM31 model and the A2 scenario GHG emissions, labeled "statistical d-s"; (b) using AAB projected with meteorological inputs from dynamical downscaling of a climate realization with the CGCM30 model and the A2 scenario GHG

emissions, labeled "dynamical d-s", and (c) using historical mean AAB for 1992-2010, labeled "historical". The study found the following:

- Wildfire area burned, and the resulting emissions of $PM_{2.5}$ in the Southeast for 2010-2060 are a result of two competing drivers, climate and socioeconomics, each with its own spatiotemporal variability. This may not always lead to uniform increases in wildfire activity and emissions in future climate regimes.
- Historical mean AAB are higher than those estimated from statistically downscaled meteorology in most of the future time slices, and higher in all of them than those estimated with dynamically downscaled meteorology.
- Historically based estimates of wildfire emissions in the Southeast are consistently higher (by 13% - 62%) for $PM_{2.5}$ than those estimated by either of the projection methodologies.
- The large differences among the three methods in the temporal variability and spatial patterns of $PM_{2.5}$ emissions in future years compared to historical values are partly attributable to the temporal variability of the future changes in climate and socioeconomics underlying the AAB projections, and partly to the dynamically downscaled meteorology used to estimate future daily fire activity.

Study 2

This study compared the two wildfire emissions projection methods to the empirically based National Emissions Inventory for wildfires compiled by the U.S. EPA, by using them in AQ simulations of a historical period (2010). The modeled ambient concentrations of 1-hr ozone, maximum daily 8-hr average ozone (MDA8), and $PM_{2.5}$ and its constituents were compared

among the three cases simulated with these inventory methods, and between each modeled case and air quality observations from various ground-based networks.

The study found the following in its ozone analyses:

- There is nearly identical performance for all three cases against AQS network observations for hourly ozone. The O_3 differences among the cases are 0.08% - 0.93%, but the biases are much larger for any of the cases with respect to AQS observations (13% - 25%) over the entire year. Ozone has acceptable performance in spring through mid-summer, but degrades (MFE > 50%) in the cooler months, particularly in the fire-free winter. These results indicate that wildfire emissions, which are the only difference between the modeled cases, are not a major contributor to the model errors in ozone.
- The larger AAB estimates for the statistical d-s result in its large positive difference in O_3 from the other two methods at locations in October downwind of high fire activity.
- Large ozone differences between the two downscaling methods occur mostly in the northeastern quadrant of the domain, and downwind from peak differences in VOC and NO_x column emissions from wildfires in eastern Missouri and Appalachia. These results indicate that transport and secondary chemical transformations of precursor emissions from high fire activity areas to fire-free areas downwind drive the largest O_3 differences seen between the two downscaling methods.

The $PM_{2.5}$ analyses in this study found the following:

- Much smaller (1% - 8%) intermodel differences among the three wildfire emission methods for $PM_{2.5}$ than their individual biases with respect to observations (-14% - +51% at IMPROVE sites) during the fire season indicate that wildfire emissions do not contribute the larger part of the model bias.

- The $PM_{2.5}$ model performance against observations from the IMPROVE network is acceptable throughout the year for all three methods, but is the result of compensating biases in SO_4 (positive) and OC (negative) in almost every month.
- EC and NH_4; which are primarily emitted in wildfires also have good-to acceptable performance in almost all months. OC, which has a larger contribution from secondary chemical reactions, has its largest underpredictions (beyond acceptable levels) for the NEI in the summer. As OC is co-emitted with EC in wildfires, these findings together indicate that the OC underpredictions are likely due to other VOC sources or secondary chemical production in the AQ model, as these are common to all three modeled cases.
- The dramatically better OC model performance at urban sites compared to rural sites indicates potential underestimates of residential wood combustion and biogenic emissions in rural areas.
- Particulate NO_3 is lower in the summer than in the other seasons, and correlated with larger overpredictions of SO_4 and smaller overpredictions of NH_4 in that season, since less NH_3 is available for NO_3 formation. Gas-particle partitioning in the thermodynamics model is recognized as one of the contributors to NO_3 underpredictions in the AQ model, and may be a factor in these summertime NO_3 results.
- The severe overprediction of NO_3 in combination with larger overpredictions in NH_4 in the rest of the fire season indicates possible overestimates in the emissions of NH_3 or anthropogenic NO_x; the latter is more likely, as NH_4 stays within acceptable performance levels over these months.
- Differences in $PM_{2.5}$ between the two downscaling cases also confirm the previous conclusions from the ozone analyses, that the biggest impact of their differences is in

fire-free locations downwind of high fire activity due to the transport of fire emission plumes, but with a bigger contribution from primary PM emissions.

- Of the two downscaling methods, dynamical d-s compares more closely with the NEI, which has the smallest biases with respect to observations except in summer. Summertime PM is underpredicted by both these methods, but for different reasons: underprediction of under-canopy fires by the NEI, and overprediction of summer precipitation by the WRF model used in the dynamical d-s.
- The largest errors in $PM_{2.5}$ occur in SO_4, which has a very small contribution from wildfires, and in the case of ozone, in the fire-free winter months, pointing to chemical production pathways of these pollutants from non-wildfire sources as fruitful targets for future model improvements.

Study 3

This study examines future-year concentrations of ozone and $PM_{2.5}$ projected with the two wildfire emissions projection methods using the same AQ simulation model, with the same configuration and model inputs as in the second study, with the exception of the emissions. These were projected for the four future time slices, 2043, 2048, 2053 and 2058, for wildfires as well as the energy, transportation, industrial, aviation, commercial marine freight, and agricultural sectors. The projections from the GCAM (Thomson et al., 2011) were based on the Representative Concentration Pathway (RCP) 4.5, which assumes measures to limit GHG emissions to stabilize radiative forcing at 4.5 W m^{-2} by 2100. In the energy sector, this involves the reduction of fossil fuel usage through replacement with more renewable energy sources, resulting in reductions in SO_x, NO_x, EC and OC, and non-methane Volatile Organic Compounds (NMVOCs). However, there are increases in VOC emissions from oil and gas activity in these

projected emissions. The AQ model results are compared between the two downscaling methods, and across all the simulation years, including the retrospective year, 2010.

This study found the following from the ozone analysis:

- The wildfire emissions from the two projection methods differ less in their hourly ozone predictions in the future years than in 2010 with smaller mean and maximum differences over the entire fire season, and in spring, summer and autumn.
- Warmer and drier summers projected in the future shift the time of occurrence of the maximum ozone difference between the projection methods over the fire season to the summer (from late autumn in 2010). This accounts for the higher monthly-average ozone levels in the locations of these maximum differences by ~ 20 ppb compared to the ozone level in October 2010. Spatially, these maximum intermodel ozone differences occur in locations of higher AAB, projected to be along the Atlantic seaboard and the Gulf coast in Texas and Florida in the future years.
- The inter-year variability in these maximum intermodel differences follows that of their AAB differences; the greatest O_3 difference occurs in 2048, and the smallest in 2043.
- The impact of wildfires on 1-hour ozone averaged over each season have Southeast-wide maxima ranging from < 0.01 ppb in autumn to 1.5 ppb in the summer. The biggest impacts are seen in the summer in 2043 and 2058, and occur mostly over the South Florida, Appalachia and the Ohio valley.

The following were the findings of the $PM_{2.5}$ analyses:

- The intermodel differences in $PM_{2.5}$ concentrations projected in the future years are smaller than those in 2010 due to lower AAB (by up to 32%) and primary wildfire $PM_{2.5}$ emissions (by up to 40%) from their 2010 values. As with ozone, the locations of

maximum intermodel difference in future years shift east and south to Virginia and Florida in July and August, from the 2010 location in the Midwest in autumn, due to warmer and drier summers and higher AAB projected in these areas.

- The impact of wildfires on predicted 1-hour $PM_{2.5}$ averaged over each season show Southeast-wide maxima ranging from 1.5 $\mu g\ m^{-3}$ in autumn (2043) to 14 $\mu g\ m^{-3}$ in the summer (2058), discounting a value of < 0.01 $\mu g\ m^{-3}$ in autumn 2058. The biggest impacts are in the summers in all years, with 2058 being an outlier. These impacts occur mostly over the South Florida (spring), Appalachia and the Ohio valley (spring and summer) and the central Midwest (autumn). Overall, these seasonal maximum impacts indicate a wildfire contribution of well over 50% to the total ambient $PM_{2.5}$ concentration.
- The temporal variability of the AAB and the resulting wildfire PM emissions dictate the $PM_{2.5}$ concentration variability within each modeled case over the future years.
- Key wildfire PM species (OC, Other PM and NH_4) remain constant or increase slightly over the future years despite reductions in the anthropogenic sector emissions of EC by 24% - 60% and of the major contributors to $PM_{2.5}$ mass (SO_x, and NO_x) to ~ 20% their 2010 levels. The net impact on $PM_{2.5}$ is a 4.5% increase in the summers for 2043-2058 from the analysis of composition trends.

General Conclusions

The wildfire emissions estimated from the historical mean AAB, even from the most recent 19-year period, are not representative of how the climate and socioeconomic variables driving wildfire activity and emissions could change in future decades. Our results therefore suggest that the use of historical AAB is not sufficient to construct wildfire emission inventories for

simulating future-year air quality by mid-21st century, be they for climate change impact assessments, or for projecting population health risks from wildfire smoke.

Data availability from the climate model data archives limited this study to one climate model for one-to-one comparisons of the two downscaling methods, even though statistically downscaled meteorology from a suite of nine climate realizations was used in the initial AAB estimation models. Better inferences of temporal trends in the future wildfire emissions can be obtained in the dynamical downscaling by ensemble simulations that bracket the extremes in climate and societal change over the 2011-2060 period using representative high- and low-fire frequency years from among a number of climate realizations.

The wildfire emissions estimates from dynamical d-s are much lower than from statistical d-s, partly due to differences between the large-scale dynamics of the climate models and the mesoscale circulation in the dynamical d-s, but also possibly due to a high precipitation bias in the WRF meteorology used for the dynamical downscaling in estimates of both annual and daily fire activity. This is already evidenced by the PM underpredictions in the 2010 summer by both downscaling methods, with greater underpredictions by the dynamical d-s method.

Overall, both downscaling methods perform comparably to the NEI in simulating ozone throughout the 2010 fire season, and better than the NEI in simulating total $PM_{2.5}$ in the summer and primary PM species (EC and NH_4) throughout the fire season. Both ozone and secondary PM species (SO_4, OC, NO_3) have large biases in the simulations with all three inventories, which are found to be attributable to non-wildfire emissions, or secondary chemical production mechanisms in the AQ model. Thus, the simulation results at least partially confirm the hypothesis that the wildfire emissions projection methods will be within acceptable AQ model performance standards, and produce comparable results to an empirically-based emissions

inventory for a retrospective period. They show that the wildfire emissions projection methods are able to support simulations of current-day wildfire AQ impacts, with the added benefit of enabling such impact assessments much farther into the future.

Both the downscaling methods perform much more comparably than in 2010 in projecting future-year air quality. Spatially, they differ from 2010 in the locations of their maximum differences, and temporally, in the season of their occurrence in both ozone and PM. The locations of these maximum differences shift to areas along the eastern seaboard and the Gulf Coast of Texas and Florida. Temporally, the maximum difference shifts from October in 2010 to the late spring and summer months in the future years, driven by much less precipitation and more fuel aridity projected for those months by mid-century. This also changes the ambient ozone concentrations in these months of maximum difference in future years by ~ +20 ppb.

The impact assessment shows a wildfire contribution of well over 50% to ambient fine PM in some areas by mid-century in the summers. Concentration increases of 4.5% in $PM_{2.5}$ are projected on average during the future summers from 2043 to 2058. This is the net effect of projected decreases in the energy sector emissions from 2010 to 2055 by an average of 80% in the major PM precursors (SO_x and NO_x), the somewhat smaller (13% - 62%) decreases in projected wildfire $PM_{2.5}$ emissions relative to 2010 (Figure 2.6). The net result, for this particular scenario of future-year reductions in energy sector emissions, is an increased contribution of wildfire to total $PM_{2.5}$ by the mid-21st century summer from their 2010 levels, largely driven by OC and Other PM.

In addition to these differences in magnitude from their 2010 levels, the projected $PM_{2.5}$ concentrations also capture the inter-year variability of the wildfire emissions dictated by the climate and socioeconomic drivers of the underlying AAB, which cannot be represented with

empirically based (static) inventories such as the NEI (see Figure 2.6). These results confirm the hypothesis that the projected wildfire emissions will lead to considerably different ozone and $PM_{2.5}$ spatial distributions and concentrations from their 2010 levels by mid-21st century.

There are several areas of uncertainty, which should be explored to improve the robustness of these assessments. One is that these projected wildfire impacts on AQ are based on key assumptions about reductions in anthropogenic emissions in a variety of sectors, each affecting the atmospheric constituents in very different ways. Wildfire emissions will have a greater proportional impact on future PM levels if anthropogenic controls on SO_x and NO_x as assumed here are implemented. An important caveat is that this is only one of several possible future emission scenarios for the energy sector, and does not take into account possible changes in other sectors, e.g., agriculture, or policy shifts that could occur in the intervening years regarding the use of fossil fuels. These will play a critical role in the significance of these wildfire emissions for ambient PM concentrations and composition in the future. For example, there is an assumption of about a two-thirds reduction in SO_x and NO_x emissions from the energy and transportation sectors by 2060 relative to 2010. A deviation from this trajectory can have dramatic impacts in the formation of nitrate if wildfire emissions grow at 4% over the Southeast as projected (Prestemon et al., 2016), and agricultural ammonia emissions increase. The resulting composition could be very different from the nearly constant compositions projected here.

Another area of uncertainty is introduced by the interannual variability of the AAB captured in the sparse sample of four years used in the future-year modeling. The AAB and wildfire emissions are both projected to be lower by 13% - 62% in these years. Selecting a different set of years, e.g., by choosing years that only have high or low fire activity, could change this trend entirely, as also the PM compositions from their nearly constant projected levels in the future

years modeled here. This again points to the need for an ensemble approach to bracket uncertainties by choosing a larger sample of years to model that are representative of both high and low AAB projections. Related to this uncertainty is the gap in the WRF inputs for the daily AQ predictions from 2020-2040. Filling this gap in the modeling can lead to very different conclusions about the projected impacts of wildfire on future AQ, and their trajectory from the present to mid-century.

Precipitation is a critical input in wildfire emissions estimates due to its impact on daily fire activity, due to its influence on fire weather, and soil and fuel moisture. Reducing the high precipitation bias in WRF will greatly change the model results, at least for the dynamical d-s projections, and increase the already high impact of wildfires projected for summertime AQ. As dynamical downscaling is the most widely used way to provide consistent meteorological inputs from estimating emissions, to driving air-quality simulations, correcting biases in this method would more reliably support natural resource management and wildfire health risk assessments.

Public response to recent fire events indicates that future fuel loads may change not only due to climate change but also due to evolving wildfire mitigation strategies. No changes were made to fuel loads in these wildfire emissions projections, although land use changes included in the AAB projections indirectly account for them in the aggregate. While this omission does not have an impact on the AAB projections, it does have an impact on the wildfire emissions estimates, which are based on current FCCS fuel loads (McKenzie et al., 2007). Removal of fuels by fire, also omitted in these emissions estimates, will somewhat offset this impact. Appropriately representing fuel loads in long-term wildfire impact assessments such as the one presented here could benefit regional fuel management decisions regarding where, when and what to control.

REFERENCES

Abatzoglou J. T., and Kolden C. A., Climate change in Western US deserts: Potential for increased wildfire and invasive annual grasses, Rangeland Ecol. Manage., 64, 471–478, doi:10.2111/REMD- 09-00151.1, 2011.

Abatzoglou, J. T., and Kolden, C. A.: Relationships between climate and macroscale area burned in the western United States, Int. J. Wildland Fire, 22, 1003–1020, 2013.

Abatzoglou, J. T. and Williams, A. P.: Impact of anthropogenic climate change on wildfire across western US forests, Proc. Natl. Acad. Sci. USA, 113, 11 770-11 775, doi: 10.1073/pnas.1607171113, 2016.

Alapaty, K., Herwehe, J. A., Otte, T. L., Nolte, C. G., Bullock. O., R., Mallard, M. S., Kain, J. S., Dudhia, J.: Introducing subgrid-scale cloud feedbacks to radiation for regional meteorological and climate modeling, Geophys. Res. Lett., 39, L24809, 2012.

Appel, K. W., Bhave, P., Gilliland, A., Sarwar, G., Roselle, S.: Evaluation of the Community Multiscale Air Quality (CMAQ) model version 4.5: Sensitivities impacting model predictions: Part II—Particulate matter, Atmos. Environ., 42**,** 6057–6066, 2008.

Appel, K. W., Gilliam, R. C., Davis, N., Zubrow, A., and Howard S. C.: Overview of the Atmospheric Model Evaluation Tool (AMET) v1.1 for evaluating meteorological and air quality models, Environ. Modell. Softw., 26, 4, 434-443, 2011.

Appel, K.W., Gilliland, A., Sarwar, G, and Gilliam, R.: Evaluation of the Community Multiscale Air Quality (CMAQ) model version 4.5: Sensitivities impacting model predictions: Part I—Ozone, Atmos. Environ., 41**,** 9603–9615, 2007.

Balch, J. K., Bradley, B. A., Abatzoglou, J. T., Nagy, R. C., Fusco, E. J., and Mahood, A. L., Human-started wildfires expand the fire niche across the United States, Proc. Natl. Acad. Sci. USA, 114, 2946-2951, 2017.

Balch, J. K., Schoennagel, T., Williams, A. P., Abatzoglou, J. T., Cattau, M. E., Mietkiewicz, N. P., and St. Denis, L. A: Switching on the Big Burn of 2017, Fire, 1, 17, doi:10.3390/fire1010017, 2018.

Baek, B. H., and Seppanen, C.: Sparse Matrix Operator Kernel Emissions (SMOKE) modeling system, https://doi.org/ /10.5281/zenodo,1421403, 2018.

Bailey, R. G.: Description of the Ecoregions of the United States (2nd ed.), USDA Forest Service Miscellaneous Publication Number 1391, 1995.

Barbero, R., Abatzoglou, J. T., Larkin, N. K., Kolden, C. A., and Stocks, B.: Climate change presents increased potential for very large fires in the contiguous United States, Int. J. Wildland Fire, 24, 892-899, https://doi.org/10.1071/WF15083, 2015.

Blanchard, C. L., Hidy, G. M., Tanenbaum, S., Edgerton, E. S. and Hartsell, B. E.: The Southeastern Aerosol Research and Characterization (SEARCH) study: Spatial variations and chemical climatology, 1999–2010, J. Air Waste Manag. Assoc., 63, 260-275, doi: 10.1080/10962247.2012.749816, 2013.

Bond, T. C., Doherty, S. J., Fahey, D. W., Forster, P. M., Bemsten, T., DeAngelo, B. J., Flanner, M. G., Ghan, S., Kärcher, B., Kock, D., Kinne, S., Kondo, Y., Quinn, P. K., Sarofim, M. C., Schultz, M. G., Schultz, M., Venkataraman, C., Zhang, H., Zhang, S., Bellouin, S., Guttikunda, S. K., Hopke, P. K., Jacobson, M. Z., Kaiser, J. W., Klimont., Z., Lohmann, U., Schwarz, J. P., Shindell, D., Storelvmo, T., Warren, S. G., and Zender, C. S.: Bounding the role of black carbon in the climate system: A scientific assessment, J. Geophys. Res. Atmos., 118, 5380-5552, doi:10.1002/jgrd50171, 2013.

Boylan, J. W. and Russell, A. G.: PM and light extinction model performance metrics, goals, and criteria for three-dimensional air quality models, Atmos. Environ., 40, 4946-4959, 2006.

Butry, D. T., Mercer, D. E., Prestemon, J. P., Pye, J. M., Holmes. T. P.: What is the price of catastrophic wildfire? J. Forest., 99, 9 –17, 2001.

Byun, D. and Schere, K. L.: Review of the governing equations, computational algorithms, and other components of the Models-3 Community Multiscale Air Quality (CMAQ) modeling system, Appl. Mech. Rev., 59, 51-76, doi: 10.1115/1.2128636, 2006.

Cal Fire, Top 20 largest California wildfires. Available at http://www.fire.ca.gov/communications/downloads/fact_sheets/Top20_Acres.pdf, 2018. [Verified 10 February 2019]

Chang, J. S., Hanna, S. R.: Air quality model performance evaluation, Meteorol. Atmos. Phys., 87, 167-196, DOI 10.1007/s00703-003-0070-7, 2004.

Collins, W. D., Rasch, P. J., Boville, B. A., Hack, J. J., McCaa, J. R., Williamson, D. L., Kiehl, J. T., and Briegleb, B.: Description of the NCAR Community Atmosphere Model (CAM 3.0), NCAR Tech. Note NCAR/TN–464+STR. 214 pp, 2004. (Boulder CO)

Coumou, D., and Rahmstorf, S., A decade of weather extremes, Nat. Clim. Change, 2, 491–496, 2012.

Daly, C., Gibson, W. P., Taylor, G. H., Johnson, G. L., and Pasteris, P.: A knowledge-based approach to the statistical mapping of climate, Clim. Res., 22, 99–113, 2002.

Dawson, J. P., Adams, P. J., and Pandis, S. N., Sensitivity of ozone to summertime climate in the eastern USA: A modeling case study, Atmos. Environ. 41, 1494-1511, https://doi.org/10.1016/j.atmosenv.2006.10.033, 2007.

Dennis, R., Fox, T., Fuentes, M., Gilliland, A., Hanna, S., Hogrefe, C., Irwin, J., Rao, S. T., Scheffe, R., Schere, K., Steyn, D., and Venkatram, A.: A framework for evaluating regional-scale photochemical modeling systems, Environ. Fluid Mech., 10, 471-489, doi:10.1007/s10652-009-9163-2, 2010.

Dennison, P. E., Brewer, S. C., Arnold, J. D., and Moritz, M. A.: Large wildfire trends in the western United States, 1984-2011, Geophys. Res. Lett., 41, 2928-2933, doi: 10.1002/2014GL059576, 2014.

Donahue, N., Chuang, W., Epstein, S., Kroll, J., Worsnop, D., Robinson, A., Adams, P., and Pandis, S.: Why do organic aerosols exist? Understanding aerosol lifetimes using the two-dimensional volatility basis set, Environ. Chem., 10, 151–157, 2013.

Eidenshink, J., Schwind, B., Brewer, K., Zhu, Z., Quayle, B., and Howard, S.: A project for monitoring trends in burn severity, Fire Ecol., 3, 3-21, 2007.

Fann, N., Alman, B., Broome, R. A., Morgan, G. G., Johnston, F. H., Pouliot, G., and Rappold, A.: The health impacts and economic value of wildland fire episodes in the U.S.: 2008-2012, Sci. Total Environ., 610-611, 802-809, http://dx.doi.org/10.1016/j.scitotenv.2017.08.024, 2018.

Fann, N., Fulcher, C. M., and Baker, K.: The recent and future health burden of air pollution apportioned across U. S. sectors, Environ. Sci. Technol., 47, 3580–3589, 2013.

Flato, G. M.: The third version of the Canadian Centre for Climate Modeling and Analysis Coupled Global Climate Model (CGCM3), 2005. Available at http://www.ec.gc.ca/ccmac-cccma/default.asp?n=1299529F-1. [Verified 10 February 2019]

Fox, D. G.: Judging air quality model performance: A summary of the AMS Workshop on Dispersion Model Performance, B. Am. Meteorol. Soc., 62**,** 599–609, 1981.

Gachon, P., Harding, A., and Radojevic, M.: Predictor datasets derived from the CGCM3.1 T47 and NCEP/NCAR reanalysis. Montréal, QC, 2008.

Gaither, C. J., Poudyal, N. C., Goodrick, S., Bowker, J. M., Malone, S., and Gan, J.: Wildland fire risk and social vulnerability in the Southeastern United States: An exploratory spatial data analysis approach, For. Policy Econ., 13, 24-36, doi:10.1016/j.forpol.2010.07.009, 2011.

Grell, G. A.: Prognostic evaluation of assumptions used by cumulus parameterizations, Mon. Wea. Rev., 121, 764-787, 1993.

Grell, G. A. and Devenyi, D.: A generalized approach to parameterizing convection combining ensemble and data assimilation techniques, Geophys. Res. Lett., 29, 1693-1697, 2002.

Gullett, B., Touati, A., and Oudejans, L.: PCDD/F and aromatic emissions from simulated forest and grassland fires, Atmos. Environ., 42, 7997-8006, 2008.

Hong, S. Y. and Lim, J. O. J.: The WRF single-moment 6-class microphysics scheme, Journal of the Korean Meteorological Society, 42, 129-151, 2006.

Hong, S. Y., Dudhia, J., and Chen, S. H.: A revised approach to ice microphysical processes for the bulk parameterization of clouds and precipitation, Mon. Wea. Rev., 132, 103-120, 2004.

Hong, S. Y., Noh, Y., and Dudhia, J.: A new vertical diffusion package with an explicit treatment of entrainment processes, Mon. Wea. Rev., 134, 2318–2341, 2006.

Houyoux, M. R., Vukovich, J. M., Coats, C. J. C. Jr, Wheeler, N. J. M., and Kasibhatla, P. S.: Emission inventory development and processing for the Seasonal Model for Regional Air Quality (SMRAQ) project, J. Geophys. Res., 105, 9079-9090, 2000.

Iacono, M. J., Delamere, J. S., Mlawer, E. J., Shephard, M. W., Clough, S. A., and Collins, W. D.: Radiative forcing by long–lived greenhouse gases: Calculations with the AER radiative transfer models, J. Geophys. Res., 113, D13103, 2008.

Jeong, D., St-Hilaire, A., Ouarda, T., and Gachon, P.: CGCM3 predictors used for daily temperature and precipitation downscaling in southern Québec, Canada. Theor. Appl. Climatol., 107, 389–406, 2012.

Joyce, L. A., Price, D. T., Coulson, D. P., McKenney, D. W., Siltanen, R. M., Papadopol, P., and Lawrence, K.: Projecting climate change in the United States: A technical document supporting the Forest Service RPA 2010 Assessment, USDA Forest Service, Rocky Mountain Research Station, General Technical Report RMRS-GTR-320, 2014. (Fort Collins, CO)

Katragkou, E., García-Diéz, M., Vautard, R., Sobolowski, S., Zanis, P., Alexandri, G., Cardoso, R. M., Colette, A., Fernandez, J., Gobiet, A., Goergen, K., Karacostas, T., Knist, S., Mayer, S., Soares, P. M. M., Pytharoulis, I., Tegoulias, I., Tsikerdekis, A., and Jacob, D.: Regional climate hindcast simulations within EURO-CORDEX: evaluation of a WRF multi-physics ensemble, Geosci. Model Dev., 8, 603-618, doi:10.5194/gmd-8-603-2015, 2015.

Keetch, J. J. and Byram, G. M.: A Drought Index for Forest Fire Control, USDA Forest Service Research Paper SE-38, Southeastern Forest Experiment Station, 1968. (Asheville, NC)

Kelly, J. T., Baker, K. R., Nowak, J. B., Murphy, J. G., Markovic, M. Z., VandenBoer, T. C., Ellis, R. A., Neuman, J. A., Weber, R. J., Roberts, J. M., Veres, P. R., de Gouw, J. A., Beaver, M. R., Newman, S., and Misenis, C.: Fine-scale simulation of ammonium and nitrate over the South Coast Air Basin and San Joaquin Valley of California during CAL-NEX 2010, J. Geophys. Res. Atmos., 119, 3600-3614, doi:10.1002/2013JD021290, 2014.

King, A. W., Hayes, D. J., Huntsinger, D. N., West, T. O., and Post, W. M.: North American carbon dioxide sources and sinks: Magnitude, attribution, and uncertainty, Front. Ecol. Environ., 10, 512–519, 2012.

Koo, B., E. Knipping, E., and Yarwood, G.: 1.5-Dimensional Volatility Basis Set approach for modeling organic aerosol in CAMx and CMAQ, Atmos. Environ., 95, 158–164, 2014.

Koplitz, S. N., Nolte, C. G., Pouliot, G. A., and Vukovich, J. M.: Influence of uncertainties in burned area estimates on modeled wildland fire $PM_{2.5}$ and ozone pollution in the contiguous U.S., Atmos. Environ., 191, 328-229, 2018.

Larkin, N. K., O'Neill, S. M., Solomon, R., Raffuse, S., Rorig, M., Peterson, J., and Ferguson, S. A.: The BlueSky smoke modeling framework, Int. J. Wildland Fire, 18, 906–920, 2009.

Larkin, N. K., Raffuse, S. M., Strand, T. M.: Wildland fire emissions, carbon and climate: U.S. emissions inventories, For. Ecol. Manage., 317, 61-69, 2014.

Leonard, S. S., Castranova, V., Chen, B. T., Schwegler-Berry, D., Hoover, M., Piacitelli, C., Gaughan, D. M.: Particle size-dependent radical generation from wildland fire smoke, Toxicology**,** 236, 103–113, 2007.

Leonard, S. S., Wang, S., Shi, X., Jordan, B. S., Castranova, V, and Dubick, M. A.: Wood smoke particles generate free radicals and cause lipid peroxidation, DNA damage, NF-kappaB activation and TNF-alpha release in macrophages, Toxicology**,** 150,147–157, 2000.

Linacre, E. T.: A simple formula for estimating evaporation rates in various climates using temperature data alone, Agr. Meteorol., 18, 409-424, 1977.

Littell, J. S., McKenzie, D., Peterson, D. L., and Westerling, A. L.: Climate and wildfire area burned in western U.S. ecoprovinces, 1916-2003, Ecol. Appl., 19, 1003-1021, 2009.

Littell, J. S., McKenzie, D., Wan, H. Y., and Cushman, S. A.: Climate change and future wildfire in the western USA: an ecological approach to non-stationarity, Earths Future, 6, 1097-1111, https://doi.org/10.1029/2018EF000878, 2018.

Littell, J. S., Oneil, E. A., McKenzie, D., Hicke, J. A., Norheim, R. A., and Elsner, M. M.: Forest ecosystems, disturbance, and climate change in Washington State, USA, Clim. Change, 102, 129–158, 2010.

Littell, J. S., Peterson, D. L., Riley, K. L., Liu, Y., and Luce, C. H.: A review of the relationships between drought and forest fire in the United States, Global Change Biol., 22, 2353–2369, doi:10.1111/gcb.13275, 2016.

Liu, J. C., Mickley, L. J., Sulprizio, M. P., Domenici, F., Yue, X., Ebisu, K., Anderson, G. B., Khan, R. F. A., Bravo, M. A., and Bell, M. L.: Particulate air pollution from wildfires in the western US under climate change, Clim. Change, 135, 655-666, DOI:10.1007/s10584-016-1762-6, 2016.

Liu, S., Bond-Lambert, B., Hicke, J. A., Vargas, R., Zhao, S., Chen, J., Edburg, S. L., Hu, Y., Liu, J., McGuire, A. D., Xiao, J., Keane, R., Yuan, W., Tang, J., Luo, Y., Potter, C., and Oeding, J., Simulating the impacts of disturbances on forest carbon cycling in North America: Processes, data, models, and challenges, J. Geophys. Res. – Biogeosci., 116, G00K08, doi:10.1029/2010JG001585, 2011.

Liu, Y., Goodrick, S. L., Stanturf, J., and Tian, H.: Impacts of mega-fires on large U.S. urban area air quality under changing climate and fuels. Final Report to the Joint Fire Science Program, US Bureau of Land Management, Joint Fire Science Program, Final Project Report 11-1-7-2, 2014, 29p. (Boise, ID)

Liu, Y., Goodrick, S. L., and Stanturf, J.: Future U.S. wildfire potential trends projected using a dynamically downscaled climate change scenario, For. Ecol. Manage., 294,120–135, doi:10.1016/j.foreco.2012.06.049, 2013.

Liu, Y., Prestemon, J. P., Goodrick, S., Holmes, T. P., Stanturf, J. A., Vose, J. M., and Sun, G.: Future wildfire trends, impacts, and mitigation options in the southern United States. In Climate change adaptation and mitigation management options A guide for natural resource managers in southern forest ecosystems, (Eds J. M Vose and K. D. Klepzig), pp. 85-125, 2014. (CRC Press: New York, NY)

Liu, Y., Stanturf, J., and Goodrick, S.: Trends in global wildfire potential in a changing climate, For. Ecol. Manage.**,** 259, 685-697, doi:10.1016/j.foreco.2009.09.002, 2010.

McKenzie, D., O'Neill, S. M., Larkin, N., and Norheim, R. A.: Integrating models to predict regional haze from wildland fire, Ecol. Modell.*,* 199, 278-288, 2006.

McKenzie, D., Raymond, C. L., Kellogg, L. K. B., Norheim, R. A., Andreu, A. G., Bayard, A. C., Kopper, K. E., and Elman, E.: Mapping fuels at multiple scales: Landscape application of the fuel characteristic classification system, Can. J. For. Res., 37, 2421–2437, 2007.

McKenzie, D., Shankar, U., Keane, R. E., Stavros, E. N., Heilman, W. E., Fox, D. G., and Riebau, A. C.: Smoke consequences of new wildfire regimes driven by climate change, Earths Future, 2, 35-59, doi:10.1002/2013EF000180, 2014.

Mearns, L. O., Gutowski, W. J., Jones, R., Leung, L-Y, McGinnis, S., Nunes, A. M. B., and Qian, Y.: A regional climate change assessment program for North America, Earth Obs. Sys., 90, 311-312, 2009.

Mercer, D. E., and Prestemon, J. P.: Comparing production function models for wildfire risk analysis in the Wildland-Urban Interface, For. Policy Econ., 7, 782–795, 2005.

Moss, R., Edmonds, J., Hibbard, K., Carter, T., Emori, S., Kainuma, M., Kram, T., Manning, M., Meehl, J., Mitchell, J., Nakicenovic, N., Riahi, K., Rose, S., Smith, S., Stouffer, R., Thomson, A. M., vanVuuren, D., Weyant, J., and Willbanks. T.: The next generation of scenarios for climate change research and assessment, Nature, 463:747-756, 2010.

Nakicenovic, N. and Steward, R. (Eds): Special Report on Emissions Scenarios: A Special Report of Working Group III of the Intergovernmental Panel on Climate Change, Cambridge University Press: Cambridge, UK, 2000. Available at http://www.grida.no/climate/ipcc/emission/index.htm [Verified 10 February 2019].

Napelenok, S., Vedantham, R., Bhave, P. V., Pouliot, G. A., and Kwok, R. H. F.: Source-receptor reconciliation of fine-particulate emissions from residential wood combustion in the southeastern United States, Atmos. Environ., 98, 454-460, 2014.

National Fire and Aviation Management: Southern Area Coordination Center firefighting costs (suppression only), 2017. Available at https://fam.nwcg.gov/fam-web/ [Verified 10 February 2019].

National Interagency Fire Center: Federal firefighting costs (suppression only), 2017a. Available at http://www.nifc.gov/fireInfo/fireInfo_documents/SuppCosts.pdf [Verified 10 February 2019].

National Interagency Fire Center: Total wildland fires and acres (1960-2015), 2017b. Available at http://www.nifc.gov/fireInfo/fireInfo_stats_totalFires.html [Verified 10 February 2019].

National Park Service: Chimney Tops 2 Fire Review Report, 2017. Available at https://www.wildfirelessons.net/orphans/viewincident?DocumentKey=5bfa19b8-ca1e-4f4a-882f-9dad173ec28c [Verified 10 February 2019]

Niu. G. Y., Yang, Z. L., Mitchell, K. E., Chen, F., Ek, M. B., Barlage, M., Kumar, A., Manning, K., Niyogi, D., Rosero, E., Tewari, M., and Xia, Y.: The community Noah land surface model with multiparameterization options (Noah–MP): 1. Model description and evaluation with local–scale measurements, J. Geophys. Res., 116, D12109, 2011.

Ottmar, R. D., Prichard, S. J., Vihnanek, R. E., and Sandberg, D. V.: Modification and validation of fuel consumption models for shrub and forested lands in the Southwest, Pacific, Northwest, Rockies, Midwest, Southeast, and Alaska. US Bureau of Land Management, Joint Fire Sciences Program, Final Project Report 98-1-0-06, 2006. (Boise, ID)

Pouliot, G., Pace, T., Roy, B., Pierce, T., and Mobley, D.: Development of a biomass burning emission inventory by combining satellite and ground-based information, J. Appl. Remote Sens., 2, 021501, doi: 10.1117/1.2939551, 2008.

Pouliot, G., Pierce, T., Van der Gon, H. D., Schaap, M., Moran, M., and Nopmongcol, U.: Comparing emission inventories and model-ready emission datasets between Europe and North America for the AQMEII project, Atmos. Environ. 53, 4-14, 2012.

Prestemon, J.P., and Butry, D. T.: Time to burn: modeling wildland arson as an autoregressive crime function, Am. J. Agric. Econ., 87, 756–770, 2005.

Prestemon, J. P., Hawbaker, T. J., Bowden, M., Carpenter, J., Scranton, S., Brooks, M. T., Sutphen, R., and Abt, K. L.: Wildfire Ignitions: A Review of the Science and Recommendations for Empirical Modeling, USDA Forest Service General Technical Report SRS-171, 2013. (Asheville, NC)

Prestemon, J. P., Pye, J. M., Butry, D. T., Holmes, T. P., and Mercer, D.: Understanding broad scale wildfire risks in a human-dominated landscape, For. Sci., 48, 685-693, 2002.

Prestemon, J. P., Shankar, U., Xiu, A., Talgo, K., Yang, D., Dixon, E., McKenzie, D., and Abt, K.: Projecting wildfire area burned in the south-eastern United States, 2011-2060, Int. J. Wildland Fire, 25, 715-729, http://dx.doi.org/10.1071/WF15124, 2016.

Prospero, J. M.: Long-range transport of mineral dust in the global atmosphere: Impact of African dust on the environment of the southeastern United States, Proc. Natl. Acad. Sci. USA, 96, 3396-3403, 1999.

Prospero, J. M., Collard, F-X., Molinié, J., and Jeannot, A.: Characterizing the annual cycle of African dust transport, to the Caribbean Basin and South America and its impact on the environment and air quality, Global Biogeochem. Cycles, 29, 757-773, doi:10.1002/2013GB004802, 2014.

Pye, H. O. T., Luecken, D. J., Xu, L., Boyd, C. M., Ng, N. L., Baker, K. R., Ayres, B. R., Bash, J. O., Baumann, K., Carter, W. P. L., Edgerton, E., Fry, J. L., Hutzell, W. T., Schwede, D. B., and Shepson, P. B.: Modeling the current and future roles of particulate organic nitrates in the Southeastern United States, Environ. Sci. Technol., 49, 14 195-14 203, 2015.

Rappold, A. G., Cascio, W. E., Kilaru, V. J., Stone, S. L., Neas, L. M., Devlin, R. B., and Diaz-Sanchez, D.: Cardio-respiratory outcomes associated with exposure to wildfire smoke are modified by measures of community health, Environ. Health-Glob., 11, 71-80. doi: 10.1186/1476-069X-11-71, 2012.

Rappold, A. G., Fann, N. L., Crooks, J., Huang, J., Cascio, W. E., Devlin, R. B., and Diaz-Sanchez, D.: Forecast-based interventions can reduce the health and economic burden of wildfires, Environ. Sci. Technol., 48, 10 571-10 579, doi: 10.1021/es5012725, 2014.

Rappold, A., Stone, S. L., Cascio, W. E., Neas, L. M., Kilaru, V. J., Carraway, M. S., Szykman, J. J., Ising, A., Cleve, W. E., Meredith, J. T., Vaughan-Batten, H., Deyneka, L., Devlin, R. B.: Peat bog wildfire smoke exposure in rural North Carolina is associated with cardiopulmonary emergency department visits assessed through syndromic surveillance, Environ. Health Perspect., 119, 1415–1420, 2011.

Reff, A., Bhave, P. V., Simon, H., Pace, T. G., Pouliot, G. A., Mobley, J. D., and Houyoux, M.: Emissions inventory of $PM_{2.5}$ trace elements across the United States, Environ. Sci. Technol., 43, 5790-5796, 2009.

Ruminski, M., Kondragunta, S., Draxler, R., and Zeng, J.: Recent changes to the Hazard Mapping System. 15th International Emission Inventory Conference: Reinventing Inventories—New Ideas in New Orleans, EPA, New Orleans, LA, 15-18 May, 2006. Available at https://www3.epa.gov/ttn/chief/conference/ei15/session10/ruminski_pres.pdf [Verified 10 February 2019].

Sarwar, G., Appel, K.W., Carlton, A.G., Mathur, R., Schere, K., Zhang, R., and Majeed, M.A.: Impact of a new condensed toluene mechanism on air quality model predictions in the US, Geosci. Model Dev., 4, 1-11, 2011.

Shankar, U., McKenzie, D., Prestemon, J., Baek, B., Omary, M., Yang, D., Xiu, A., Talgo, K., and Vizuete, W.: Evaluating emissions projection methods in comparisons of simulated and observed air quality, Atmos. Chem. Phys. Discuss., https://doi.org/10.5194/acp-2018-1296, in review, 2019.

Shankar, U. Prestemon, J. P., McKenzie, D., Talgo, K., Xiu, A., Omary, M., Baek, B. H., Yang, D., and Vizuete, W.: Projecting wildfire emissions over the south-eastern United States to mid-century, Int. J. Wildland Fire, 27, 313-328, https://doi.org/10.1071/WF17116, 2018.

Short, K. C.: Sources and implications of bias and uncertainty in a century of US wildfire activity data, Int. J. Wildland Fire, 24, 883–891, 2015.

Short, K. C.: A spatial database of wildfires in the United States, 1992-2011, Earth Syst. Sci. Data, 6, 1-27, doi:10.5194/ESSD-6-1-2014, 2014.

Simon, H. and Bhave, P. V.: Simulating the degree of oxidation in atmospheric organic particles, Environ. Sci. Technol., 46, 331-339, 2012.

Sisler, J. F., Huffman, D., Latimer, D. A., Malm, W. C., and Pitchford, M. L.: Spatial and temporal patterns and the chemical composition of the haze in the United States: An analysis of data from the IMPROVE network, 1988 – 1991, Cooperative Institute for Research in the Atmosphere, Colorado State University, ISSN No. 0737-5352-26, 1993. (Fort Collins, CO)

Skamarock, W., Klemp, J. B., Dudhia, J., Gill, D. O., Barker, D. M., Duda, M. G., Huang, X-Y., Wang, W., and Powers, J. G.: A Description of the Advanced Research WRF Version 3, NCAR/TN-475+STR, 2008. (Boulder, CO)

Soja, A. J., Al-Saadi, J., Giglio, L., Randall, D., Kittaka. C., Pouliot. G., Kordzi. J. J., Raffuse, S., Pace, T. G., Pierce, T. E., Moore, T., Roy, B., Pierce, R. B., and Szykman, J. J.: Assessing satellite-based fire data for use in the National Emissions Inventory. J. Appl. Remote Sens., 3, 031504, https://doi.org/10.1117/1.3148859, 2009.

Spero, T. L., Otte, M. J., Bowden, J. H., and Nolte, C. G.: Improving the representation of clouds, radiation, and precipitation using spectral nudging in the Weather Research and Forecasting model. J. Geophys. Res. Atmos., 119, 11,682-11,694, doi:10.1002/2014JD022173, 2014.

Stavros, E. N., Abatzoglou, J., Larkin, N. K., McKenzie, D., and Steel, E. A.: Climate and very large wildland fires in the contiguous western USA, Int. J. Wildland Fire, 23, 899-914, http://dx.doi.org/10.1071/WF13169, 2014.

Syphard, A. D., Keeley, J. E., Pfaff, A. H., and Ferschweiler, K.: Human presence diminishes the importance of climate in driving fire activity across the United States, Proc. Natl. Acad. Sci. USA, 114, 13 750-13 755, doi:10.1073/pnas.1713885114, 2017.

Thomson, A. M., Calvin, K. V., Smith, S. J., Kyle, G. P., Volke, A., Patel, P., Delgado-Arias, S., Bond-Lamberty, B., Wise, M. A., Clarke, L. E., and Edmonds, J. A., Climatic Change, 109, 77, https://doi.org/10.1007/s10584-011-0151-4, 2011.

US Bureau of Economic Analysis (2013a) Interactive data. Available at http://www.bea.gov/itable/ [Verified 10 February 2019]

US Bureau of Economic Analysis (2013b) Current-dollar and "real" GDP. Available at http://www.bea.gov/national/index.htm[Verified 10 February 2019]

US Census Bureau: Population estimates, 2018. Available at https://www.census.gov/programs-surveys/popest/data/data-sets.All.html. [Verified 10 February 2019]

USDA Forest Service: 2010 RPA Assessment population and income data (xlsx), 2014. Available at http://www.fs.fed.us/research/rpa/assessment/ [Verified 10 February 2019]

U.S. EPA: Guidance on the use of models and other analyses for demonstrating attainment of air quality goals for ozone, $PM_{2.5}$, and regional haze. U.S. Environmental Protection Agency Report EPA -454/B-07-002, U.S. Environmental Protection Agency, Office of Air Quality Planning and Standards, Research Triangle Park, NC 27711, USA, April 2007. Available at https://www3.epa.gov/scram001/guidance/guide/final-03-pm-rh-guidance.pdf. [Verified 10 February 2019]

USGCRP, Impacts, Risks, and Adaptation in the United States: Fourth National Climate Assessment, Volume II [Reidmiller, D. R., C. W. Avery, D. R. Easterling, K. E. Kunkel, K. L. M. Lewis, T. K. Maycock, and B. C. Stewart (eds.)]. U.S. Global Change Research Program, Washington, DC, USA, 1515 pp, December 2018, doi: 10.7930/NCA4.2018, 2018.

Van Wagner, C. E., and Pickett, T. L.: Equations and FORTRAN program for the Canadian Forest Fire Weather Index System. Canadian Forest Service, Forestry Technical Report 33 (Ottawa, ON, Canada), 1985.

Vennam, L. P., Arunachalam, S., Bowden, J., Baek, B. H., Omary, M. O., Vizuete, W., Olsen, S.: Modeled Trends in Impacts of Landing and Takeoff Aircraft Emissions on Surface Air-Quality in U.S for 2005, 2010 and 2018. 13th Annual CMAS Conference, Chapel Hill, NC, 27 – 29 October 2014, 2014. Available at https://www.cmascenter.org/conference/2014/agenda.cfm - inline1530. [Verified 10 February 2019]

Viedma, O., Urbieta, I. R., and Moreno, J. M., Wildfires and the role of their drivers are changing over time in a large rural area of west-central Spain, Sci. Rep., 8, Article No. 17797, doi: 10.1038/s41598-018-36134-4, 2018.

Wear, D. N.: Forecasts of land uses. In 'The Southern Forest Futures Project: Technical Report.' (Ed. DN Wear, JG Greis) USDA Forest Service General Technical Report SRS-GTR-178, pp. 45–71, 2013. (Asheville, NC).

Wegesser, T. C., Pinkerton, K. E., and Last, J. A.: California wildfires of 2008: Coarse and fine particulate matter toxicity, Environ. Health Perspect., 117, 893–897, 2009.

Westerling, A. L., Bryant, B. P., Preisler, H. K., Holmes, T. P., Hidalgo, H., Das, T., and Shrestha, S., Climatic change and growth scenarios for California wildfire, Clim. Change, 109, 445–463, doi:10.1007/S10584-011- 0329-9, 2011a.

Westerling, A. L., Turner, M. G., Smithwick, E. A. H., Romme, W. H., and Ryan, M. G., Continued warming could transform greater Yellowstone fire regimes by mid-21st century, Proc. Natl. Acad. Sci. USA, 108, 13,165–13,170, doi:10.1073/PNAS.1110199108, 2011b.

Whitten, G. Z., Heo, G., Kimura, Y., McDonald-Buller, E., Allen, D. T., Carter, W. P. L., and Yarwood, G.: A new condensed toluene mechanism for Carbon Bond: CB05-TU, Atmos. Environ., 44, 5346-5355, 2010.

Wilkins, J. L., Pouliot, G., Foley, K., Appel, W., and Pierce, T.: The impact of US wildland fires on ozone and particulate matter: a comparison of measurements and CMAQ model predictions from 2008 to 2012, Int. J. Wildland Fire, https://doi.org/10.1071/WF18053, 2018.

Wong, D. C., Pleim, J., Mathur, R., Binkowski, F., Otte, T., Gilliam, R., Pouliot, G., Xiu, A., Young, J. O., and Kang, D.: WRF- CMAQ two-way coupled system with aerosol feedback: Software development and preliminary results, Geosci. Model Dev., 5, 299-312, 2012.

Woody, M. C., Baker, K. R., Hayes, P. L., Jiminez, J. L., Koo, B., and Pye, H. O. T.: Understanding sources of organic aerosol during CalNex-2010 using CMAQ-VBS, Atmos. Chem. Phys., 16, 4081-4100, 2016.

Yang, Z. L., Niu, G. Y., Mitchell, K. E., Chen, F., Ek, M. B., Barlage, M., Longuevergne, L., Manning, K., Niyogi, D., Tewari, M., and Xia. Y: The community Noah land surface model with multiparameterization options (Noah–MP): 2. Evaluation over global river basins. J. Geophys. Res., 116, D12110, 2011.

Yu, S., Eder, B., Dennis, R., Chu, S-H., and Schwarz, S.: New unbiased symmetric metrics for evaluation of air quality models, Atmos. Sci. Lett., 7, 26-34, 2006.

Yue, X., Mickley, L. J., Logan, J. A., Hudman, R. C., Martin, M. V., and Yantosca, R. M.: Impact of 2050 climate change on North American wildfire: consequences for ozone air quality, Atmos. Chem. Phys., 15, 10033-10055, doi:10.5194/acp-15-10033-2015, 2015.

Yue, X., Mickley, L. J., Logan, J. A., and Kaplan, J. O.: Ensemble projections of wildfire activity and carbonaceous aerosol concentrations over the western United States in the mid-21st century, Atmos. Environ., 77, 767-780, 2013.